NUMERICAL ANALYSIS OF THE ANDERSON LOCALIZATION

P. Markoš[1]

Institute of Physics, Slovak Academy of Sciences, 845 11 Bratislava, Slovakia

The aim of this paper is to demonstrate, by simple numerical simulations, the main transport properties of disordered electron systems. These systems undergo the metal insulator transition when either Fermi energy crosses the mobility edge or the strength of the disorder increases over critical value. We study how disorder affects the energy spectrum and spatial distribution of electronic eigenstates in the diffusive and insulating regime, as well as in the critical region of the metal-insulator transition. Then, we introduce the transfer matrix and conductance, and we discuss how the quantum character of the electron propagation influences the transport properties of disordered samples. In the weakly disordered systems, the weak localization and anti-localization as well as the universal conductance fluctuation are numerically simulated and discussed. The localization in the one dimensional system is described and interpreted as a purely quantum effect. Statistical properties of the conductance in the critical and localized regimes are demonstrated. Special attention is given to the numerical study of the transport properties of the critical regime and to the numerical verification of the single parameter scaling theory of localization. Numerical data for the critical exponent in the orthogonal models in dimension $2 < d \leq 5$ are compared with theoretical predictions. We argue that the discrepancy between the theory and numerical data is due to the absence of the self-averaging of transmission quantities. This complicates the analytical analysis of the disordered systems. Finally, theoretical methods of description of weakly disordered systems are explained and their possible generalization to the localized regime is discussed. Since we concentrate on the one-electron propagation at zero temperature, no effects of electron-electron interaction and incoherent scattering are discussed in the paper.

Contents

---

[1]E-mail address: peter.markos@savba.sk

1 Introduction

Localization of electrons in disordered system has fascinated scientists for almost fifty years. In 1958, Anderson [1] predicted that randomly distributed impurities in the crystal lattice can localize an electron in a certain spatial region. The localization is given by the quantum character of electron propagation: electron wave function is scattered on randomly distributed impurities, and mutual interference of scattered components cancel the wave function on large distances. Localization of the electron is responsible for a new kind of insulators - the Anderson insulator, which possesses zero electric conductivity, σ, in a part of the energy bands, where the density of states, $\rho(E)$, is non-zero. Propagation of the electron in disordered systems is therefore qualitatively different from that in periodic structures. Although the electron wave function is reflected also by a periodic potential, the interference of the reflected and the transmitted waves in a regular lattice gives rise to bands and gaps in the electron energy spectrum. In the bands, where the density of states is non-zero, the electron propagates freely throughout the structure.

Of course, disorder is always present in the real world, and it influences the electric transport. Scattering on weak impurities causes diffusive propagation of electrons. The electrical conductivity can be expressed through the diffusive coefficient, $D(E)$, and the density of states, $\rho(E)$,

$$\sigma = e^2 D(E)\rho(E). \tag{1}$$

In the derivation of the expression (1), it is assumed that an electron on its travel through the sample is scattered on individual impurities. This assumption is correct only if the electron wavelength, λ_F, which is determined by the wave vector, k_F on the Fermi energy, is smaller than the electron mean free path due to the coherent scattering on impurities, ℓ,

$$\frac{\ell}{\lambda_F} \gg 1. \tag{2}$$

[2]. The mean free path represents, in the first approximation, the mean distance between two impurities. Clearly, ℓ is large in the limit of weak disorder, and decreases when disorder increases. Therefore, condition (2) is violated for strong disorder and localization is expected when $\ell \sim \lambda_F$. The last relation is known as the Lifshitz criterion for localization.

Increase of disorder changes the transport regime considerably. In the limit of very strong disorder, all electronic states become localized. The wave function of localized electron decreases exponentially as a function of distance from the localization center, $\vec{r_0}$,

$$\Psi(\vec{r}) \sim \exp-\frac{|\vec{r} - \vec{r_0}|}{\lambda}, \tag{3}$$

where λ is the *localization length.*

Anderson showed in his pioneering work [1] that all electronic states become insulating when disorder increases above the critical value. The transition from metal to insulator due to the increase in disorder is called the *Anderson transition.* Similar to the theory of phase transitions, it is believed that Anderson transition is universal and can be described by the one-parameter *scaling theory* [3]. The key parameter of the scaling theory is the conductance, g. Introduced by Landauer [4], the conductance measures the transmission properties of disordered systems both in the metallic and the localized regime.

The scaling theory of localization analyzes the size dependence of the conductance in the limit of large system size. Only three transport regimes exist in this limit: the system is either in the metallic, localized or critical regime. In the metallic regime, the conductance increases with the system size, and the system possesses non-zero electric conductance. In the localized regime, all electronic states are localized, and g decreases exponentially due to further increase of the system size. The system is in the critical regime only at the critical value of the disorder.

While the localized regime exists in any system, provided the disorder is sufficiently strong, the existence of the metallic regime is not guaranteed, especially for systems with lower spatial dimension. It is well-known that all electronic states are localized in any one dimensional (1d) disordered system [5]. Spin-less electrons are always localized already in the two dimensional (2d) systems, with the only exception caused by an external magnetic field.

The scaling theory of localization predicts that the metal-insulator transition is universal. The size and disorder dependence of the conductance in the neighborhood of the critical point is governed only by universal critical exponents. All the parameters, which define the microscopic structure of the model, become irrelevant when the size of the system is sufficiently large. Verification of the universality of the metal-insulator transition and the calculation of the critical parameters - the critical disorder and critical exponents - for systems of various dimension and physical symmetry are the main theoretical and numerical problems of the theory of localization.

Contrary to the scaling theory of localization which discusses the transport regimes in the limit of $L \to \infty$, in everyday life we must deal with systems of finite size. Here, the transport regime depends on the relation of the system size, L, to the characteristic lengths. For instance, if

$$\ell \ll L \ll \lambda, \tag{4}$$

then the system exhibits metallic behavior with the conductivity given by Eq. (1). This happens in 2d systems, where the localization length λ is extremely huge for weak disorder [6]. Since the electron diffuses through the sample, we called the transport regime, defined by inequalities (4), the *diffusive regime*. Of course, an increase of the system size over the localization length causes localization of all electronic states and the conductivity decreases to zero.

There are small quantum corrections to the conductivity (1) when the conditions (4) are fulfilled. For instance, if the size of the two dimensional (2d) sample is much larger than the mean free path, $L \gg \ell$, the mean value of the conductance decreases logarithmically when the size of the system increases. This effect - weak localization corrections to the conductance - is the first manifestation of the quantum character of the electron propagation. Similar weak localization corrections to the conductivity exist also in one and three dimensions and in quasi-one dimensional (quasi-1d) geometry.

In the opposite limit of very small systems, $L \ll \ell$ we observe the *ballistic* regime. In this regime, the electron, in its travel through the sample, is scattered only on a few impurities. Clearly, the sample is almost transparent and the conductance might be large already in 1d systems.

While the weakly disordered systems can be described analytically, for instance by the Dorokhov-Mello-Pereyra-Kumar (DMPK) equation [7], or perturbation Green's function methods [8,9], the theoretical description of the critical regime is still not complete. The main problem is the absence of small parameter, since the critical disorder is of the order or even larger than the

bandwidth in three dimensional systems. The critical disorder is small only when the dimension of the system, d, decreases to the lower critical dimension, $d_c = 2$ [10]. Analytical theories in dimension $d = 2 + \epsilon$ [10–12] calculate critical parameters of the model in powers of ϵ.

Since each sample contains randomly distributed scatterers, the measured quantities, like the conductance g, fluctuate from sample to sample and must be averaged over random disorder. One possibility is to average the conductance over the statistical ensemble of macroscopically equivalent samples, which differ only in the microscopic realization of the disorder. The ergodic hypothesis [13] states that the same statistical ensemble can be constructed with the use of the single sample by varying the Fermi energy or the magnetic field. This enables us to compare the theoretical or numerical results, which use the ensemble averaging, with experiments, where usually only a few samples are analyzed.

The key parameter of the scaling theory, the conductance, g, is not a self-averaged quantity. Already in the metallic regime, the conductance becomes sample-dependent. Measured values of the conductance [14] fluctuate around the mean value. These fluctuations, of the order of e^2/h, depend neither on the size of the system, nor on the mean value [9] and they lead to the *absence of self-averaging* of the conductance. In the localized regime, the fluctuations of the conductance [15] are so strong that the mean value, $\langle g \rangle$, is not a representative quantity [16].

The absence of self-averaging and huge fluctuations of the conductance which do not disappear in the limit of infinite size of the system must be included in the theoretical description of the localization. First, it is not clear how the averaging over the disorder should be performed. Moreover, not only the mean values, but also the higher cummulants of the conductance must be calculated. Contrary to the classical systems, the higher cummulants do not diminish in the limit of large system size. Also, the averaged quantity must be carefully chosen. In the localized regime, it is more suitable to average the *logarithm* of the conductance than the conductance itself. The average procedure is easier in the numerical simulations than in the analytical theory. This is the reason why numerical methods, based on the finite size scaling [17] provides us with the most reliable information about the Anderson transition in higher dimensions.

In this Paper, we discuss the basic ideas of the localization theory. We concentrate on numerical methods of investigation of disordered electronic systems. Numerical simulations enable us to describe the metallic, the critical and the strongly localized regime. They verify theoretical predictions, and, last but not least, they provide us with data necessary for the analytical description of the localization.

As already mentioned, both the weak localization and the localization are quantum effects, caused by the mutual interference of the scattered components of the electron wave function. The quantum coherence of the electron propagation is destroyed by the incoherent scattering. Since the incoherent mean free path, L_ϕ, increases when the temperature decreases [18], we expect that the best experimental conditions for the analysis of the localization effects are those in the limit of small temperature, when $L_\phi \gg L$. In this paper, we restrict our discussion only to the limit of zero temperature, when $L_\phi \to \infty$. For the case of non-zero temperature, when $L_\phi > L$, we can obtain a qualitative estimation of the transport in the diffusive regime if the size of the system is replaced by L_ϕ. The transport in the strongly localized regime, $L_\phi > \lambda$ requires more detailed analysis [19, 20] which is above the scope of this paper.

We will consider only the one-electron problem. Although the electron-electron interaction might play important role in the localization [21], numerical analysis of systems of disordered

interacting electrons is too difficult to be able at present to answer the main questions of the scaling theory.

Since the single electron localization is caused by interference of electron wave function, the theory can be easily applied also to propagation of classical waves in disordered media. Of special interest is propagation of electromagnetic waves through random dielectrics [22–24].

The Paper is organized as follows.

In Sect. 2 we describe the Anderson localization and demonstrate the localization of electron in two dimensional (2d) strongly disordered system. In Sect. 3 we introduce several models, used in numerical simulations. For numerical convenience, all the models are based on the propagation of electrons on the d - dimensional lattice, with disorder represented by the random on site energies. The Anderson transition is explained briefly in Sect. 4. Spatial structure of the electron wave functions and spectra of eigenenergies is shown in Sect. 5. Transfer matrix and the conductance are introduced in Sect. 6.

In the most simple case of the one-dimensional (1d) disordered chain, it was proved [5] that all electronic states are localized even for weak disorder provided that the system is sufficiently long (longer than localization length, λ). We discuss the transport in the 1d systems in Sect. 7. The one dimensional systems are not only easy to simulate numerically, but allow also to derive exact analytical results. The statistics of the conductance and the resistance is discussed in details, and the quantum origin of the localization is explained.

Section 8 analyzes the electronic transport in the diffusive regime. The scaling theory of localization, formulated in terms of the conductance, is introduced in Sect. 9. It is argued that the metal - insulator transition is a universal phenomenon, and the conductance, g, is a function of only one parameter in the critical regime. This scaling hypothesis is verified numerically. First, in Sect. 10 and 11 we discuss statistical properties of the conductance in the critical and localized regime. The critical conductance distribution is presented and discussed in detail. Then, in Sect. 12, we review the numerical scaling analysis of the Anderson transition in the Anderson model. Sect. 13 presents the critical exponent, obtained by numerical scaling analysis of systems with dimension $2 < d \leq 5$. Obtained numerical data are compared with theoretical predictions. The two dimensional critical regime is discussed in Sect. 14. Finally, Sect. 15 discusses two possibilities of the analytical description of the localized regime.

The Paper contains five Appendices, which present some technical details useful for the understanding of discussed numerical data. Properties of the transfer matrix are reviewed in Appendix A. The next two Appendices introduce two successful theories of the transport in diffusive regime: the DMPK equation in App. B and random matrix theory in App. C. Lyapunov exponents of the product of transfer matrices are introduced in Appendix D. The last Appendix E discusses numerical algorithms for calculation of the conductance.

Various aspects of the electronic transport in disordered systems were reviewed recently. The weak localization effects are discussed in [25]. Refs. [26–28] review the main ideas of the localization theory. Experimental and theoretical aspects of the localization are reviewed in [30]. The Quantum Hall effect is discussed in refs. [31, 32]. Supersymmetric field theory and its application to electron transport is explained in [33]. Statistical properties of spectra and wave functions are reviewed in [34]. Random matrix theory and its application to electronic transport is reviewed in [35]. The development of research is in conference proceedings [36–38].

Wave transport in disordered media is a subject of many textbooks and monographs. We

want to mention the classical book of Economou [39] and Mott and Davis [40]. Transport of electrons in mesoscopic systems is discussed in [41–43]. The book of Mehta [44] presents the theory of random matrices.

2   Localization

Localization of an electron in disordered system was predicted by Anderson [1]. Anderson calculated the probability p that an electron, being at time $t = 0$ at point $\vec{r_0}$ with the wave function $\Psi(\vec{r}, t = 0) = \delta(\vec{r} - \vec{r_0})$ returns to the same point in time $t > 0$. It is evident that $p = 0$ for regular lattice, since the electron propagates freely, provided that its energy lies in the allowed energy band The question is whether there are such disordered systems, where $p \to 1$ in the limit $t \to \infty$. If yes, then the electron is localized in the space around $\vec{r_0}$. If not, then electron can propagate through the sample, in spite of the disorder.

To demonstrate Anderson's idea, we simulated numerically the time evolution of a single electron wave function in two-dimensional disordered lattice. At time $t = 0$, we add the electron to the center of the lattice and solve the time-dependent Schrödinger equation,

$$i\hbar\frac{\partial\Psi(\vec{r}, t)}{\partial t} = \mathcal{H}\Psi(\vec{r}, t),$$ (5)

where $\mathcal{H}$ is the *Anderson Hamiltonian*,

$$\mathcal{H} = W\sum_r \varepsilon_r c_r^\dagger c_r + V\sum_{[rr']} c_r^\dagger c_{r'}.$$ (6)

Following Eq. (6), the electron moves on the d-dimensional lattice of size L^d. The first sum is a local term, where $\vec{r}$ counts sites on the lattice and the disorder is given by random on-site energies ε_r. The second term in Hamiltonian enables the hopping of electron between the nearest neighbor sites. Parameter V is given by the overlap of the wave functions localized on neighboring sites, and W defines the strength of the disorder. The distance between two neighboring sites, a, is used as a unit length, $a = 1$.

Figure 1 shows the time development of the electron wave function in the strongly disordered two-dimensional (2d) lattice. At the beginning, the electron wave function broadens with time. However, later this broadening becomes slower and finally stops. The electron is localized in the central part of the lattice and its wave function far away from the localization center is negligibly small. Figure 2 shows the detailed spatial distribution of the wave function at time $t = 2800V/\hbar$.

The presented data show that indeed the electron might be localized for sufficiently strong disorder. Anderson calculated the critical strength of the disorder, W_c, such that the electron is delocalized (and the system is a metal) when $W < W_c$, and the electron is localized and the system becomes an insulator when $W > W_c$. The transition of the system from the metallic to insulating regime due to increase of the disorder is called metal-insulator transition.

We will not reproduce Andersons analysis here, only present his main result: there is indeed the critical disorder which separates localized and delocalized electron states. In the most simple approximation, critical disorder can be found as

$$\frac{W_c}{V} \approx 2eK\ln(eK),$$ (7)
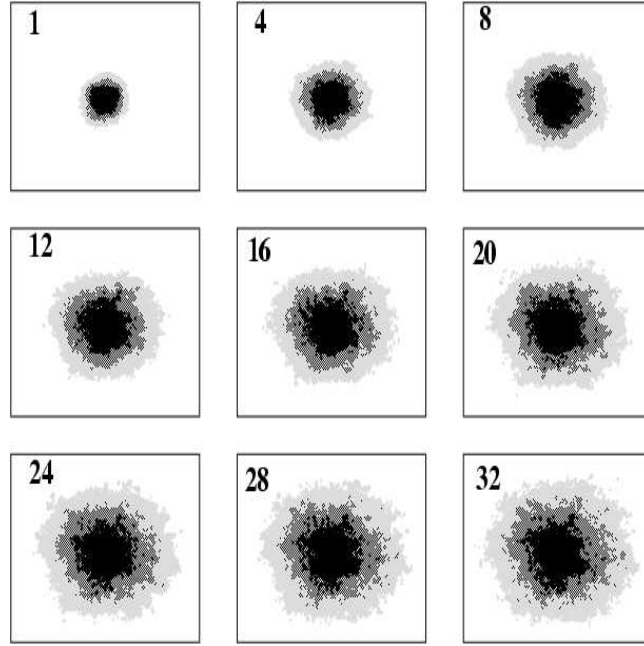
Fig. 1. The time dependence of the wave packet in the two dimensional disordered system defined by Hamiltonian (6) with Box disorder and $W = 6$. This disorder corresponds to the localization length $\lambda \approx 50$ [45]. Different colors distinguish points where the wave function $|\Psi(\vec{r})| > 0.0001$ (gray), $|\Psi(\vec{r})| > 0.0010$ (dark gray), and $|\Psi(\vec{r})| > 0.0050$ (black) at different times shown in legend. The time is measured in units of $100\hbar/V$ with hopping term $V = 1$. The size of the lattice is 512×512 (in units of lattice spacing a). The initial wave function, $\Psi(\vec{r}, t = 0)$, is the eigenfunction of the sub-lattice of the size $N_h \times N_h$ ($N_h = 24$) of the system, located in the middle of the lattice. The eigenfunction belongs to the eigenenergy closest to the band center, $E = 0$. From the time development of the wave packet, one can see that the electron is indeed localized in the center of the lattice.

where K is a connectivity of the lattice. A detailed discussion of Anderson analysis is given in Refs. [46].

Note, relation (7) does not contain the dimension d of the system. Later [10] it became clear that, similarly to critical phenomena in statistical physics, the dimension of the system is crucial for the existence of the Anderson transition. The dimension $d = 2$ is a lower critical dimension; there is no metallic state for $d < 2$. That means, all electron states are localized in space when $d < 2$. However, localization can be observed only when the system is large enough,

$$L \gg \lambda. \tag{8}$$

In 2d, the localization length is extremely large for weak disorder [6]. This is the reason why good metallic behavior is observed in numerical simulations performed on 2d weakly disordered samples of finite size, L. (Sect. 8).

Analytical estimation of the critical disorder is possible only when the dimension of the
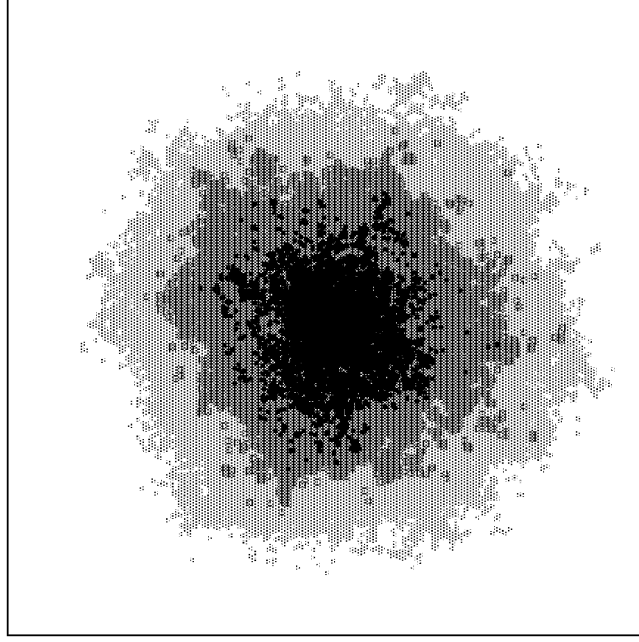
Fig. 2. The wave function of the electron in time $t = 2800\ \hbar/V$. The size of the lattice is 512×512 (in units of lattice spacing, a). Note that the radius of occupied region is much larger than the localized length, which is in this case $\lambda \approx 50$. The localization length determines only the exponential decrease of the wave function at large distances, not the size of the region in which the electron is localized.

system is close to 2, $d = 2 + \epsilon$ with $\epsilon \ll 1$. In realistic three dimensional systems, W_c can be obtained only numerically. Various methods of calculation of W_c and of other critical parameters will be explained in Sect. 12.

3   Models and symmetries

The most suitable model for the numerical analysis of the localization is Andersons model, defined by the Hamiltonian (6). It represents an isotropic model, in which the hopping term, V, is the same in all directions. In the isotropic models, we consider $V = 1$. This also defines the scale of the energy.

It is often suitable to consider anisotropic models, with different hopping terms in different directions. For instance, we will use the three-dimensional (3d) model

$$\mathcal{H} = W \sum_r \varepsilon_r c_r^\dagger c_r + t \sum_{[rr']} c_{xyz}^\dagger c_{x'yz} + t \sum_{[rr']} c_{xyz}^\dagger c_{xy'z} + V \sum_{[rr']} c_{xyz}^\dagger c_{xyz'}, \tag{9}$$

where $t < V$. The hopping term, V, defines the scale of the energy. We often use $V = 1$.

Random energies ε_n are distributed either with the Box distribution,

$$P_B(\varepsilon) = (2/W)\Theta(W/2 - |\varepsilon|) \tag{10}$$

or with the Gaussian distribution,

$$P_G(\varepsilon) = (2\pi W^2)\exp-(\varepsilon^2/2W^2). \tag{11}$$

The parameter W measures the strength of the disorder. Other distributions of random energies (binary, Lorentzian) are often used in the literature too.

The Anderson model defined by Eq. (6) will be used in the present paper to demonstrate numerically the basic ideas of the localization theory. For zero disorder, $\varepsilon_r \equiv 0$, we easily find all the eigenenergies of Hamiltonian (6). For instance, for the 3d anisotropic model we have

$$E = 2t\cos k_x + 2t\cos k_y + 2V\cos k_z. \tag{12}$$

The energy band spans between $-V - 2t$ and $V + 2t$. We define the bandwidth,

$$B = 2V + 4t. \tag{13}$$

Andersons model, given by Hamiltonian (6), belongs to models with time reversal symmetry. It describes the propagation of a single *spin-less* particle in the disordered lattice. Such models are called *orthogonal*. Systems with *orthogonal* symmetry do not exhibit the metal-insulator transition in dimension $d_c = 2$. This changes when the hopping between neighboring sites becomes dependent on the orientation of the spin of the electron [10]. Evangelou and Ziman [47], and Ando [48] showed numerically that the two dimensional (2d) systems with spin dependent hopping (called *symplectic* models) exhibit the metal-insulator transition already at $d_c = 2$. In this paper we will discuss the Ando model which is defined by the Hamiltonian

$$\mathcal{H} = W\sum_r \varepsilon_r c_r^\dagger c_r + V_x \sum_{[rr']} c_{xy}^\dagger c_{x'y} + V_y \sum_{[rr']} c_{xy}^\dagger c_{xy'} \tag{14}$$

with spin dependent hopping terms given by Ando [48],

$$V_x = \begin{pmatrix} c & s \\ -s & c \end{pmatrix}, \text{ and } V_y = \begin{pmatrix} c & -is \\ -is & c \end{pmatrix}, \tag{15}$$

with $c^2 + s^2 = 1$. Note how hopping depends on the direction of propagation. Also, the wave function, c_r, has two components,

$$c_r = \begin{pmatrix} c_{r\uparrow} \\ c_{r\downarrow} \end{pmatrix}, \tag{16}$$

for different orientations of the spin of electron. Another 2d model with *symplectic* symmetry is the Evangelou-Ziman model. In this model, the hopping term has the form

$$V = \begin{pmatrix} 1 + ivt_z & -v(t_y - it_x) \\ v(t_y + it_x) & 1 - ivt_z \end{pmatrix}, \tag{17}$$

where t_x, t_y and t_z are real random variables chosen from box distribution, and v measures the strength of (random) spin-orbit hopping. In Refs. [49], SU(2) model is analyzed, with the random hopping term

$$V = \begin{pmatrix} e^{i\alpha}\cos\beta & e^{i\gamma}\sin\beta \\ e^{-i\gamma}\sin\beta & e^{-i\alpha}\cos\beta \end{pmatrix}, \tag{18}$$

where random phases α and γ are uniformly distributed in the interval $(0, 2\pi)$ and the distribution of random phase β is $p(\beta)d\beta = \sin(2\beta)d\beta$ for $0 \le \beta \le \pi/2$.

An external magnetic field breaks the time reversal inversion of the electron propagation. Such systems belong to the *unitary* universality class. Magnetic field can be added to the two dimensional Hamiltonian (6) by Peierls factor,

$$\begin{aligned} \mathcal{H} &= \sum_r \varepsilon_r c_r^\dagger c_r + \sum_{xy} c_{x,y+a}^\dagger x_{xy} + \sum_{xy} c_{x,y-a}^\dagger x_{xy} \\ &+ \sum_{xy} e^{+i\phi y} c_{x+a,y}^\dagger c_{xy} + \sum_{xy} e^{-i\phi y} c_{x-a,y}^\dagger c_{xy}, \end{aligned} \tag{19}$$

where $\phi = B(ea)^2/\hbar$ is a magnetic flux through the elementary plaquette of the size a^2.

Hamiltonian (19) is used for the numerical analysis of the critical quantum Hall regime of 2d disordered system in a strong magnetic field. Although this model does not exhibit metal-insulator transition, there is, in each Landau band, the critical energy, E_c, at which the electron is delocalized [31]. The existence of the critical - delocalized - state inside the energy band is crucial for the transmission of the system between two neighboring quantum Hall plateaus [50]. Another model, often used in the numerical analysis of the critical quantum Hall regime is the model of Chalker and Coddington [32, 51].

4   Anderson transition

The Anderson transition is the transition from the metallic (extended) regime to the localized regime. Before describing the scenario of the Anderson transition, we must understand how the disorder influences the density of electronic states in the conducting band. Then, we introduce the mobility edge, describe qualitatively the transition from metal to insulator, and define critical exponents.

4.1   The density of states

For zero disorder, $W = 0$, the energy of the electron in the Anderson model is given by the dispersion relation

$$E = 2V\cos k_x + 2V\cos k_y + 2V\cos k_z, \tag{20}$$

where $\vec{k} = (k_x, k_y, k_z)$ is the wave vector of electron. The density of states,

$$\rho(E) = \frac{1}{2\pi}\frac{\partial k}{\partial E}. \tag{21}$$

can be calculated analytically [39], and is shown in Fig. 3. The energy band spans from $-6V \le E \le +6V$ and is symmetric, $\rho(E) = \rho(-E)$. This symmetry is typical for tight-binding Hamiltonians given by Eq. (6).
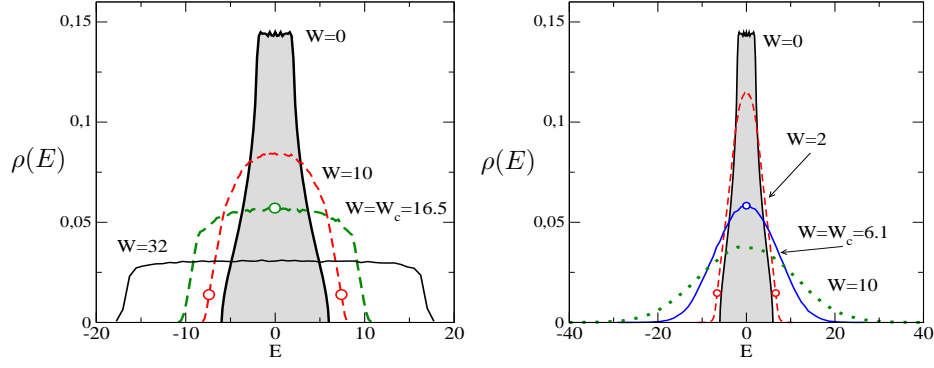
Fig. 3. The density of states, $\rho(E)$, of the three-dimensional Anderson model with box (left) and Gauss (right) distribution of random energies ε_n, defined by Eqs. (10) and (11), respectively. As expected, the energy band becomes broader when disorder increases. In the tails of the band, the electronic states become localized (Fig. 5). Open circles show the position of three critical points, one for $E = 0$ and $W = W_c$, and two other for fixed disorder $W < W_c$ and the mobility edge $E_{c1} = -E_{c2}$. Note, for weak disorder ($W = 10$ in the left figure) the mobility edges lie outside the unperturbed energy band, $|E_c| > B$.

Note that the density of states, given by Eq. (21) does not include the degeneracy of the electron system due to the two possible orientations of the spin. When spin of the electron is included, $\rho(E)$ must be multiplied by a factor of 2.

Figure 3 demonstrates the effect of disorder on the energy spectrum of the three dimensional Anderson model for Box and Gaussian disorder. As expected, the band becomes broader when disorder increases. This is more pronounced for the Gaussian disorder which allows larger fluctuations of random energies. Open circles indicate the position of the mobility edge, discussed in the next Section.

For completeness, we also show in Fig. 4 the density of states of the disordered two dimensional Anderson model.

4.2   Mobility edge

Intuitively, we expect that the localized states appear first in tails of the energy band. These states are namely created by large random energies, ε_r. One expects that the states with the energy close to the band center are less affected by randomness. Another argument for the localization in tails was given by Lifshitz [2]. The classical scattering of electrons on impurities, which led to an expression for the conductance, given by Eq. (1), is only possible when the mean free path, ℓ, is much larger than the wavelength of the electron, λ_F, given as the inverse of the Fermi wave vector, k_F. When both lengths become comparable,

$$\lambda_F \sim \ell, \tag{22}$$

then the spatial extent of the electron wave function is comparable with the typical distance between two impurities, so that we cannot discuss the propagation of electron in terms of individual
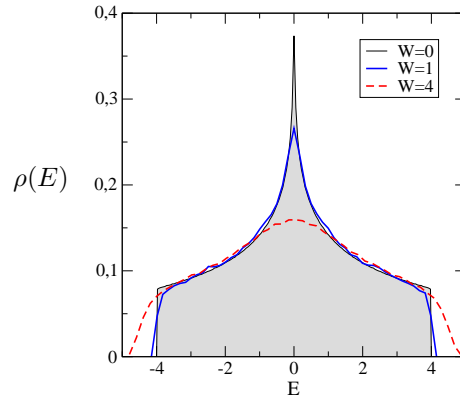
Fig. 4. The density of states for the disordered two dimensional Anderson model. Note the typical singularity of the density of states at the band center for the unperturbed tight binding Hamiltonian ($W = 0$) [39].
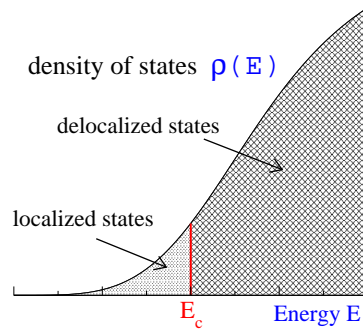
Fig. 5. The mobility edge, E_c, separates the localized states in the band tail from the conducting states. By changing the Fermi energy, E_F, the system exhibits a transition from the metallic regime ($E_F > E_c$) into the localized regime ($E_F < E_c$).

scattering procedures. The electron wavelength, λ_F, is small, comparable with the lattice distance, a, at the band center, but increases with the distance of the Fermi energy from the band center. Consequently, the Lifshitz criterion for the localization, given by Eq. (22) is fulfilled first in the band tails.

Separation of the energy spectra into localized and delocalized intervals is schematically shown in Fig. 5. For a given strength of the disorder, W, there is an energy, E_c, called the *mobility edge*, which separates the localized states from the delocalized states. When $E_F < E_c$, the system is an insulator, since all states at the Fermi energy are localized (we remind the reader that the temperature $T = 0$). We call this insulator *the Anderson insulator* to emphasize the fact, that the system possesses the zero electric conductance, although the density of states is non-zero. When the Fermi energy crosses the mobility edge, the system undergoes the transition

Fig. 6. Schematic phase diagram for the 3d Anderson model with the Gaussian disorder. Metallic (conductive) states are separated from the localized states by the critical line, which is an envelope of the shadow region. Open circles show the position of three critical points, one for $E = 0$ and $W = W_c = 6.1$, and two other for fixed disorder $W = 2 < W_c$ and the mobility edge $E_{c1} = -E_{c2} 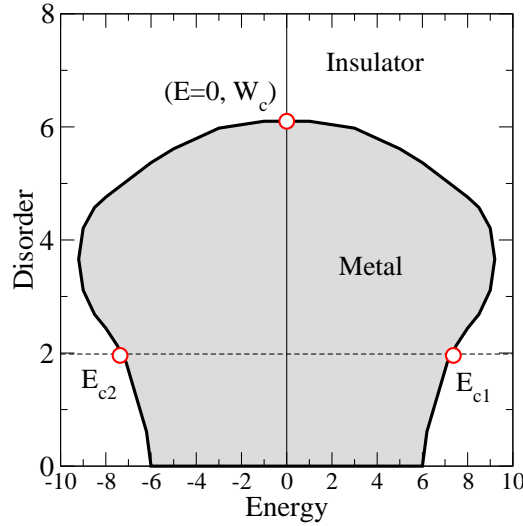= 6.58$. Note, these mobility edges lie outside the unperturbed energy band. When disorder reaches its critical value, $W = W_c$, two mobility edges reach the band center, $E_{c1} = E_{c2}$. No metallic states exist when $W > W_c$.

from insulator to metal. For $E_F > E_c$, the system possesses a finite electric conductivity.

Note that there are two mobility edges, E_{c1} and E_{c2} which separate localized states in the upper and lower band tails from the delocalized states in the central part of the band. For a particular disorder, we show the mobility edges in Fig. 3. Of course, the position of the mobility edges depends on the strength of the disorder. With increasing disorder, both mobility edges move to the band center. There is a critical value of the disorder, W_c, for which $E_{c1} = E_{c2}$ approach the band center. For $W > W_c$ there are no propagating states in the spectrum. The function $E_c = E(W)$ defines the critical line, which separates the metallic and the localized states in the phase diagram. An interesting feature of the Anderson transition is that the disorder creates propagating states *outside* the unperturbed energy band. We see that for non-zero disorder, the metallic regime exists also for energies $|E| > 6V$.

The phase diagram of the three dimensional Anderson model is shown schematically in Fig. 6. For $W = 0$, all the electron states inside the energy band, $|E| < 6V$ are delocalized. Increasing disorder broadens the density of states, and the interval E_{c1}, E_{c2} of the metallic states becomes broader, too. Only for rather strong disorder, close to to the critical disorder, W_c, the mobility edge starts to converge towards the band center. For the disorder $W > W_c$, all electron states are localized. The *phase diagram* for the 3d Anderson model was calculated numerically in Ref. [52].
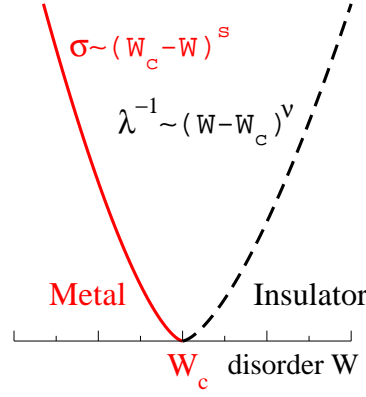
Fig. 7. Definition of the critical exponents. At the metallic side of the critical point, the conductance σ decreases to zero as $\sigma \propto (W_c - W)^s$, whereas at the insulating side the localization length diverges as $\lambda \propto (W - W_c)^{-\nu}$.

4.3   Critical exponents

The metallic states are separated from the localized ones by the critical line. Any crossing of the critical line is accompanied by the metal insulator transition. The common belief, supported by the scaling theory of localization [3] is that this transition is universal. This means that the transition from metal to insulator should not depend on microscopic details of the model, and on the position of the critical point, lying at the critical line. However, it depends on the dimension and on the physical symmetry of the model. We can, similarly to the theory of phase transitions, formulate the theory of the metal insulator transition in terms of the order parameter and of the critical exponents [10]. The critical exponents are defined in terms of the energy or disorder dependence of the metallic conductivity and localization length (Fig. 7).

Metallic conductivity, σ, characterizes the transport properties of the metallic regime. We have non-zero conductivity $\sigma > 0$ in metal, and σ decreases when the system approaches the critical point. For many years it was not clear whether the conductivity *at the critical point*, σ_c, is zero or not. Mott [40, 53] suggested that the conductance possesses non-zero value at the critical point and drops discontinuously to zero on the insulating side of the transition. At present, the common belief is that the critical conductivity $\sigma_c = 0$ in 3d orthogonal systems. The decrease of the conductivity in the neighborhood of the critical point is determined by the critical exponent s,

$$\sigma \sim (W_c - W)^s. \tag{23}$$

On the insulating side of the transition, we can characterize the electronic states by the localization length, λ. By definition, the localization length which characterizes the exponential decrease of the localized wave function far away from the localization center $\vec{r}_0$, is given by Eq. (3),

$$\Psi(\vec{r}) \propto \exp -\frac{|\vec{r} - \vec{r}_0|}{\lambda}. \tag{24}$$

It is intuitively clear that λ should increase when system approaches critical point, and become infinite at the critical point,

$$\lambda \sim (W - W_c)^{-\nu}. \tag{25}$$

As discussed in the Sect. 4.1, the Anderson transition is induced either by a change of the Fermi energy with fixed disorder strength, or by an increase in the disorder, W, for fixed energy ($E = 0$). Therefore, we expect also that

$$\sigma \sim (E_c - E)^s, \qquad \lambda \sim (E - E_c)^{-\nu} \tag{26}$$

for the case when the Fermi energy crosses the mobility edge.

Scaling theory of localization [3] assumes that the metal-insulator transition is universal. That means that critical exponents, s and ν, are universal, depending only on the dimension of the system, and on the physical universality class. They do not depend on the microscopic details of the model. The scaling analysis gives [10]

$$s = (d - 2)\nu. \tag{27}$$

Proof of the universality of critical exponents and their dependence on the dimension of the system represents the main problem of the theory of Anderson localization.

5 Wave functions and energy spectrum of disordered systems

For the case of a regular lattice ($W = 0$), all the eigenenergies and eigenfunctions of the Hamiltonian can be found analytically. Of course, disorder influences the spectrum of eigenenergies, and also the form of the corresponding wave functions. In this Section, we describe briefly the main qualitative and quantitative properties of the wave functions and of the energy spectra both in the limit of weak and strong disorder, and discuss the non-homogeneous spatial distribution of electrons in the critical regime.

5.1 The wave function

Following Anderson [1], we expect that an electron is delocalized if disorder is small, and localized if disorder is strong. To verify this assumption, we calculate numerically all the eigenenergies and eigenvectors of the 2d Ando model, defined by Eqs. (14,15). We will see later that the Ando model exhibits MIT for critical disorder $W_c = 5.838$. Thus, for $W \ll W_c$ the system is in the metallic regime and we expect that the electronic wave function is almost homogeneously distributed throughout the sample. On the other hand, the electron should be localized in some small region. if $W \gg W_c$.

These expectations are confirmed by numerical results presented in Fig. 8 where we compare the spatial distributions of two electron eigenstates. The "metallic" eigenstate ($W = 2 \ll W_c$) is almost homogeneously distributed within the sample[2]. Also, the localized eigenstate, calculated numerically for the system with disorder $W = 8 \gg W_c$, is spatially localized in a certain region of the sample, and is orders of magnitude smaller elsewhere.

---

[2]Note, similar result can be obtained also in the 2d orthogonal systems, if the localized length is larger than the size of the system, $L \ll \lambda$.
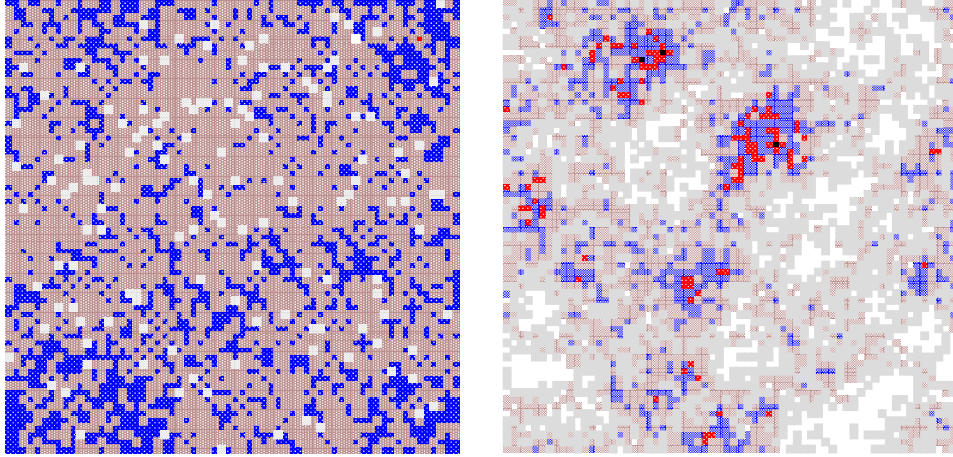
Fig. 8. The spatial distribution of the electron, given by the absolute value of the eigenvector, $|\Psi(\vec{r})|^2$, with the eigenenergy closest to the band center $E = 0$ for the two-dimensional Ando model. In the metallic regime (left, $W = 2$), the electron is homogeneously distributed in the system, while in the localized regime (right, $W = 8$), the electron is localized in a small part of the lattice and its wave function is very small elsewhere. The size of the system is 64×64 lattice sites. The critical disorder of the Ando model is $W_c = 5.838$. The data was obtained by numerical diagonalization of the random 2d Hamiltonian (6) using the LAPACK subroutines.

The critical point deserves special attention. Figure 9 shows the electron wave function for two eigenstates close to the band center for the Ando model with $W = W_c$. Detailed analysis shows that the wave function at the critical point possesses the *multi-fractal* spatial structure. To define multifractality, we introduce the quantities [34]

$$I_q(E_n) = \sum_{\vec{r}} |\Psi_n(\vec{r})|^{2q}. \tag{28}$$

In Eq. (28), E_n is the eigenenergy of the Hamiltonian, and $\Psi_n(\vec{r})$ is the corresponding eigenfunction. It is evident that $I_1(E_n) \equiv 1$ for all eigenstates. The quantity I_2 is the *inverse participation ratio*, often used for the characterization of the eigenvectors in disordered systems (Fig. 10).

We can easily estimate the size dependence of the parameters I_q. If the eigenstate n belongs to the metallic part of the energy spectra, then the wave function is homogeneously distributed throughout the sample. Assuming that $|\Psi_n(\vec{r})| \sim L^{-d/2}$ for all lattice sites $\vec{r}$, we immediately see that in the metallic regime

$$I_q \sim L^d \times \left[L^{-d/2} \right]^{2q} = L^{-(q-1)d}. \tag{29}$$

On the other hand, in the localized regime, we expect, in agreement with the right panel of Fig. 8, that the wave function is localized in a certain small region and is almost zero in the rest
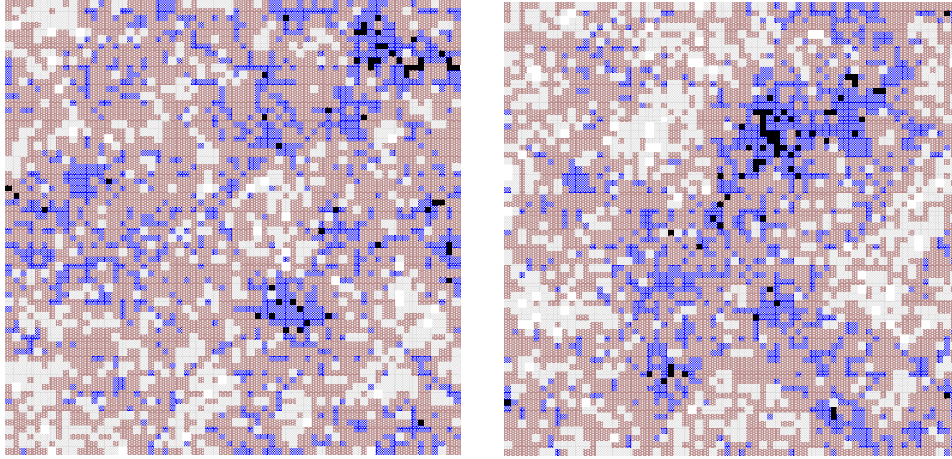
Fig. 9. Two electron eigenstates, $|\Psi(\vec{r})|^2$, in the critical regime of the two-dimensional Ando model. The size of the system is 64×64, and $W = W_c = 5.838$ for the electron energy $E = 0$ [54]. For a given realization of disorder, we calculate two eigenvalues closest to the band center ($E = -0.028$ and $E = -0.01476$ for the left and right figure, respectively). The spatial distribution of the electron is more complicated than in the metallic or localized regime. Detailed analysis of the wave function (discussed in Sect. 14) shows that the wave function $\Psi(\vec{r})$ possesses the *multi-fractal* spatial structure.
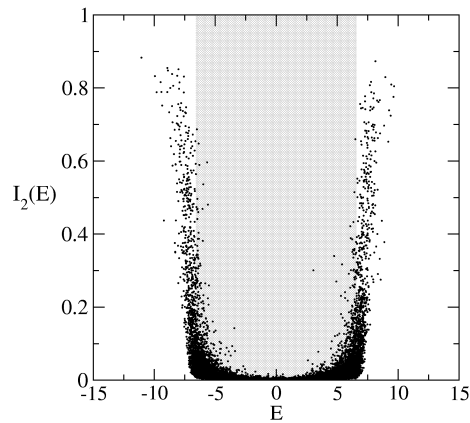
Fig. 10. The inverse participation ratio, I_2, as a function of energy for the 3d Anderson model with Gaussian disorder $W = 2$. The size of the lattice is $L = 16$. The shaded area indicates propagating states, $|E| < |E_c| = 6.58$ [56], where I_2 is very small. In the tails of the energy band, the electronic states are localized and I_2 is close to 1. Note, I_2 wildly fluctuates and see Fig. 11 for the probability distribution of I_2.
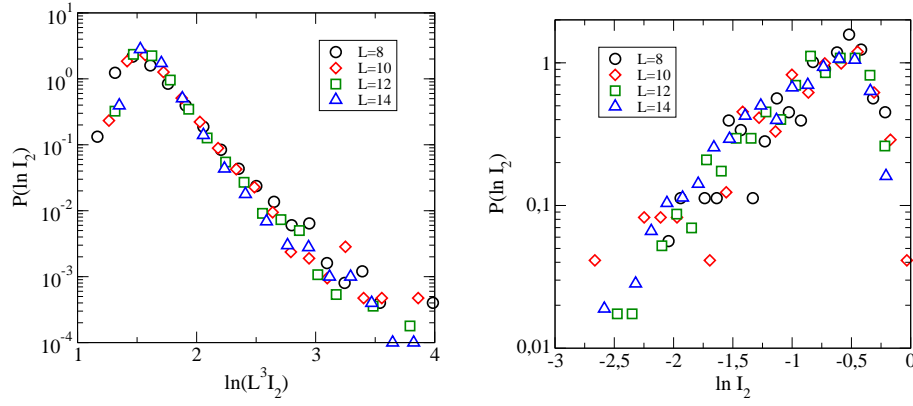
Fig. 11. The probability distribution of the *logarithm* of the inverse participation ratio, $\ln I_2$, defined by Eq. (28) for the 3d Anderson model with Gaussian disorder $W = 2$ and for system size given in the legend. Left: data for all eigenstates with energies $|E_n| < 0.2$ (band center). From the phase diagram, shown in Fig. 6, we know that these eigenstates are metallic. We indeed see that the typical values of I_2 decrease as L^{-3}, in agreement with Eq. (29). The distribution decreases exponentially for large values of $I_2 \gg L^{-3}$ indicating that there are no insulating states in the metallic phase. Right: the data for the eigenstates with $7.5 < |E_n| < 7.7$. These states are localized (see Fig. 6). The typical values of I_2 are of the order of 1, as expected.

of the system. Then, the wave function $|\Psi_n(\vec{r})| \sim 1$ in the localization region and is almost zero otherwise. Inserting this Ansatz into the definition (28) we obtain that $I_q \sim 1$ for all $q > 1$.

At the critical point, the wave function is multifractal [55]. That means, by definition, that

$$I_q(E_n) \sim L^{-(q-1)d_q} \tag{30}$$

[34]. In Eq. (30), $d_q < d$ are *fractal dimensions*. Note, d_q depends on q.

To understand the meaning of multifractality of the wave function, note that the wave function $|\Psi(\vec{r})| < 1$, for all $\vec{r}$. Therefore, the value of $|\Psi(\vec{r})|^{2q}$ decreases when q increases. Hence, the higher q projects out such sites on the lattice, where $|\Psi(\vec{r})|$ is large. For each value of q, these sites create a fractal structure. Since different q projects different fractal structures, the complete description of the spatial distribution of the wave function requires the knowledge of d_q for all values of q.

Figure 10 shows values of I_2 calculated for all eigenstates of the 3d Anderson model with Gaussian disorder $W = 2$. Data confirm our qualitative estimations, namely that I_2 is small in the metallic part of the spectra, $|E| \ll |E_c| = 6.58$, but possesses values of order of 1 in the band tails, where localization is expected. We also see that I_2 is a statistical variable, which might fluctuate from one eigenstate to another. It is therefore useful to calculate the mean value over all eigenvalues lying in a given narrow interval of energies, δE. Also, since I_2 might fluctuate in many orders of magnitude, we analyze $\ln I_2$. This is useful especially in the metallic regime. Figure 11 shows the probability distribution of $\ln I_2$ for the three dimensional Anderson model. In the metallic regime, the maximum of the distribution $p(\ln I_2)$ is around the values
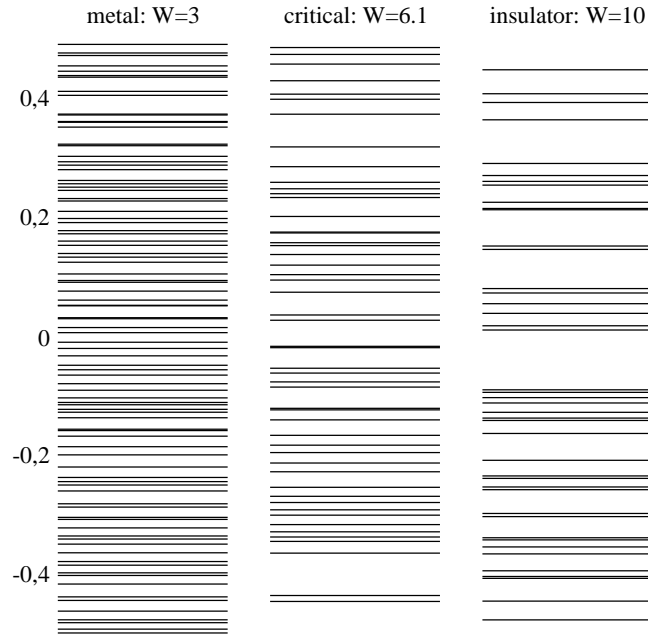
Fig. 12. Eigenenergies of disordered three dimensional Anderson model with Gaussian disorder. The size of the system $L = 10$. Left: metallic regime. The spectrum is almost equidistant, there are no degenerate energies. Right: localized regime. The degeneracy of the energy spectra is more probable than in the metallic regime. Middle: spectrum at the critical point.

$\sim L^{-3}$, in agreement with Eq. (29). Also, the distribution decreases exponentially on both sides of the maxima, indicating, that the probability to find $I_2 \sim 1$ rapidly decreases when L increases. This agrees with the commonly accepted paradigm, that there are no localized states inside the metallic phase. In the localized regime, I_2 possess values of ~ 1, as expected. Again, the probability to find delocalized state in the tail is very small.

5.2   Level statistics

Other important information about the transport regime can be obtained from the analysis of the spectrum of the eigenenergies of the disordered Hamiltonian. In Fig. 12 we show a typical spectrum of the eigenenergies for the metallic, critical and insulating regime. One sees that the three spectra are qualitatively different. This difference can be quantitatively measured by the statistical distribution of *differences*

$$s_n = E_{n+1} - E_n \tag{31}$$

of two neighboring eigenenergies of the random Hamiltonian (6).

Because of the randomness of the Hamiltonian, s is a statistical variable. It turns out that the probability distribution $p(s)$ converges in the limit $L \to \infty$ to three characteristic universal

functions, depending on whether the system is in the metallic, critical or localized regime.

If the system is in the metallic regime, then the hopping term between sites causes level repulsion, typical for random matrix theory. (Random matrix theory is discussed in Appendix C). Random matrix theory states that the distribution $p(s)$ of *normalized* differences s, defined by Eq. (31) is universal, and depends on the physical symmetry. For orthogonal systems, we have

$$p_1(s) = \frac{\pi}{2} \, s \, \exp{-\frac{\pi}{4}s^2}. \tag{32}$$

For unitary and symplectic systems, we have the Wigner distributions given by

$$p_2(s) = \frac{32}{\pi^2} \, s^2 \, \exp{-\frac{4}{\pi}s^2}, \tag{33}$$

and

$$p_4(s) = \frac{2^{18}}{3^6\pi^3} \, s^4 \, \exp{-\frac{64}{9\pi}s^2}, \tag{34}$$

respectively. Note, all three distributions can be obtained analytically if we assume that

$$p_\beta(s) = c_0 \, s^\beta \, \exp{-c_1 s^2}, \tag{35}$$

where $\beta = 1$, 2 and 4 for orthogonal, unitary and symplectic symmetry, respectively, and coefficients c_0 and c_1 are given by the requirement of normalization,

$$\int_0^\infty d\,s\,p_\beta(s) = 1, \tag{36}$$

and by the normalization,

$$\langle s \rangle = \int_0^\infty d\,s\,sp_\beta(s) = 1. \tag{37}$$

A characteristic property of the Wigner distribution is level repulsion. We indeed see in left panel of Fig. 12 that the spectrum in the metallic phase is almost equidistant, and the probability to find two degenerate energies is very small. The absence of the degeneracy can be understood already in the simple case of the 2×2 matrix,

$$\begin{pmatrix} \Lambda & v \\ v & \Lambda \end{pmatrix}, \tag{38}$$

which can represent the two site Hamiltonian. Without the overlap of the wave functions ($v = 0$), the spectrum is degenerate, $E_1 = E_2 = \Lambda$. However, any non-zero overlap removes the degeneracy, and the eigenenergies become $E_{1,2} = \Lambda \pm v$. Similarly, in more complicated systems, we expect that the overlap of wave functions prevents the eigenenergies being degenerate. In random matrix theory, the absence of degeneracy follows from the probability distribution of the eigenvalues of random matrices, which is derived in Appendix C.

The energy spectrum of the insulator is different. The simplest model of localized systems is the Hamiltonian given by Eq. (6) with $V = 0$. In this limit, the energy spectrum consists of
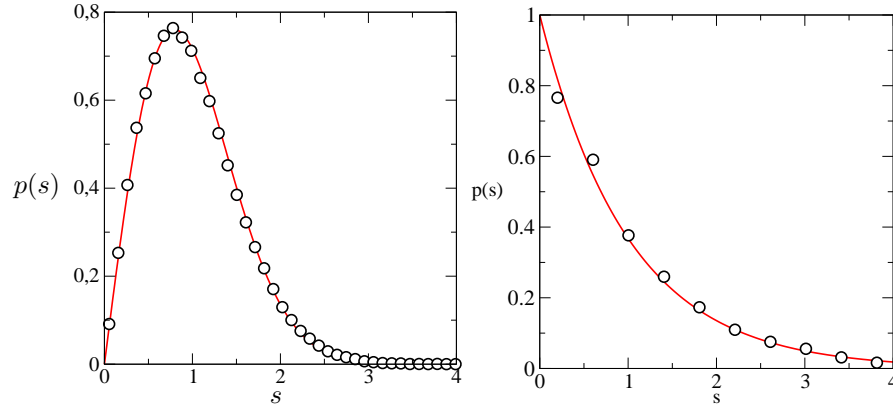
Fig. 13. The probability distribution $p(s)$ of the *normalized* differences, s, between two neighboring eigenenergies in the 3d Anderson model. Only eigenstates close to the band center, $|E_n| < 0.5$, were considered. Left panel shows the distribution for the model with Gaussian disorder $W = 2$, which is smaller than the critical disorder, $W_c \approx 6.1$. The system is in the metallic regime and the distribution $p(s)$ is close to the Wigner distribution $p_1(s)$, given by Eq. (32). (solid line). The size of the system $L = 14$ and $N_{\text{stat}} = 450$. Right panel shows data for the box disorder $W = 32$, $L = 10$. System is in the localized regime, and $p(s)$ is close to the Poison distribution, $p(s) = \exp -s$.

random energies ε. It is well known [44] that the differences of random *uncorrelated* numbers are distributed with the Poisson distribution,

$$p_{\text{loc}}(s) = e^{-s}. \tag{39}$$

We therefore expect that in the localized regime, the distribution $p(s)$ will be close to the Poisson distribution. This is confirmed in the right panel of Fig. 13. Note, however, that the overlap $V \neq 0$ in any disordered system. Therefore, the level repulsion is always present in the energy spectra, independent of the strength of the disorder, and $p(s) \to 0$ when $s \to 0$ also in the strongly localized models [57].

In numerical analysis of the level statistics, it is important to note that the mean difference, $\langle s \rangle$, depends also on the density of states. Indeed, $\langle s \rangle$ would posses smaller values in that part of the energy band where the density of states, $\rho(E)$, is larger. Therefore, we restricted our analysis of the statistics $p(s)$ to the energy interval $E, E + \delta E$, where the density of states is approximately constant. The analysis of the entire energy band requires rescaling the differences s by $1/\rho(E)$.

When the system undergoes the metal-insulator transition, the distribution $p(s)$, transforms from the Wigner distribution, given by Eq. (32), to the Poisson distribution, given by Eq. (39). There is the third universal distribution, characteristic for the critical point [58]. We do not know the analytical form of the critical distribution, but we can calculate it numerically. In Fig. 14 we show the critical distribution $p_c(s)$ for the 3d Anderson model. Data confirms the theoretical expectation that $p_c(s)$ must decrease to zero when $s \to 0$. From the symmetry considerations, it follows that $p_c(s) \sim s^\beta$ for $s \ll 1$. There is no agreement about the form of exponential

PSfrag replacements
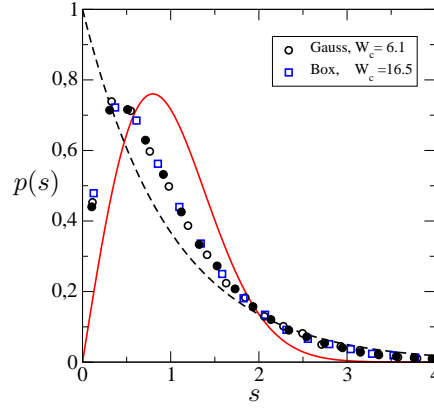
Fig. 14. The critical distribution $p_c(s)$ of the normalized differences s. Both the Gaussian and box disorder were considered. The size of the system $L = 10$. The solid circles show data for the Gaussian disorder and the system size $L = 14$. The data confirm that the distribution $p(s)$ does not depend on the microscopic details of the model. Also, $p(s)$ is independent on the size of the system. Only the eigenenergies $|E_n| < 0.5$ were considered so that the density of states can be considered as constant. For comparison, we show also the Wigner distribution, given by Eq. (32) (solid line) and the Poisson distribution, $p_{\mathrm{loc}}(s) = \exp -s$ (dashed line).

decrease for large $s \gg 1$. Exponential decrease, $p_c(s) \sim \exp(-s^\alpha)$, with $\alpha = 1 + 1/(d\nu)$, was found in Ref. [59], while the semi-Poisson distribution,

$$p_c(s) = 4se^{-2s}, \tag{40}$$

was proposed for the orthogonal critical regime by other groups [60]. Numerical analysis [61] did not distinguish between these two distributions.

Figure 14 also confirms the universality of the critical distribution which does not depend on the size of the system and on the distribution function of random energies. However, it was found that p_s depends on the choice of the boundary conditions [60].

5.3 Boundary conditions

The sensitivity of the electron eigenstates to the boundary conditions provides us with another criterion for localization [62, 63]. Consider a disordered d dimensional system of size L. We can calculate all the eigenenergies of the system with periodic boundary conditions,

$$\Psi(x + L) = \psi(x), \tag{41}$$

and then repeat the same calculation with the *anti-periodic* boundary conditions,

$$\Psi(x + L) = -\psi(x). \tag{42}$$

The change of the boundary conditions influences the spectrum of eigenenergies,

$$E_n \to E_n + \delta E_n, \tag{43}$$

where δE_n is a change of the eigenenergy due to the change of the boundary conditions. Clearly, δE_n depends on the character of the electron eigenstate.

Suppose first that the electron in the nth eigenstate is delocalized. Then its wave function is spread over the sample. We expect therefore that the change of the boundary conditions influences strongly the position of the eigenenergy, E_n, so that δE_n might be comparable or even larger than the typical spacing between two neighboring eigenenergies. Since the wave function is delocalized for any system size, δE will not decrease when L increases. On the other hand, If the electron is localized in a certain region inside the sample, then its wave function decreases exponentially as a function of the distance from the center. If the size of the system is larger than the localization length λ, the localized eigenstate is almost insensitive to the boundaries and th localized electron does not know what happens on the boundary of the system, so that δE_n decreases exponentially when the size of the system increases, $\delta E \sim \exp{-L/\lambda}$.

To measure the sensitivity to the change of the boundary conditions quantitatively, consider a small interval of energies, $E \pm \delta$, and calculate the parameter

$$g_T(E) = \frac{e^2}{h} \frac{\langle \delta E \rangle}{\Delta E}, \tag{44}$$

where ΔE is a typical difference between two neighboring eigenenergies,

$$\Delta E = \frac{1}{L^d \rho(E)}, \tag{45}$$

and $\langle \delta E \rangle$ is a typical change of eigenenergies lying in the interval $E \pm \delta$. Then, from the size dependence of g, we can distinguish between the metal and insulator.

In Fig. 15 we show how the eigenenergies E_n of the disordered system depend on the boundary conditions. We consider the 3d Anderson Hamiltonian, given by Eq. (6) with the random on-site energies, ε_n, and the boundary conditions determined by the real parameter, θ,

$$\begin{aligned}
\Psi(L, y, z) &= e^{i\theta} \Psi(0, y, z) \\
\Psi(x, L, z) &= e^{i\theta} \Psi(x, 0, z) \\
\Psi(x, y, L) &= e^{i\theta} \Psi(x, y, 0).
\end{aligned} \tag{46}$$

Clearly, $\theta = 0$ corresponds to the periodic boundaries, Eq. (41), and $\theta = \pi$ gives us anti-periodic boundary conditions, (42).

It was shown in Ref. [62] that if the energy E belongs to the metallic part of the spectra, then

$$g_T = \sigma L^{d-2} \quad \text{metal}, \tag{47}$$

where σ is the conductivity of the sample. When the eigenenergies around the energy E are localized, g_T decreases exponentially with the system size,

$$g_T \sim e^{-L/\lambda} \quad \text{insulator}. \tag{48}$$

The quantity g_T is called the Thouless conductance. It played an important role in the formulation of the scaling theory of localization [3].

The mean value, $\langle \delta E \rangle$, is called the *Thouless energy*, E_T. By comparison of the expressions (44,47) with the formula for the metallic conductivity, $\sigma = e^2 D \rho$, we find that

$$E_T = \frac{hD}{L^2}. \tag{49}$$
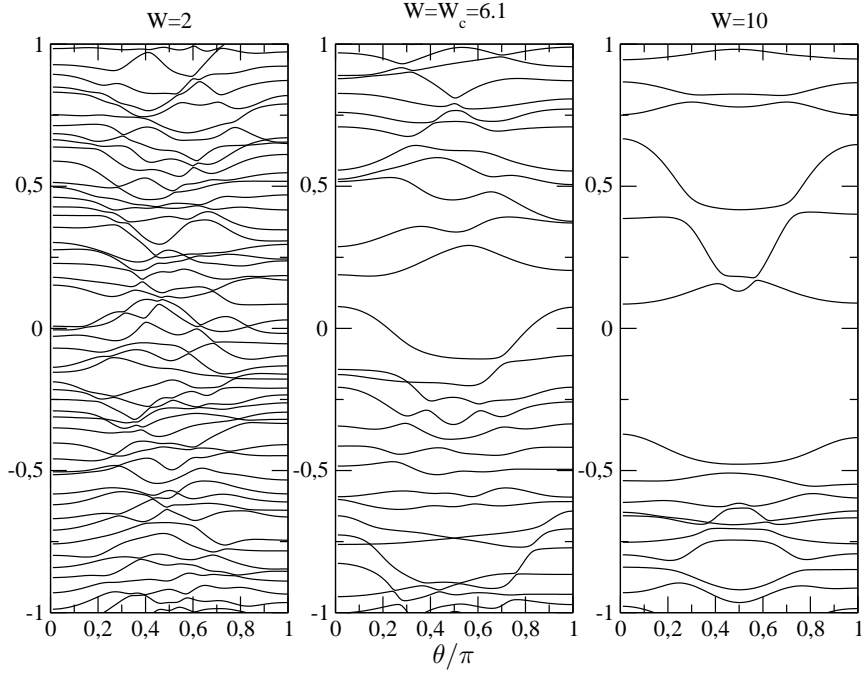
Fig. 15. Dependence of eigenvalues, $E_n(\theta)$ on the boundary conditions, given by Eq. (46). in the metallic (left), critical (middle) and the localized regime. Only eigenvalues close to the band center are shown. The size of the system is $L = 6$.

The corresponding Thouless time,

$$\tau_T = h/E_T,\tag{50}$$

represents the typical time, L^2/D, which the electron needs to diffuse from one side of the sample to the opposite side.

To the best of our knowledge, the relation (44) has so far not been used for the numerical analysis of the metal-insulator transition. The reason is that both δE_n and ΔE fluctuate not only as a function of the microscopic realization of disorder in a given sample, but also as a function of the energy within one given sample. Also, it is not clear which averaging procedure - arithmetic or geometrical - is more appropriate for the calculation of mean value, $\langle E_n \rangle$. Nevertheless, an introduction of the variable g_T provided the first step toward the scaling theory of localization. Since it is rather easy to estimate how both differences, δE and ΔE, depend on the system size, L, we can estimate the size dependence of the Thouless conductance, g_T.

6   Transfer matrix and conductance

As discussed in the introduction, the electron localization affects the transport properties of disordered systems. Therefore, the theory of localization concentrates mostly on the electron propa-
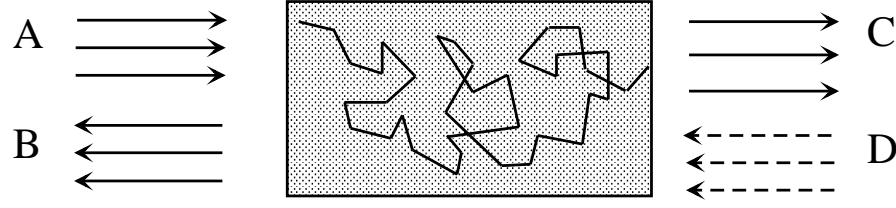
Fig. 16. Definition of amplitudes A - D.

gation. A key role in this study is played by the conductance, a quantity defined by Landauer [4] and Economou and Soukoulis [64]. The conductance is expressed in terms of the transmission and reflection amplitudes of the electron.

Consider scattering experiment shown in Fig. 16. The sample is connected on both sides to the semi-infinite ideal leads. We are interested in the probability that an electron, coming either from the left or from the right side of the sample, can transfer to the opposite side. Thus, we want to characterize the sample in terms of four matrices: transmission of the wave from the left to the right, t^+, from the right to the left, t^-, and by the reflection coefficient from the right to the right, r^+, and from the left to the left, r^-. In the most simple case of one-dimensional conductors, all the above parameters are complex numbers.

Transmission and reflection amplitudes define the *scattering matrix* **S**:

$$\mathbf{S} = \begin{pmatrix} t^+ & r^- \\ r^+ & t^- \end{pmatrix}. \tag{51}$$

Figure 16 shows that the scattering matrix, S, expresses the wave functions of outgoing waves B and C, in terms of the wave functions of the incoming waves, A and D,

$$\begin{pmatrix} C \\ B \end{pmatrix} = \mathbf{S} \begin{pmatrix} A \\ D \end{pmatrix} \tag{52}$$

Linear relation (52) can be re-written into the form

$$\begin{pmatrix} C \\ D \end{pmatrix} = \mathbf{T} \begin{pmatrix} A \\ B \end{pmatrix}. \tag{53}$$

where **T** is the transfer matrix, which determines the fields on one side of the sample with the fields on the another side. An explicit form of the transfer matrix, derived in AppendixA reads

$$\mathbf{T} = \begin{pmatrix} t^+ - r^-(t^-)^{-1}r^+ & r^-(t^-)^{-1} \\ -(t^-)^{-1}r^+ & (t^-)^{-1} \end{pmatrix}. \tag{54}$$

Some useful properties of the transfer matrix are given in Appendix A. If the system possesses time reversal symmetry, then the transmission amplitudes t^+ and t^- are related by

$$t^+ = (t^-)^T. \tag{55}$$

In the special case of 1d system, we have that $t^+ = t^-$ Therefore, we omit the superscripts in the transmission amplitudes in the following discussion.
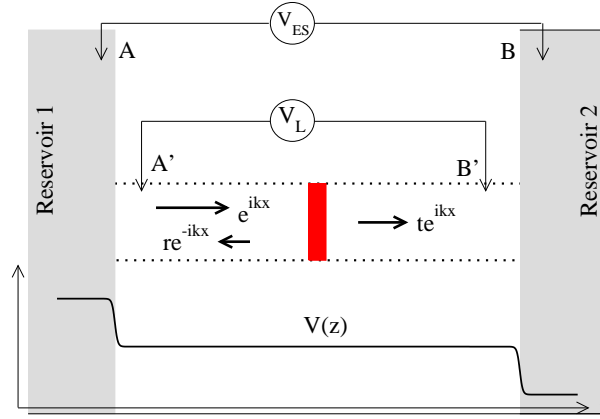
Fig. 17. Experimental setup for the measurement of the conductance g. Two semi-infinite leads are attached to the sample. Electrons are emitted from the left reservoir, propagate through the left lead and scatter on the sample. The transmitted electrons are absorbed in the reservoir on the opposite side, the reflected electrons propagate back. There is no scattering in the leads. There are two possibilities of the measurement of the voltage. Voltmeter V_L measures the voltage on leads; resulting conductance is then $g_L = j/V_L$, given by Eq. (57). The voltmeter V_{ES} measures the voltage on reservoirs. In this measurement, we obtain Economou-Soukoulis conductance g_{ES}, given by Eq. (58). We show also the voltage for the case when the sample is totally transparent to show the voltage drops due to the contact resistances between the reservoirs and leads.

6.1   Conductance

Consider the one dimensional experimental setup shown in Fig. 17. The sample is connected to two semi-infinite ideal leads, which transfer electrons from two reservoirs. The current through the sample is proportional to the voltage difference, ΔV, and to the conductance, g,

$$j = g\Delta V. \tag{56}$$

To find the conductance, we have to measure the voltage, ΔV. Two possibilities were considered. Landauer [4] proposed to measure the voltage difference between the leads, and obtained the conductance

$$g_L = \frac{e^2}{h} \frac{T}{1-T}. \tag{57}$$

On the other hand, Economou and Soukoulis [64] considered the voltage difference on reservoirs (Fig. 17), and derived an alternative formula,

$$g_{ES} = \frac{e^2}{h}T. \tag{58}$$

Both formulas are equivalent to each other only in the limit of small transmission, $T \rightarrow 0$. However, they lead to different results when the sample becomes transparent ($T \rightarrow 1$). Landauer

formula predicts that the conductance diverges (as it should be since the resistance is zero). On the other hand, expression (58) converges to e^2/h.

The origin of the difference between two formulas lies in the presence of a contact resistance between leads and reservoirs. We can write

$$\frac{e^2}{h}\frac{1}{g_{ES}} = \frac{1}{T} = \frac{1-T}{T} + 1 = \frac{e^2}{h}\frac{1}{g_L} + 1 \tag{59}$$

or, in terms of resistances,

$$\rho_{ES} = \frac{1}{g_{ES}} = \rho_L + \frac{h}{e^2}. \tag{60}$$

Thus, in the measurement of Economou and Soukoulis, the total resistance included in the measurement contains also contact resistance, $\rho_c = h/e^2$, measured on the contact of leads and reservoirs.

In numerical simulations, we will calculate the conductance g_{ES}. When necessary, we can extract the effect of contact resistance with the help of Eq. (59).

Historically, both quantities, g_L and g_{ES}, are called "Landauer conductance" in the literature.

6.2 Conductance of multi-channel system

In the previous Section, we have introduced the conductance of the one dimensional systems. For a given energy, we have only one possible value of the wave vector. This is the reason why the maximum value of the conductance is 1 (in units of e^2/h). In the real world, the leads might be quasi one dimensional, which means that the electron can propagate also in directions perpendicular to the propagation direction. Since the cross section of the leads is finite, the wave vector in the transversal direction, $k_\perp$, is quantized and possesses only discrete values. Each value of the transversal wave vector defines one channel (Fig. 18). It might happen that transmission is not possible for some values of $k_\perp$. We call such channels evanescent, or closed. For simplicity, we do not consider evanescent channels in the present discussion. Evanescent waves are discussed in Appendix A.5. The number of channels N_o, defines the size of the transmission matrices, t^+ and t^-. The physical meaning of the matrix element is clear: t_{ab}^+ is the transmission amplitude of the electron from the channel a to the channel b. Similarly, we define the matrix r^+ which contains reflection amplitudes from channel a to channel b. Then,

$$T_{ab}^+ = |t_{ab}^+|^2 \tag{61}$$

is the probability that the electron, coming in channel a, is transmitted through the sample into channel b, and

$$R_{ab}^+ = |r_{ab}^+|^2 \tag{62}$$

is the probability that the electron is reflected back into channel b.

It is useful to introduce the probability

$$T_a^+ = \sum_b t_{ab}^+(t_{ab}^+)^* = \sum_b T_{ab}^+ \tag{63}$$
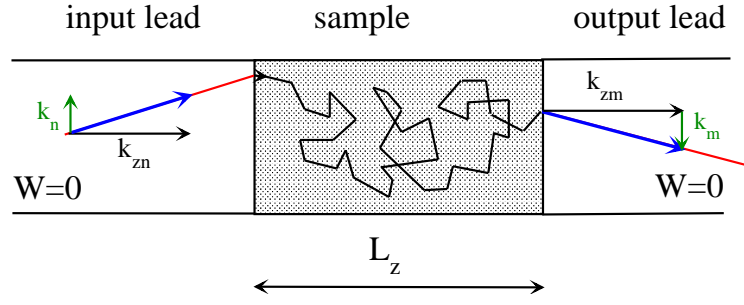
Fig. 18. Transmission of electron through disordered sample. The sample is connected to two semi-infinite metallic leads. Channels are determined by transversal momentum, or, equivalently, by incident angle, $\alpha = \tan^{-1}(k_n/k_{zn})$.

of the electron coming in the channel a to be transmitted through sample, and

$$T^+ = \sum_b T_a^+ = \sum_{ab} T_{ab}^+ \tag{64}$$

is the total probability that the electron transmits through the sample from left to right. Similarly,

$$R^+ = \sum_{ab} |r_{ab}^+|^2 \tag{65}$$

is the probability that the electron is reflected back. Since electrons can not be absorbed in the sample, we have

$$T^+ + R^+ = N_o, \tag{66}$$

as is proved in Appendix A. Then, generalization of expression (58) to the multi-channel system is straightforward,

$$g_{ES} = \frac{e^2}{h} \mathrm{Tr}\, t^\dagger t, \tag{67}$$

[65–68].

Multi-channel conductance is fully determined by eigenvalues of the matrix $t^\dagger t$. Using the parametrization of the transfer matrix, derived in appendix A.3, we obtain

$$g_{ES} = \frac{e^2}{h} \sum_a^{N_o} \frac{1}{1 + \lambda_a} = \frac{e^2}{h} \sum_a^{N_o} \frac{1}{\cosh^2 x_a/2}, \tag{68}$$

where $1/(1 + \lambda_a)$ is the ath eigenvalue of the matrix $t^\dagger t$ and parameters x_a are defined by the relation

$$\lambda_a = \frac{1}{2}\left(\cosh x_a - 1\right). \tag{69}$$

It was proved in Refs. [66, 67] that in the metallic regime, the conductance g, given by Eq. (67) is related to the conductivity σ, given by Eq. (1), by

$$g_{ES} = \sigma L^{d-2}. \tag{70}$$

6.3 Relation between the Thouless conductance and g_{ES}

In Sect. 5.3 we introduced the Thouless conductance, g_T, which measures the sensitivity of the energy spectra to the change of the boundary conditions. In the diffusive regime, g_T is given by Eq. (47). Comparison with Eq. (70), indicates that two quantities, g_T and g_{ES} are closely related to each other. This equivalence was studied numerically in Ref. [69]. Instead of changing the boundary conditions from periodic to anti-periodic, the *level curvature*,

$$c = \left. \frac{\partial^2 E_n(\theta)}{\partial \theta^2} \right|_{\theta=0}. \tag{71}$$

was studied numerically and compared with the conductance g_{ES}. The curvature, c, measures the sensitivity of the energy spectra to the change of the boundary conditions. In the metallic regime, the curvature c is related to g_{ES} by the relation [69]

$$g_{ES} = \pi \rho(E) L^d \langle |c| \rangle. \tag{72}$$

Also, in the strongly localized regime it was confirmed in Ref. [69] that

$$\langle \ln g_{ES} \rangle \propto \langle \ln |c| \rangle \tag{73}$$

Owing to Eqs. (72) and (73) we identify the conductance g_T with g_{ES} and conclude that the conductance g_{ES} not only measures the transmission properties of the sample, but also provides us with information about the sensitivity of the wave functions to the change of boundary conditions. In what follows we discuss only the conductance g_{ES}, defined by Eqs. (58). and use the notation

$$g = g_{ES}. \tag{74}$$

7 One-dimensional systems

It is instructive to analyze first the most simple problem, namely the one dimensional disordered (1d) chain. The simplest system which exhibits localization is the 1d Anderson model. If Ψ_n is the wave function of the electron on site n, then the Schrödinger equation reads

$$(\varepsilon_n - E)\Psi_n + \Psi_{n-1} + \Psi_{n+1} = 0. \tag{75}$$

It is well known [5] that all electron states in the disordered 1d system are localized. Localization is characterized by the localization length, which defines the exponential decrease of the wave function,

$$\Psi_n = \exp -L_z/\lambda, \tag{76}$$

where $L_z = an$ is the length of the system.

We can calculate the conductance, given by Eq. (365). It is more useful to start with the analysis of statistical properties of the variable x, related to the conductance by

$$g = \frac{1}{\cosh^2(x/2)} \tag{77}$$
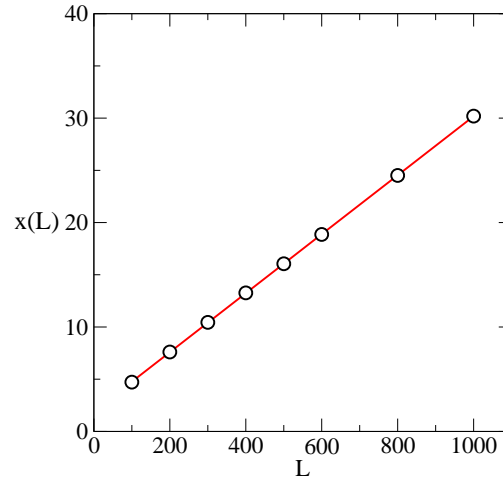
Fig. 19. The size dependence of parameter x defined by Eq. (77). Energy $E = 1$ and disorder $W = 1$. By combining the linear fit, $x(L_z) = 1.94 + 0.0282 L_z$, shown by solid line, with Eq. (78) we estimate the localization length, $\lambda = 70.92$. This agrees with the analytical estimation, $\lambda = [\text{Re } \gamma]^{-1}$ for the real part of the Lyapunov exponent, $\text{Re } \gamma(E) = 1/24(4 - E^2) = 1/72$, given by Eq. (334).

(in units of e^2/h).

Since all states are localized in 1d, we expect that conductance decreases exponentially when the length of the system increases, so that

$$x(L_z) = 2L_z/\lambda, \quad L_z \to \infty \tag{78}$$

as is shown in Fig. 19. This follows also from the Oseledec's theorem, discussed in Appendix D.

Conductance g is a statistical variable. To describe the transport properties of the systems with given disorder, we must study the statistical ensemble of samples, which differ in the microscopic realization of random energies, and calculate the mean, $\langle g \rangle$, and higher cummulants, or the entire conductance distribution, $p(g)$. We prefer to study the probability distribution of the parameter x, shown in Fig. 20 for a finite system length L_z. We see that the distribution $p(x)$ is similar to Gaussian. However, $p(x)$ differs from Gaussian when x is small. Indeed, $p(x) \to 0$ when $x \to 0$ since no negative values of x are allowed. Detailed numerical analysis confirmed (inset of Fig. 20, [20]) that

$$p(x) \sim x \quad x \ll 1. \tag{79}$$

Note, no negative values of x are allowed. Thus, to first approximation, $p(x)$ can be written in the form

$$p(x) = \propto x \, e^{-(x-a)^2/2b}, \tag{80}$$

where

$$a = \langle x \rangle + O(1) \tag{81}$$
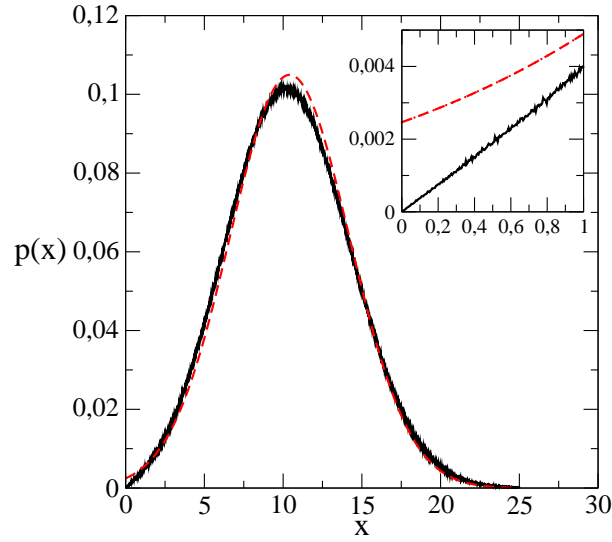
Fig. 20. The probability distribution, $p(x)$, of the parameter x for the one-dimensional disordered chain of the length $L_z = 300$, disorder $W = 1$ and $E = 1$. For comparison, we show also the Gaussian distribution with the same mean value, $\langle x \rangle = 10.41$ and variance, var $x = 14.45$ (dashed line). Inset shows how the two distributions differ for small x. Note, $p(x) \sim x$ for small x. To calculate the distribution, the statistical ensemble of $N_{\text{stat}} = 10^9$ samples was considered [20].

and

$$b = \alpha \langle x \rangle. \tag{82}$$

Here, α is a constant of order 1. In the limit of $L_z \to \infty$, $\alpha \to 2$ but $\alpha < 2$ for finite L_z. For instance, $\alpha = 1.388$ for system analyzed in Fig. 20.

From known distribution of $p(x)$, we can calculate the distribution of conductance,

$$p(g) = \int_0^\infty d\,x\, p(x)\delta\left[g - \frac{1}{\cosh^2 x/2}\right], \tag{83}$$

or the mean values

$$\langle g^n \rangle = \int_0^1 d\,g\, p(g)g^n = \int_0^\infty d\,x\, p(x)\frac{1}{\cosh^{2n} x/2}. \tag{84}$$

We evaluate the integral in the r.h.s of Eq. (84) by the steepest descent method. The function $p(x)\cosh^{-2n} x/2$ possess a sharp maximum around x_n, which solves the equation

$$\frac{\partial}{\partial x}\left\{-\frac{(x-a)^2}{2b} + \ln x - 2n \ln \cosh(x/2)\right\}\bigg|_{x=x_n} = 0. \tag{85}$$

Fig. 21. Conductance calculated for $N_{\text{stat}} = 200$ realization of disorder on the 1d system of the length $L = 200$ and box distribution of the disorder with $W = 1$. The localization length $\lambda \approx 100$.

It is easy to find that $x_n \sim O(1)$. Then, neglecting in Eq. (84) x_n with respect to a which is $\propto L_z \gg 1$ we find that

$$\langle g^n \rangle = \frac{c_n}{L_z^{3/2}} e^{-a^2/2b} \propto e^{-\langle x \rangle/2\alpha} \tag{86}$$

with the constant c_n independent of the length $L_z{}^3$.

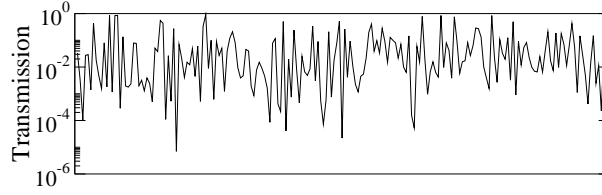Equation (86) agrees for $n = 1$ with the analytical result derived in Refs. [70,71]. For $n > 1$, we recover the universality of the moments of the conductance, derived in Refs. [71,72], namely that the ratio

$$\frac{\langle g^n \rangle}{\langle g \rangle} = \frac{c_n}{c_1} \tag{87}$$

does not depend on the system length.

Also, note that since $\langle g^2 \rangle \sim \langle g \rangle \gg \langle g \rangle^2$, we obtain that the ratio

$$\frac{\sqrt{\text{var } g}}{\langle g \rangle} = e^{+\langle x \rangle/4\alpha} \gg 1 \tag{88}$$

increases exponentially when the length of the system increases. Therefore, the mean value, $\langle g \rangle$, is not a good representative of the statistical ensemble. It follows from the derivation of Eq. (86 that all the moments of the conductance are determined only by a vanishingly small number of samples of the ensemble. These samples with small x are by no means representative. The same conclusion can be drawn out from numerical data in Fig. 21 which shows the conductance calculated for $N_{\text{stat}} = 200$ samples which differ from each other only by the microscopic realization of disorder. We see that the conductance fluctuates from sample to sample in many orders of magnitude. The mean value, $\langle g \rangle$, is determined by a few samples with $g \sim 1$, while the most probable value of the conductance is in many order of magnitude smaller.

Since x possesses a good probability distribution, and the transmission, $T = \cosh^{-2} x/2$, it is evident that for long systems it is more convenient to analyze the distribution of the *logarithm* of the transmission $\ln T$. We introduce a typical conductance,

$$g_{\text{typ}} = e^{\langle \ln g \rangle} \propto e^{-a} \propto e^{-\langle x \rangle}, \tag{89}$$

---

^{3}The factor $L_z^{-3/2}$ arises form the normalization constant of the distribution $p(x)$.

Comparing the typical conductance with the mean conductance,

$$\ln\langle g \rangle \sim \langle x \rangle/(2\alpha) \tag{90}$$

we obtain that

$$\ln g_{\text{typ}} = \langle \ln g \rangle = \frac{1}{2\alpha} \ln\langle g \rangle. \tag{91}$$

The typical conductance is orders of magnitude smaller than the mean conductance. This is typical for the localized regime. The conductance, g, is therefore not a good variable for description of transport in the localized regime.

The same holds for the resistance. Using $\rho = R/T$, we have

$$\rho = \sinh^2(x/2) \tag{92}$$

and

$$\langle \rho^n \rangle = \int dx p(x) \sinh^2(x/2) \approx e^{an+bn^2/2}. \tag{93}$$

In particular, for $n = 1$ we obtain, [4]

$$\langle \rho_L \rangle = \frac{1}{2}\left(e^{4L_z/\lambda} - 1\right). \tag{94}$$

Using the composition law or transfer matrices, derived in the next Section, the mean value of the Landauer resistance, $\langle \rho_L \rangle$, increases exponentially with the length of the system, but the *typical* resistance,

$$\rho_{\text{typ}} = e^{\langle \ln \rho \rangle} \tag{95}$$

increases much slower than the mean resistance:

$$\rho_{\text{typ}} = \frac{1}{2}\left(e^{2L_z/\lambda} - 1\right). \tag{96}$$

Again, the reason for the difference between the mean and the typical resistance is that the value of $\langle \rho^n \rangle$ is determined by very specific samples which have extremely huge resistance. Detailed analysis of the statistics of the resistance can be found in Ref. [16, 73–77]

7.1 Role of quantum coherence

In oredr to understand the physical origin of the localization and huge fluctuations of the conductance, we calculate the transmission of the quantum particle through two barriers. In Appendix A.1, we derived the transmission *amplitude* for transmission through two barriers, given by Eq. (228),

$$t_{12}^- = t_1^-\left[1 - r_2^+ r_1^-\right]^{-1} t_2^-. \tag{97}$$

---

[4] We remind the reader that $b = \alpha a$ and assume $\alpha = 2$ in the limit of $L_z \to \infty$.

From Eq. (97) we obtain the transmission *probability*,

$$T_{12} = |t_{12}^-|^2 = \frac{T_1 T_2}{1 + R_1 R_2 - 2\sqrt{R_1 R_2}\cos\phi}, \tag{98}$$

where we use $T_{1,2} = |t_{1,2}^-|^2$, $r_1^- = \sqrt{R_1}e^{i\phi_1}$, $r_2^- = \sqrt{R_2}e^{i\phi_2}$ and $\phi = \phi_1 + \phi_2$.

Equation (98) can be written in the form

$$\ln T_{12} = \ln T_1 + \ln T_2 - \ln(1 + R_1 R_2 - 2\sqrt{R_1 R_2}\cos\phi). \tag{99}$$

We can introduce the disorder by considering the phase factor, ϕ, being random with uniform distribution in the interval $(0, 2\pi)$ [16]. Then, averaging over all realization of phase gives the relation

$$\langle \ln T_{12} \rangle = \ln T_1 + \ln T_2, \tag{100}$$

since the integral of the last term on the r.h.s. of Eq. (99) is zero [16].

Relation (100) can be generalized for the N scattering centers. We obtain

$$\langle \ln T_N \rangle = N\,\overline{\ln T_1}, \tag{101}$$

where $\overline{\ln T_1}$ is the average of the transmission probability through one scatterer,

$$\overline{\ln T_1} = \frac{1}{N}\sum_{a=1}^{N} \ln T_a. \tag{102}$$

Equation (101) gives immediately the exponential decrease of the typical transmission,

$$e^{\langle T \rangle} = e^{-2L_z/\lambda}, \tag{103}$$

where the localization length is given by

$$\lambda^{-1} = \overline{\ln T_1}/2. \tag{104}$$

With the use of the expression $\rho_L + 1 = 1/T$ (Eq. 94) we recover the relation (96).

On the other hand, Ohm's law claims that the resistance of the 1d system increases linearly with the length of the system, or, equivalently, with the number N of scatterers. To obtain this result, we have to assume that electron is a classical particle. Then, instead of combination of transmission *amplitudes*, we combine the transmission and reflection *probabilities*. We obtain that

$$T_{12} = \frac{T_1 T_2}{1 - R_1 R_2}. \tag{105}$$

With the use of relations $T = 1 - R$ and $\rho = R/T$, we obtain from Eq. (105) that

$$\rho_{12} = \rho_1 + \rho_2, \tag{106}$$

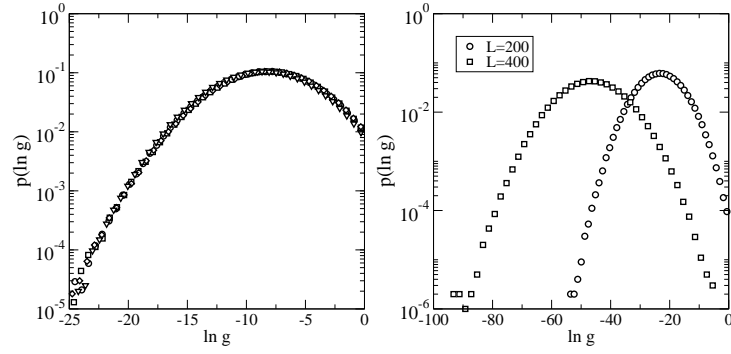which is nothing but Ohm's law as we wanted.

Fig. 22. Left: Distribution of the logarithm of the conductance, $p(\ln g)$ for the 1d disordered Anderson model. The energy of the electron is $E = 1$, and the disorder $W = 0.25, 0.5, 1$ and 2. To keep the same value of the ratio L/λ, we use the analytical result, $\lambda \sim W^{-2}$, for the localization length, discussed in Appendix D, and choose the length of the system $L_z = 4800, 1200, 300$ and 75, respectively. Note the drop of the distribution at $\ln g = 0$. This is because the conductance never exceeds 1 in the 1d systems. Right: $p(\ln g)$ for disorder $W = 2$ and two lengths of the system, $L_z = 200$ and $L_z = 400$. For a longer system, the probability to have g close to 1 is negligible and $p(\ln g)$ is Gaussian.

7.2   Distribution of the conductance

Figure 22 presents numerical data for the distribution $p(\ln g)$ for a strongly disordered 1d system. The distribution is similar to a Gaussian, in agreement with theoretical expectation discussed in Appendix D and with our estimation of the distribution $p(x)$. The main difference from the Gaussian distribution is that the distribution drops to zero at $\ln g = 0$ since the conductance never exceeds 1.

Figure 23 shows the probability distribution, $p(g)$ for 1d chains shorter than the localization length. For very short systems, $L_z \ll \lambda$, the electron "almost always" propagates through the sample. The chance to be scattered is very small. Interestingly, the distribution is almost flat when $L_z/\lambda \approx 0.5$.

Numerical data shown in Figs. 22 and 23 confirm that the distribution depends only on the ratio L_z/λ. Although the system is defined by many parameters - energy, disorder, length of the system - the only parameter which really determines the transport properties is the ratio L_z/λ. This observation simplifies considerably the theoretical investigations of the localization, and it is the key assumption in the scaling theory of localization.

7.3   Ergodic hypothesis

As discussed above, the conductance of a 1d system is a statistical quantity which wildly fluctuates as a function of distribution of random energies, ε_r. This is demonstrated in Fig. 21, which shows the conductance for $N_{\text{stat}} = 200$ realization of disorder. These data should be compared with those shown in Fig. 24 which plots the conductance of a given sample as a function of energy E of the electron. We observe that the conductance fluctuates similarly as in Fig. 21. More detailed analysis proved that the values $g(E)$ create the same statistical ensembles as the values
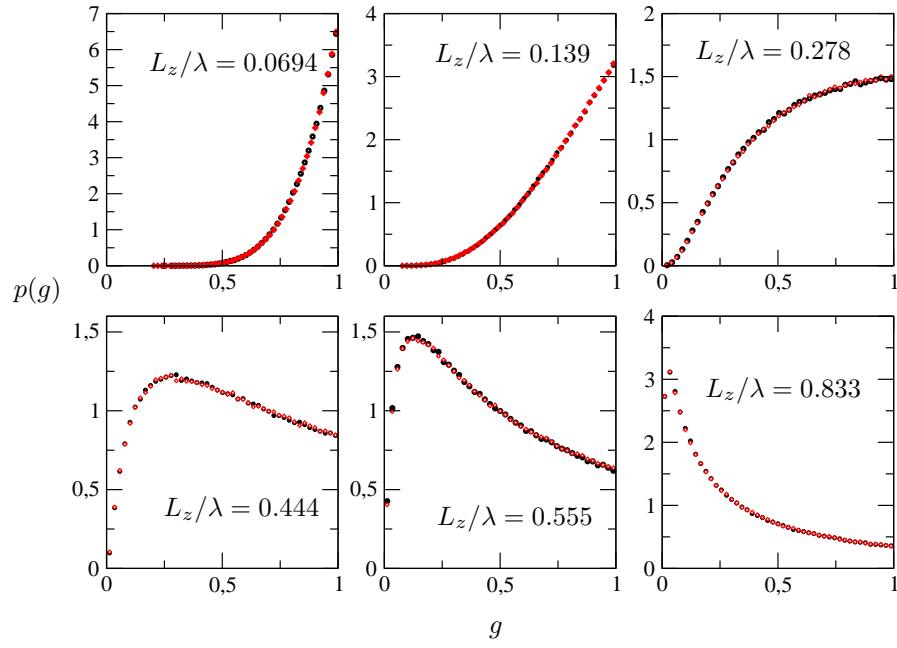
Fig. 23. Conductance distribution for the 1d Anderson model with short system length L_z. Figures contain data for $W = 0.5$ (the localization length $\lambda = 360$) and $L = 25, 50, 100, 160, 200$ and 300. These data are compared with data for $W = 0.25$ ($\lambda = 1440$) and a four times longer system, to show that systems with the same ratio L/λ have the same distribution $p(g)$. The energy of the electron is $E = 0.5$.
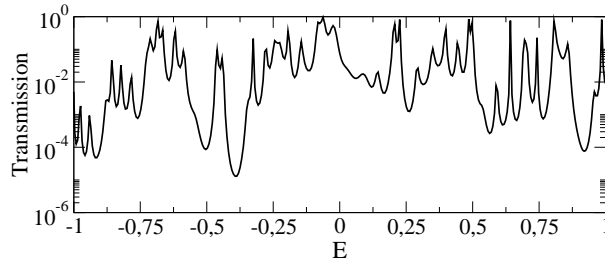
Fig. 24. The conductance of the single disordered one dimensional chain as a function of the energy E of the electron. The length of the sample is $L = 200$, disorder $W = 1$. Note, the conductance fluctuates within the same orders of magnitude as in Fig. 21. The energy dependence of the conductance is studied in details in Ref. [78]

of the conductance calculated for different samples with fixed energy. This result is known as the *ergodic hypothesis* [13].

The ergodic hypothesis plays a crucial role in the experimental studies of the transport in

disordered systems. Contrary to numerical simulations, it is impossible to study a huge number of microscopically different samples in experiments. Fortunately, due to the ergodic hypothesis, it is sufficient to use only one sample and vary the Fermi energy. Similar equivalence holds also in the metallic regime. Here, not only Fermi energy, but also the magnetic field can be varied [79]. The ergodic hypothesis in higher dimensional systems was numerically tested in Ref. [80].

8   Diffusive regime

By definition, the diffusive regime is characterized by the diffusive propagation of the electron in the sample. This happens when the mean free path is sufficiently large so that electron is scattered separately on two successive impurities. Also, the size of the system must be large enough,

$$L \gg \ell, \tag{107}$$

so that the electron scatters many impurities before it leaves the sample.

The diffusive regime can be obtained in the 3d systems with disorder $W < W_c$. Although no metallic phase exists in 2d systems, we can observe the diffusive regime if the size of the system is smaller than the localization length,

$$L \ll \lambda. \tag{108}$$

Similarly, in weakly disordered quasi one dimensional systems, described by the DMPK equation (Appendix B), the diffusive regime exists when the length L_z of the system does not exceeds localization length. Note, there is no diffusive regime in one dimensional samples since $\ell = \lambda$ [84].

The diffusive regime is characterized by the conductivity, σ, given by Eq. (1), which is related to the conductance, g, by Eq. (70), which we now write in more accurate form,

$$\langle g \rangle = \sigma L^{d-2}. \tag{109}$$

In Eq. (109), $\langle \ldots \rangle$ means ensemble averaging. The averaging is crucial in Eq. (109). Contrary to the conductivity, σ, the conductance g, is a sample dependent statistical variable, which is not self-averaged. In Sect. 8.3 we show that fluctuations of the conductance in the diffusive regime are universal, independent of the size of the system and the mean value, $\langle g \rangle$.

Owing to Eq. (107), the electrons are scattered many times inside the sample, and their wave function becomes totally randomized. Thanks to this randomization, electron transport is totally universal in diffusive regime. We discuss two main transport properties of the diffusive regime: the weak localization correction to the mean conductivity, and the universal conductance fluctuations.

8.1   Weak localization

In the derivation of the conductivity, σ, given by Eq. (1), no quantum interference processes were considered. Experimental and numerical results, however, show that these processes play an important role already in the diffusive regime, and lead to the so called *weak localization corrections*
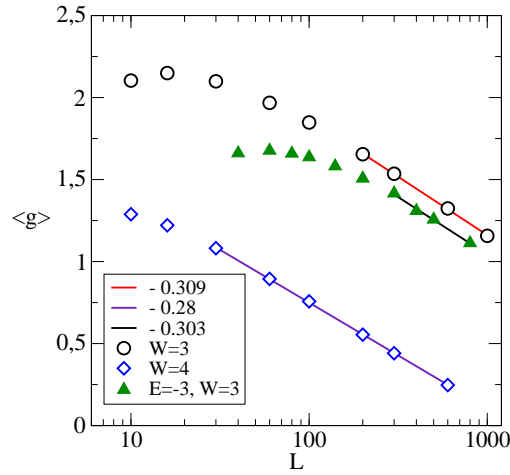
Fig. 25. The conductance (in units of e^2/h) in the 2d orthogonal system. Weak localization corrections are given by a logarithmic decrease of $\langle g \rangle$ when the size of the system increases. Symbols show numerical data for the conductance, while the lines are logarithmic fits (note logarithmic scale on the horizontal axis). Corresponding slopes are given in the legend. Theory predicts that the slope is universal, equal to $\pi^{-1} = -0.318$ (Eq. 118).
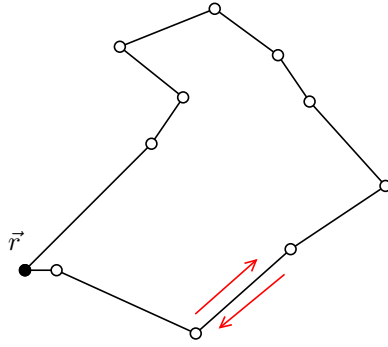
Fig. 26. The closed trajectory of the electron in a disordered 2d system. On the travel along the trajectory, the electron is *coherently* scattered. If the systems possess time reversal symmetry, then traveling in both directions gives the same contribution to the conductance.

to the conductance. We demonstrate the weak localization effects in Fig. 25 which shows that the mean conductance, $\langle g \rangle$, of the 2d disordered Anderson model depends logarithmically on the system size. This is a consequence of coherent backscattering of quantum electrons.

To understand the origin of this correction, we calculate the probability that the electron, propagating through the sample, is scattered back. Figure 26 shows the typical closed trajectory of the electron. The probability amplitude associated with the nth closed trajectory is A_n. Since

the electron is a quantum particle, the probability to return back is given by (in units of e^2/h)

$$\delta g_q = \left| \sum_n A_n \right|^2.$$ (110)

where n counts all possible closed paths. The corresponding contribution for the *classical* particle is

$$\delta g_c = \sum_n |A_n|^2.$$ (111)

Note, δg_c is included already in the conductance, σ, given by Eq. (1). Therefore, the logarithmic corrections to the conductance, shown in Fig. 25 originate form the difference

$$\delta g = \delta g_q - \delta g_c.$$ (112)

The r.h.s. of Eq. (110) can be written in the form

$$\sum_n |A_n|^2 + \sum_{n \neq n'} (A_n^* A_{n'} + A_n A_{n'}^*) = \delta g_c + \sum_{n \neq n'} (A_n^* A_{n'} + A_n A_{n'}^*).$$ (113)

In random systems, the sum of the off-diagonal terms is zero because of random phases of complex amplitudes A. However, there is an important exception, when A_n and $A_{n'}$ correspond to the same closed path, but opposite in direction to the electron propagation. Consider one loop, as shown in Fig. 26. The electron can travel this path in both directions; both possibilities give the same contribution, $|A|^2 = |A_+|^2 = |A_-|^2$. Moreover, if the system possesses time reversal symmetry (which is the case of 2d Anderson model), then also $A_+ = A_-$, and the off-diagonal terms,

$$A_+ A_-^* + A_+^* A_- = 2|A|^2$$ (114)

are real, independent of phase. Then, in the quantum case, a given loop contributes to backscattering by

$$\delta g_q = |A_+|^2 + |A_-|^2 + A_+ A_-^* + A_+^* A_- = 4|A|^2.$$ (115)

In the classical case, this contribution is only

$$\delta g_c = 2|A|^2,$$ (116)

The difference between *classical* and *quantum* backscattering, given by Eq. (112), gives rise to the *negative* weak localization corrections to the conductance.

We do not calculate δg here, only give a final result [30],

$$\delta g = \delta g_q - \delta g_c = -4 \frac{e^2}{h} L^{d-2} \frac{1}{(2\pi)^d} \int \frac{d^d \vec{q}}{q^2}.$$ (117)

Here, q is the wave vector of the electron propagating on the loop. To avoid the divergences in integral (117), we introduce the lower, $q_{\min} = 1/L$, and the upper, $q_{\max} = 1/\ell$, integration limits [81]. Then, integration gives for dimension $d = 2$ the expression

$$\delta g = -\frac{1}{\pi} \ln L/\ell, \qquad d = 2,$$ (118)
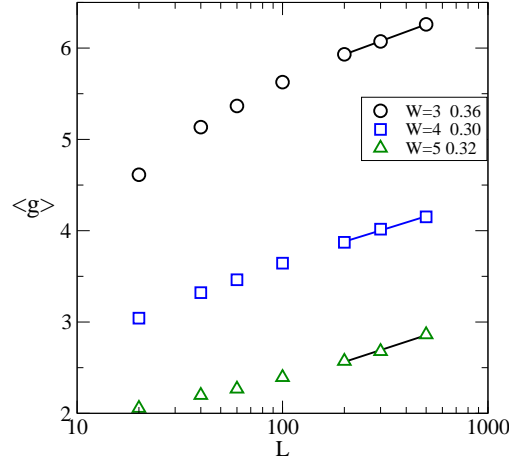
Fig. 27. The weak anti-localization corrections to the conductance for the 2d Ando model. The conductance is given in units e^2/h. The legend presents the calculated slopes. Theory predicts the slope $+\pi^{-1} = 0.318$. More accurate data for the weak anti-localization correction were obtained within the SU(2) model in Ref. [82].

and for $d = 1$ and $d = 3$ the formulas

$$
\delta g = \begin{cases} -\pi^{-2}(L/\ell - 1) & d = 3 \\[2mm] \ell/L - 1 & d = 1. \end{cases}
\tag{119}
$$

Since the backscattering is larger for the quantum particle, the correction to the conductance must be negative. Note, however, that the above results hold only in systems with time reversal symmetry. When a strong magnetic field is applied to the system, the time reversal symmetry is broken and $\delta g = 0$. Indeed, the electron acquires on the closed loop the phase

$$
\phi_n = \pm \int \vec{A}(\vec{r}) d\vec{r},
\tag{120}
$$

where $\vec{A}$ is a vector potential and the sign $\pm$ depends on the propagation direction. Then, the product $A_n A_{n'}^*$ is not real, but possesses the phase factor $e^{2i\phi_n}$. Since the phase ϕ_n depends on the length of the loop, in the summation over all loops, all complex contributions cancel.

In symplectic models, when the hopping between two neighboring sites becomes spin dependent, the quantum contribution to the backscattering changes the sign. The reason is that the wave function of the particle with spin 1/2 transforms into itself after rotation in 4π, contrary to spin-less particle [25]. The weak anti-localization corrections to the conductance for the 2d Ando model is shown in Fig. 27.
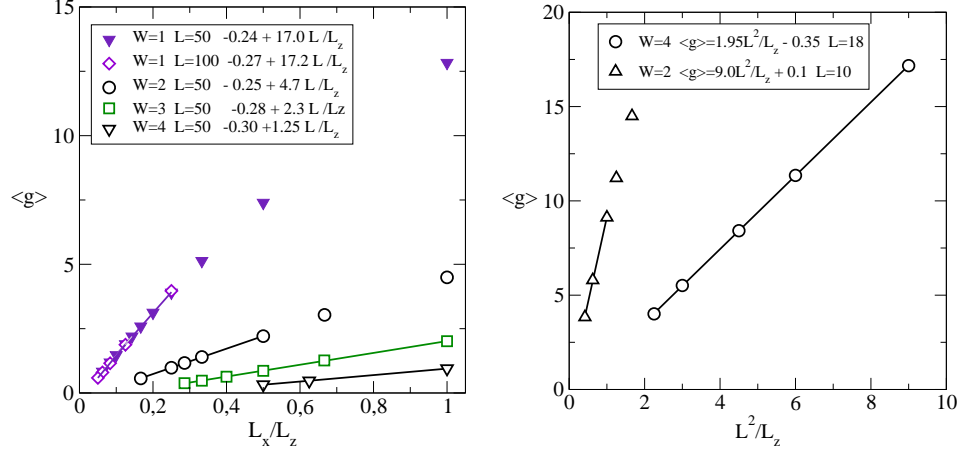
Fig. 28. The mean conductance, $\langle g \rangle$, as a function of N/L_z for the 2d systems (left) and the 3d anisotropic model (9) with $t = 0.4$ (right). The slope of the linear fit determines, due to Eq. (121), the mean free path, ℓ. Left: The 2d system, $N = L = 50$. We found $\ell = 17.0$, 4.9, 2.30 and 1.25 for $W = 1$, 2, 3 and 4, respectively. For $W = 1$, we add also data for $L = 100$. Right: The 3d systems of the size $L \times L \times L_z$. For $W = 4$ (circles) we found $\ell = 1.92$, while $\ell \approx 9$ for $W = 2$. Note, the weak localization corrections in both systems are close to $-1/3$, as predicted by DMPK equation (Appendix B). The only exception is the 3d system with $W = 2$, since $\ell \approx L$ in this case.

8.2 Weak localization in quasi-1d systems

Of particular interest is transport in weakly disordered quasi one dimensional systems. This problem is exactly solvable. In Appendix B we introduced the DMPK equation for the joint probability distribution of parameters λ of the transfer matrix. From the DMPK equation, the following expression for the mean conductance can be derived [83] (in units of e^2/h),

$$\langle g \rangle = \frac{N\ell}{L_z} - \frac{1}{3}, \tag{121}$$

(Eq. 282). The weak localization correction is constant, independent of the system length, provided that $\ell \ll L \ll N\ell$.

Note that expression (121) was derived in the limit of infinite number of transmission channels, $N \to \infty$. Therefore, it cannot be applied to the 1d models, where $N = 1$.

Figure 28 verifies both the L_z dependence of the mean conductance and the weak localization correction, $\delta g = 1/3$ for two different quasi-1d systems. Note, relation (121) can be also used for the numerical calculation of the mean free path, ℓ. Numerical data for the conductance in quasi-1d systems are presented in Fig. 28. The obtained values of the mean free path are rather small, of the order of the lattice period. Only when disorder is very weak ($W = 1$ in 2d), then $\ell \approx 17$. Note that in the Born approximation [84], the mean free path decreases with the disorder as

$$\ell \propto W^{-2}. \tag{122}$$
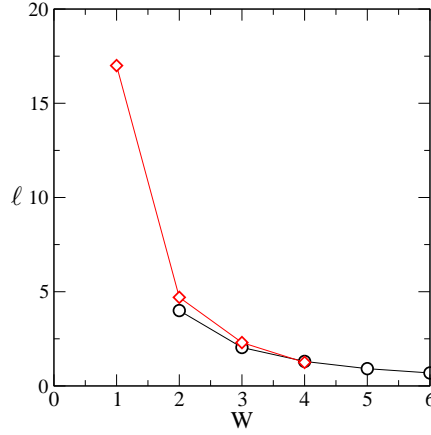
Fig. 29. The numerical data for the mean free path, ℓ, from Fig. 28 (diamonds), compared with results of Ref. [84] (circles).

The numerical data for the mean free path of 2d systems, obtained in Fig. 28 are in very good agreement with results of Ref. [84], shown in Fig. 29.

8.3   Conductance distribution. Universal conductance fluctuations

Because of the randomness, the conductance is a statistical variable, and can vary from sample to sample as a function of the distribution of random energies ε_n. In the diffusive transport regime, the conductance distribution is Gaussian, as shown in Fig. 30.

Since the disorder W is weak, the statistical properties of the conductance can be derived theoretically, either by the perturbation Green's function method [9] or within the framework of the DMPK equation, introduced in Appendix B. The distribution of the conductance is Gaussian with universal width. The variance,

$$\operatorname{var} g = \langle g^2 \rangle - \langle g \rangle^2 \tag{123}$$

is a universal number, independent on the disorder strength (provided that inequalities (107, 108) hold). var g depends only on the dimension of the system and on boundary conditions [9]. This phenomenon is known as universal conductance fluctuation.

Also, var g depends on the physical symmetry of the model. It was proved in Ref. [9] that

$$\operatorname{var} g \propto \frac{1}{\beta}. \tag{124}$$

We remind the reader that $\beta = 1,\ 2$ and 4 for the orthogonal, unitary and symplectic systems, respectively. For the quasi-1d systems, the same universality relation was derived in Ref. [83,85].

In systems with higher dimension, var g depends also on the boundary conditions in the directions perpendicular to the propagation [9]. This dependence was theoretically investigated in Ref. [86] and numerically verified in [87].
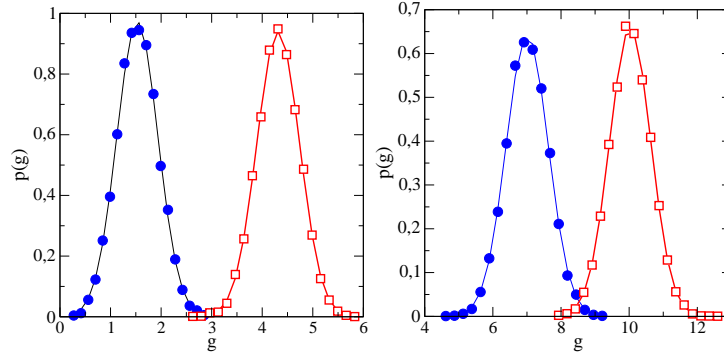
Fig. 30. The probability distribution $p(g)$ of the conductance for weakly disordered systems. Left: The 2d samples of the size 300×300. Disorder $W = 3$ (circles) and $W = 2$ (squares). Solid lines are Gaussian fits with variance 0.168 and 0.179 for $W = 3$ and $W = 2$, respectively. This is close to the theoretical prediction, 0.185, obtained for hard wall boundary conditions in Ref. [87]. Right: The 3d system with box distribution of random energies, $W = 6$ and $L = 10$ (circles) and $L = 14$ (squares). Solid lines are Gaussian fits with mean value $\langle g \rangle = 7$ ($L = 10$) and $= 10.03$ ($L = 4$). These values confirm the relation $\langle g \rangle = \sigma L$ with the conductance $\sigma = 0.7$. The width of distributions is var $g = 0.38$ and 0.366 for $L = 10$ and $L = 14$, respectively, are close to the theoretical prediction 0.314 [87,88]. Data were obtained numerically with statistical ensembles of $N_{\text{stat}} = 10^4$ samples.

The deviations of $p(g)$ from Gaussian form can be measured by the third cummulant,

$$\langle g^3 \rangle_c = \langle g^3 \rangle - 3\langle g^2 \rangle\langle g \rangle + 2\langle g \rangle^3. \tag{125}$$

It was shown analytically [89] that $\langle g^3 \rangle_c = 0$ for the quasi-one dimensional systems and is $\sim 10^{-3}\langle g \rangle^{-1}$ for the 3d system. Such small values are not observable with today's computer facilities.

The conductance fluctuations for the 2d weakly disordered systems are plotted in Fig. 31. Note how the variance of the conductance is universal only when the size of the sample is much larger than the mean free path, $L > 10 \times \ell$. However, L must be much smaller than the localization length, $L/\lambda \ll 1$. Also, for small system size, when condition (107) is not satisfied, the

Tab. 1. Universal values of the conductance fluctuations, var $g = \langle g^2 \rangle - \langle g \rangle^2$ for the d-dimensional disordered systems with the hard wall and periodic boundary conditions [88]. For other symmetry classes, var g must be divided by a factor of β, (Eq. 124). var $g \sim \epsilon^{-1}$ in the dimension $d = 4 - \epsilon$.

d	HW	periodic
1	2/15	2/15
2	0.185613	0.154078
3	0.314054	0.2194393
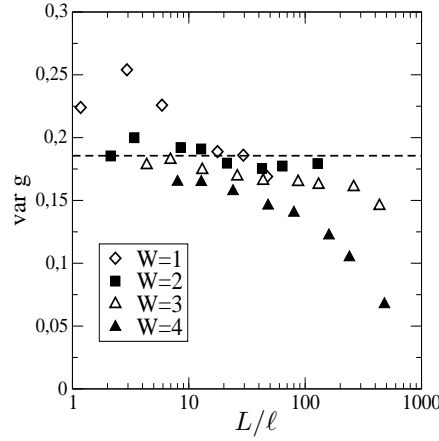
Fig. 31. Conductance fluctuations for the 2d Anderson model. Different symbols correspond to the disorder $W = 1, 2, 3, 4$ and 5. The size of the system increases from $L = 10$ to $L = 1000$. The horizontal dashed line is the theoretical prediction var $g \approx 0.1856$ of the universal conductance fluctuations for 2d orthogonal system with the hard wall boundary conditions [87]. For $W = 1$, the mean free path $\ell \sim 17$ is already comparable with L for some smaller samples. The system is in the ballistic regime and var g exceeds universal value. A more detailed analysis of the universal conductance fluctuations has been done in [87].

system is in the ballistic regime, in which the scattering of electrons is not sufficiently strong to randomize the wave function sufficiently. In this regime, the conductance is large, $g \sim N_{\mathrm{o}}$, and the fluctuations of the conductance increase. Of course, the variance decreases to zero in the limit of a regular lattice ($W = 0$).

8.4   Other universal relations

Universal conductance fluctuations are the consequence of the universality of the diffusive transport. In Appendices B and C we discuss the statistical properties of the eigenvalues λ_a of the matrix $\left[t^\dagger t \right]^{-1}$. It turns out, that in the diffusive regime the joint probability distribution of the eigenvalues λ is universal and depends only on the length of the system and the number of the transmission channels, N_{o}. The disorder, W, influences the transmission parameters only in terms of the ratio L_z/λ of the system length and the mean free path.

From the universality of the probability distribution $p(\lambda)$ we can obtain other universal relations for the transmission parameters. In Appendix C we show that the spectrum of parameters x_a, defined by Eq. (68) is linear,

$$x_a \propto a, \tag{126}$$

as shown in Fig. 76. Also, the differences, $x_{a+1} - x_a$ are distributed with the Wigner probability distribution (Fig. 74).

Here we want to show that not only the conductance, g, but also the transmission probabilities, T_{ab} and T_a, introduced in Sect. 6.2 as

$$T_{ab} = |t_{ab}|^2 \tag{127}$$
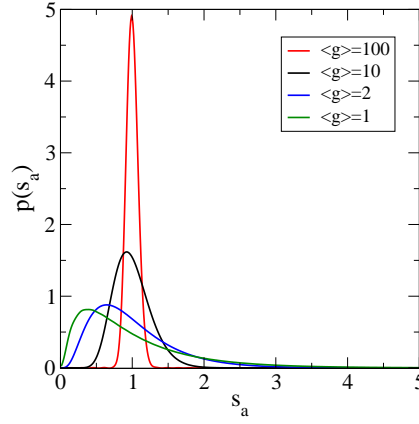
Fig. 32. Probability distribution $p(s_a)$, given by Eqs. (131,132) for various values of the mean conductance, $\langle g \rangle$.

and

$$T_a = \sum_b |t_{ab}|^2 = \sum_b T_{ab}, \qquad (128)$$

exhibit universal statistical properties. We remind the reader that T_{ab} is the probability that the electron, coming in channel a is transmitted through the sample and leaves the sample in channel b and T_a is the probability that the electron, coming in channel a, transfers through the sample. It is clear that

$$g = \sum_a T_a. \qquad (129)$$

Note, T_a is *not* the eigenvalue of the matrix $t^\dagger t$.

The universal probability distribution for the *normalized* transmission probability,

$$s_a = \frac{T_a}{\langle T_a \rangle}, \qquad (130)$$

was derived in Refs. [94,95]. The distribution $p(s_a)$ is determined only by the mean conductance, and is given by the following analytical formula,

$$p(s_a) = \int_{-i\infty}^{+\infty} \frac{dx}{2\pi i} e^{xs_a - \Phi(x)} \qquad (131)$$

where

$$\Phi(x) = \langle g \rangle \left[\ln \left(\sqrt{1 + x/\langle g \rangle} + \sqrt{x/\langle g \rangle} \right) \right]^2. \qquad (132)$$

The probability distribution $p(s_a)$ is shown in Fig. 32 for a few values of the mean conductance. Distribution $p(s_a)$ possesses universal variance,

$$\text{var } s_a = \langle s_a^2 \rangle - \langle s_a \rangle^2 = \frac{2}{3\langle g \rangle}. \qquad (133)$$
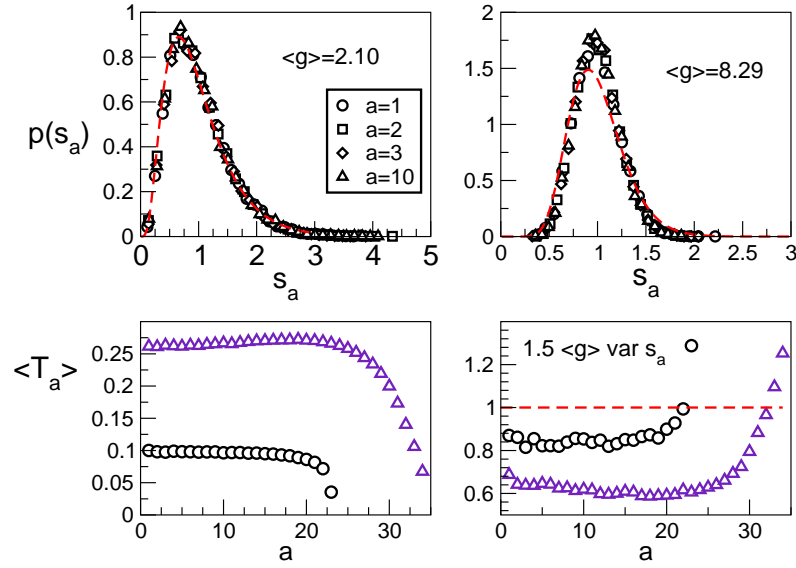
Fig. 33. Upper panels show the probability distribution of the parameters s_a, defined by Eq. (130) for the 2d Anderson model, with the random binary potential given by Eq. (134). The energy of the electron, $E = 0.14$ (left upper panel) and $E = 0.31$ (right upper panel) is measured in this particular case from the bottom of the conductance band. Different symbols represent the data for channels $a = 1, 2, 3$ and 10. The solid line is the theoretical prediction, given by Eqs. (131,132). Two lower panels show the mean transmission, $\langle T_a \rangle$ and the variance, var s_a, given by Eq. (133). Note that all channels are almost equivalent and they give the same contribution to the conductance. The number of open channels is $N_o = 23$ and $N_o = 34$ for $E = 0.14$ and $E = 0.31$, respectively. The size of the system is 192×192 [93].

Universality of the distribution (131) was confirmed experimentally in experiment with microwave electromagnetic waves [24, 95]. Numerically, it was studied in Ref. [93] for the 2d system with correlated binary disorder

$$p(\varepsilon) = (1 - x)\delta(\varepsilon) + x\delta(\varepsilon + V_b). \tag{134}$$

Spatial correlations were introduced so that random energies create randomly distributed potential wells of the size of 3×3 lattice sites.

Figure 33 shows the numerically obtained data for the system of size 192×192 and for two energies of the electron. Data confirm that indeed the channels are equivalent to each other, and they give the same value of the transmission, $\langle T_a \rangle$. This is a typical property of the diffusive regime: transmission in a given channel does not depend on the incident angle, since electron, being many times scattered inside the sample, forgets the initial direction of propagation.

8.5   Diffusion

Conductivity, σ, can be expressed through the diffusion coefficient, D, $\sigma = e^2 D \rho$, given by Eq. 1. The density of states, $\rho(E)$ was calculated in section 4.1. The diffusion coefficient can
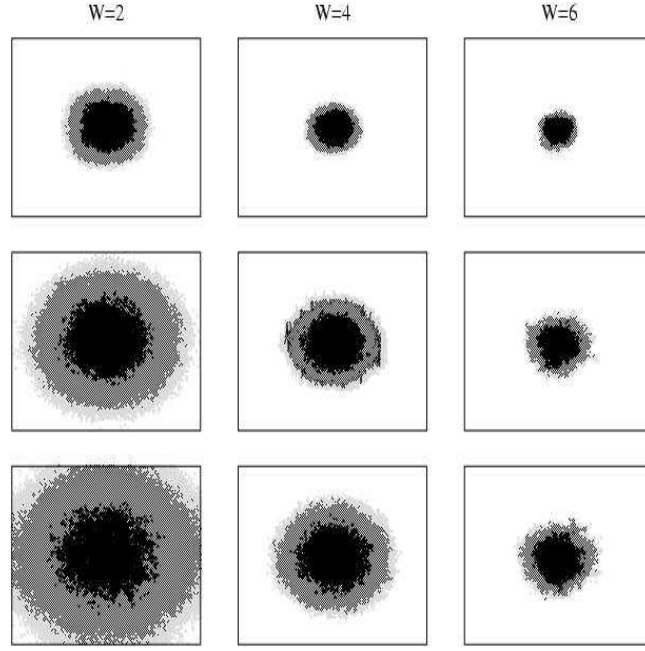
Fig. 34. The time dependence of the wave packet in the 2d disordered system, defined by Hamiltonian (6). Shown are points where $|\Psi(\vec{r})| > 0.0005$ (gray), $|\Psi(\vec{r})| > 0.0010$ (dark gray), and $|\Psi(\vec{r})| > 0.0050$ (black) at time $t = 100$, 500 and 900 (from top to bottom). The time is measured in units $\hbar/V$ with $V = 1$ and the size of the lattice is 512×512. For weak disorder, the wave function of the electron diffuses and $\rangle r^2 \langle = 2Dt$ where D is the diffusion coefficient. Clearly, D decreases when disorder increases. For $W = 6$ (right column), diffusion already stops and the electron is localized (see also Fig. 2).

be calculated numerically solving the time dependent Schrödinger equation, Eq. (5). Figure 34 shows the time evolution of the single electron wave function in disordered 2d samples with different strength of the disorder. We use the same data to calculate the width of the wave packet,

$$\langle r^2(t) \rangle = \int d\vec{r} \Psi^*(\vec{r}, t) r^2 \Psi(\vec{r}, t) \tag{135}$$

in time t. When disorder is small, the electron diffuses from the center, and we obtain that

$$\langle r^2 \rangle = 2Dt. \tag{136}$$

In the case of strong disorder, $\langle r^2 \rangle$ should converge to the time-independent quantity, when the electron is localized. This was shown already in Fig. 1 for the case of strong disorder.

Figure 35 shows the time dependence of $\langle r^2 \rangle$ for various strengths of the disorder. The diffusion constant, D, is obtained as the slope of the linear dependence $\langle r^2 \rangle$ vs t. If the density of states, $\rho(E)$ is known, then we can obtain the conductance,

$$g = \sigma = \frac{e^2}{h} hD\rho. \tag{137}$$
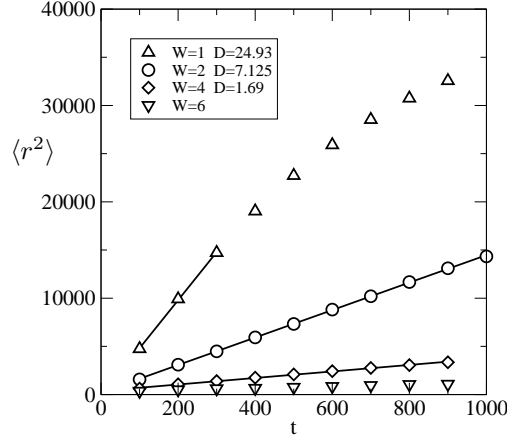
Fig. 35. Left: $\langle r^2 \rangle$ vs time t for the 2d Anderson model with box disorder. The slope of the linear dependence determines the diffusive coefficient D. The data for disorder $W = 2$ and $W = 4$ corresponds to the wave function shown in Fig. 34. For weak disorder, $W = 1$, we see already the saturation of $\langle r^2 \rangle$ due to the finite size of the system and reflection of the wave packet from boundaries. Solid lines are linear fits, $\langle r^2 \rangle = 2Dt$. Time is measured in units $\hbar/V$. The diffusion coefficient, D, measured in units $a^2V/\hbar$, is given in legend.

Using numerical data for the disorder $W = 4$: $\rho(E) \approx 0.15/a^2V$ (Fig. 4), and $D = 1.69\, a^2V/\hbar$ (Fig. 35), we obtain that $g(W = 4) = 1.59(e^2/\hbar)$. This is consistent with numerical data shown in Fig. 25.

8.6   Beyond the diffusive regime

As will be discussed in next Section, there is no true metallic regime in 2d orthogonal systems. What we have observed so far is the diffusive propagation of the electron on a *finite* square lattice of size $L \times L$. When L increases over the localization length, $\lambda = \lambda(W)$, the electron becomes localized and the L dependence of the conductance changes from the logarithmic to the exponential.

In Fig. 36 we demonstrate how the conductance distribution, $p(g)$, of the 2d disordered systems changes when the size of the system, L, increases. For disorder $W = 3$, $p(g)$ is Gaussian even for $L = 1000$. However, for the disorder $W = 4$, the localization length $\lambda \approx 50$ and the probability distribution changes its form considerably.

In the opposite limit of small L, the system is in the ballistic regime. In the limit of $L < \ell$, there is almost no scattering inside the sample, so the conductance $\langle g \rangle$ is given by the number of open channels. In 2d, this means that $\langle g \rangle \propto L$. Increase of the conductance with the system size is shown in in Fig. 37. Note, the ballistic regime can be observed also in the 1d systems. Fig. 23 shows that for sufficiently short systems, the conductance of 1d disordered system is close to 1 when $L \ll \xi$.

Since the electron is scattered only on a few impurities during its travel through a ballistic
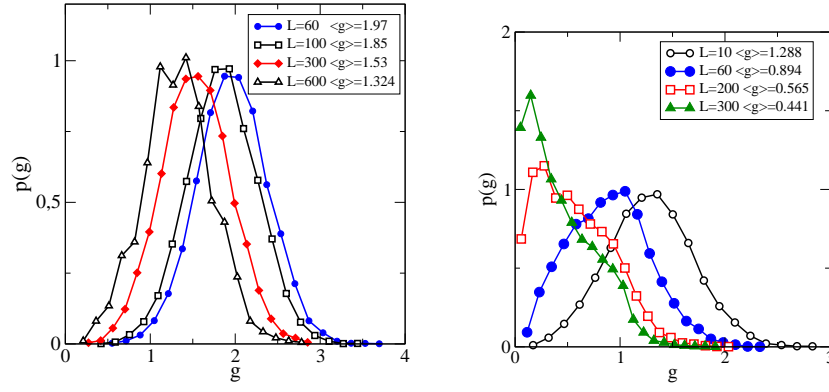
Fig. 36. The system size dependence of the conductance distribution, $p(g)$ for the 2d systems. Left: $W = 3$. The conductance is almost independent to the system size, since system is in the diffusive regime ($\ell \approx 2.3$, and $\lambda = 5046$). Right: $W = 4$. The distribution $p(g)$ is Gaussian only for very small systems ($L = 10$), and it changes considerably when L increases. The mean free path, $\ell \approx 1.3$ and localization length, $\lambda = 481$. The estimation of the localization length is taken from Ref. [6].
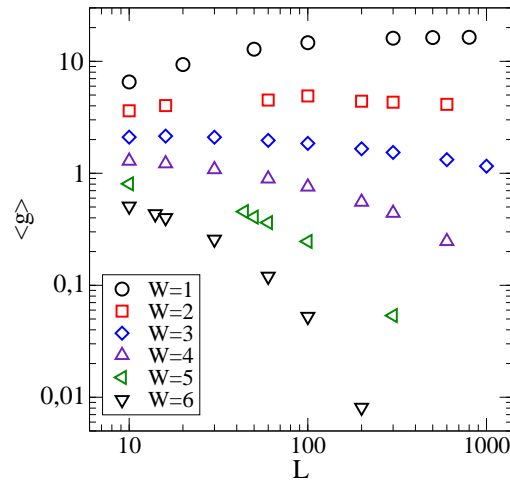
Fig. 37. The length dependence of the mean conductance, $\langle g \rangle$, for the 2d disordered systems. When disorder is weak, $\langle g \rangle$ increases for small L since the system is in the ballistic regime. Naively, this might be interpreted as a metal-insulator transition: since the mean conductance increases for $W = 1$ and decreases for $W = 5$, one might conclude that the 2d system possesses the critical point, $W_c \leq 1$, i. e. that disorder $W = 1$ corresponds to the metallic regime.

sample, the values of the conductance for a given sample depends on the actual distribution of impurities. Consequently, fluctuations of the conductance increase in the ballistic regime [96]. This is confirmed in Fig. 31.

9   Scaling theory of localization

As discussed in the Introduction, the metal-insulator transition resembles the phase transition in statistical physics. We would like to develop the theory, similar to the renormalization group theory of second order phase transitions.

The first step in this direction is to determine the relevant order parameter. It turns out that the most suitable candidate for such parameter is the Thouless conductance, g_T. First, it can be defined both in the metallic and localized regime. Second, the analysis of the sensitivity to the boundary conditions tells us how the conductance g_T develops when the size L of the system increases. Since g_T is equivalent to g_{ES} [69] both in the metallic and in the insulating regime, we will consider the conductance g_{ES} and use the simpler notation, g.

The main assumption we have to accept is that for the system size sufficiently large, the length dependence of the conductance is given only by the conductance itself:

$$\frac{\partial \ln g}{\partial \ln L} = \beta(g). \tag{138}$$

The "sufficiently large" system size L means that L exceeds all "natural" lengths which might determine the transport in the system. Some examples of such scales are the mean free path, ℓ, which determines the coherent scattering on impurities, the coherence length of the random potential, or magnetic length, which is important if the magnetic field is present. If L is much larger than all these scales, we expect that microscopic details of the model become irrelevant.

Now, we want to derive some consequences from the Eq. (138). First of all, we must admit that the form of the function $\beta(g)$ is unknown. However, we can derive its limits for $g \to \infty$ and $g \to 0$. Consider for simplicity only the orthogonal symmetry, so that the symmetry parameter $\beta = 1$. In the limit of large conductance, we can use the L-dependence of the conductance, derived in Sect. 8. The leading term of the conductance behaves as $g = \sigma L^{d-2}$. Inserting into Eq. (138), we obtain that

$$\lim_{g \to \infty} \beta(g) = d - 2. \tag{139}$$

Since the first correction to the conductance, derived in Sect. 8.1 is *negative*, we immediately see that $\beta(\ln g)$ reaches the limit (139) from below. In particular, for $d = 2$, we obtain from Eq. (118) that

$$\beta(g) = \frac{\partial \ln g}{\partial \ln L} = \frac{1}{g} \frac{\partial g}{\partial \ln L} = -\frac{1}{\pi g}. \tag{140}$$

In the opposite limit, $g \ll 1$, we have exponential localization,

$$g \sim e^{-2L/\lambda}, \tag{141}$$

so that

$$\beta(g) = -\frac{2L}{\lambda} = \ln g. \tag{142}$$
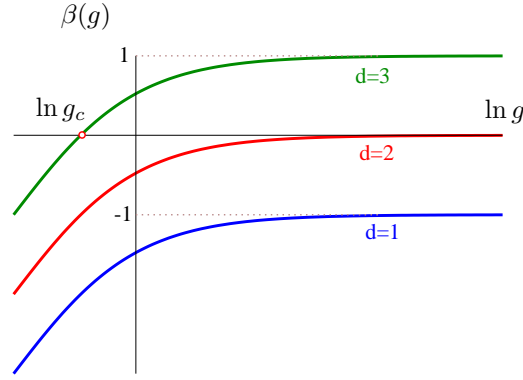
Fig. 38. The function $\beta(g)$ for the disordered *orthogonal* systems with dimension $d = 1, 2$ and 3. Notice the critical point, g_c for $d = 3$.

Now, we can interpolate between the limits (139) and (142). This is straightforward if we *assume* that the function $\beta(g)$ is always continuous and monotonous. Although we do not have a rigorous proof that $\beta(g)$ really fulfills these conditions, there is no physical reason not to accept them. Then, connecting both limits, we obtain that the function $\beta(g)$ behaves as shown in Fig. 38.

The form of the function $\beta(g)$ has some important consequences. First, we see that for $d < 2$, the function $\beta(g)$ is always negative. So starting with a sample of finite size, L_0, and conductance, g_0, the conductance, given by Eq. (138) decreases and develops to a smaller conductance when the system size, L, increases. Consequently, an infinite system with dimension $d \leq 2$ does not exhibit the Anderson transition since all electronic states are localized, independent of the strength of the disorder.

For $d > 2$ ($d = 3$, for instance), there is a critical point g_c such that

$$\beta(g_c) = 0. \tag{143}$$

When starting exactly with $g = g_c$, the conductance remains constant, independent of the system size even in the limit of $L \to \infty$. Thus, a disordered system in dimension $d > 2$ possesses a critical point. This critical point is unstable: when starting with $g = g_c + \delta g$, we end up, in the limit of $L \to \infty$, in the metallic regime with finite conductivity σ. Similarly, starting with $g = g_c - \delta g$, the system will develop into the insulating regime with exponentially small conductance.

What remains is the calculation of the function $\beta(g)$. Analytically, this is possible only for systems close to the critical dimension: $d = 2 + \epsilon$, $(\epsilon \ll 1)$ [97, 98]. We will discuss these results in Section 13.

The scaling theory of localization, formulated first in Ref. [3] represents the main milestone in our understanding of the Anderson transition. First, it estimates the lower critical dimension,

$$d_c = 2. \tag{144}$$

There is no metallic regime in the disordered system with dimension $d \le 2$. However, this statement is true only for *orthogonal* systems, i.e. for systems with time reversal symmetry. We know already that in symplectic systems the first correction to the conductance in the diffusive regime is positive (Fig. 27) so that $\beta(\ln g) \to 0^+$ when $g \gg 1$ [10]. Consequently, the 2d systems with spin dependent hopping exhibit the metal insulator transition. This was for the first time predicted in Refs. [47, 48] and confirmed numerically by many authors [49, 54, 99, 100].

Soon after formulation of the scaling theory [3] it became clear that g is a statistical quantity, which is not self-averaged in the limit of the infinite system size. In the metallic regime, the probability distribution of the conductance, $p(g)$, possesses an universal width, given by the universal conductance fluctuations. In the insulating regime, g does not represent the statistical ensemble, as discussed in Section 7, and we have to use its *logarithm*, $\ln g$. Even then, $p(\ln g)$ is Gaussian with the mean value $\langle \ln g \rangle = -2L/\lambda$ and the variance, $\langle \ln^2 g \rangle - \langle \ln g \rangle^2$, being of the same order as $-\langle \ln g \rangle$. We do not know the analytical form of the critical distribution, $p_c(g)$, but both theoretical [75, 101] and numerical [102] results confirm that $p_c(g)$ is independent on the size of the system. This is consistent with the size independence of the critical conductance, given by Eq. (143). However, since the width of the critical distribution is non-zero, the conductance is not the self-averaged quantity at the critical point. The statistical character of the conductance opens new problems in the scaling theory. First, we have to prove that both mean values, $\langle g \rangle$, and $\langle \ln g \rangle$ obey scaling relations (138). Then, it would be useful to prove the same for all cummulants of the conductance. This is, of course, an unsolvable task.

The first step in the verification of the single parameter scaling theory is to understand the statistical properties of the conductance in the critical and localized regime.

10   Statistical properties of the conductance in the critical regime

The statistical properties of the conductance at the critical point were discussed by Shapiro, [75, 101]. With the use of the Migdal-Kadanoff renormalization, he studied the size dependence of the conductance distribution and he proved that the critical conductance distribution, $p_c(g)$, is universal, independent of the system length. The later works [103] however showed that the Migdal-Kadanoff renormalization overestimates the conductance fluctuations, and is therefore not suitable for a quantitative description of the critical conductance distribution.

In dimension $d = 2 + \epsilon$, the non-universality of higher order conductance cummulants has been found analytically [12] to be

$$\langle \delta g^n \rangle = \begin{cases} \epsilon^{n-2} & n < n_0 = \epsilon^{-1} \\ \sim L^{\epsilon n^2 - n} & n > \epsilon^{-1}. \end{cases} \tag{145}$$

Expression (145) states that the higher order cummulants, $n > n_0 = \epsilon^{-1}$, depend on the size of the system. This seems to be in contradiction with universality of the critical distribution. This discrepancy was explained in Ref. [104]. Starting from the known cummulants, given by Eq. (145), the critical conductance distribution was derived. It was shown that $p_c(g)$ is indeed universal in the limit of the infinite system size. The non-universality of higher cummulants follows from the form of the critical distribution. For small ϵ, the bulk of $p_c(g)$ is approximately Gaussian near the mean value $\langle g \rangle$. The parameters of the Gaussian peak,

$$\langle g \rangle \sim \epsilon^{-1} \tag{146}$$
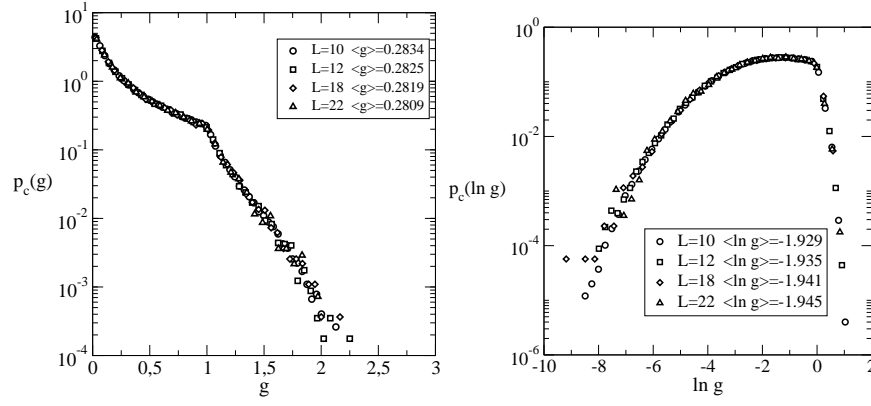
Fig. 39. The critical conductance distribution for the 3d Anderson model. The data for the samples L^3 with $10 \leq L \leq 22$ are shown. Statistical ensembles of $N_{\text{stat}} = 10^6$ (20000) sample for $L = 10$ ($L = 22$), respectively were used to create the distribution. Left: the distribution of the conductance, right: the distribution of the *logarithm* of the conductance. The legends present the mean values, which should be independent of the system size at the critical point. Note the non-analytical behavior of the distribution at $g = 1$.

and

$$\text{var } g \sim \epsilon^0, \tag{147}$$

but $p_c(g)$ possesses long tails for large values of g,

$$p_c(g) \sim g^{1-2/\epsilon}. \tag{148}$$

The power-law behavior of $p_c(g)$ explains the non-universality of higher cummulants, $\langle \delta g^n \rangle$, which are not defined for $n > 2/\epsilon$.

These analytical results were derived only for dimensions close to 2, for $\epsilon \ll 1$. Any attempt to apply them to the 3d system fails. For instance, Eq. (148) predicts that $p_c(g)^{(d=3)} \sim g^{-3}$ for large g, which is clearly not realistic. The most relevant information about the form of the critical conductance distribution was therefore obtained from numerical simulations [102, 105–108] based on the formula

$$g = \text{Tr } t^\dagger t = \sum_a \frac{1}{\cosh^2(x_a/2)}, \tag{149}$$

already used in the diffusive regime.

In Fig. 39 we plot the critical conductance distribution for the 3d Anderson model. We see that $p_c(g)$ does not depend on the system size. This is what we expect if the scaling theory really works.

The form of $p_c(g)$ is rather unusual. Numerical data enables us to understand its main properties. It turns out that it is useful to study also the distribution of the logarithm of the conductance, $p(\ln g)$, shown in the right panel of Fig. 39.
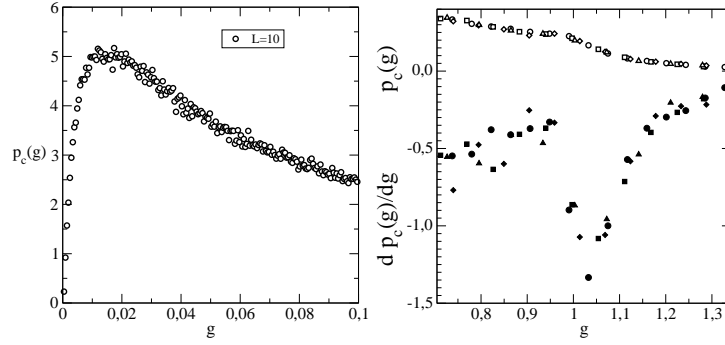
Fig. 40. Details of the critical probability distribution for the 3d Anderson model. The left figure proves that $p_c(g) \to 0$ when $g \to 0$. The right panel shows both the distribution, $p_c(g)$ and its first derivative, $\partial p_c(g)/\partial g$ in the neighborhood of $g = 1$. Numerical data indicate the non-analytical behavior of the distribution at $g = 1$.

First, we need to know the form of $p_c(g)$ for small g. The behavior of $p_c(g)$ for small g can be easier obtained from the distribution of the $\ln g$. In the right panel of Fig. 39 we see that

$$\ln p_c(\ln g) \sim -(\ln g)^2 \quad g \ll 1. \tag{150}$$

Since $p_c(g)dg = p_c(\ln g)d(\ln g)$, we immediately obtain that [105]

$$p_c(g) \propto \exp\left[-(\ln g)^2 - \ln g\right] \quad g \ll 1, \tag{151}$$

so that $p_c(g) \to 0$ when $g \to 0$. The left panel of Fig. 40 shows details of the critical distribution for $g < 0.1$. The data, collected from the ensemble of the $N_{\text{stat}} = 10^7$ samples of the size $L = 10$ confirm that $p_c(g)$ indeed decreases to zero when $g \to 0$. However, the probability to obtain small values of g is very small.

Other properties of the critical distribution, namely the form of the tail for large values g and the non-analytical behavior in the neighborhood of $g = 1$, are more convenient to analyze in terms of parameters x_a [102, 105], introduced in Eq. (68). We remind that x_a determine the eigenvalues of the matrix $t^\dagger t$ and that the conductance is expressed in terms of x_a by the following formula

$$g = \sum_a \frac{1}{\cosh^2 x_a/2}. \tag{152}$$

Numerical data [91, 102, 128] showed that the spectrum of x_a consists of two qualitatively different parts. In the lower part of the spectra, for $a \leq L$, $\langle x_a \rangle$ are independent on the size of the system

$$\langle x_a \rangle = \text{const} \qquad a < L. \tag{153}$$

This is what we expect, since the mean conductance, $\langle g \rangle$, is size-independent at the critical point. The size independence of x_a was confirmed numerically in Ref. [128] and will be discussed in
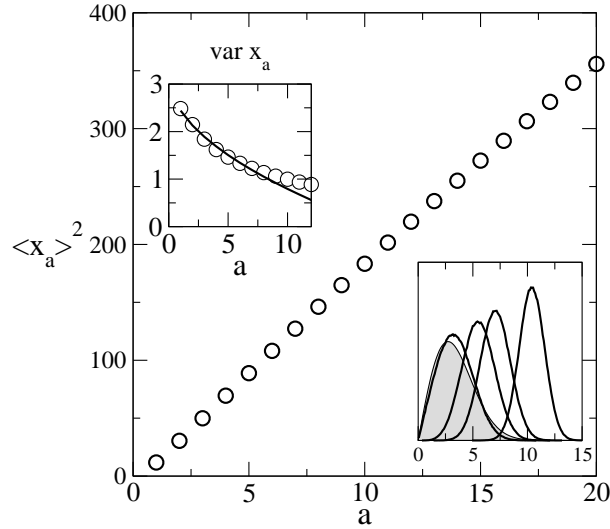
Fig. 41. The index dependence of the parameters x_a at the critical point in the 3d Anderson model. The data confirm that $\langle x_a \rangle^2 \propto a$. Left inset shows that the variance, var x_a decreases as a function of index a. The solid line is a fit $a_0 + a_1 x^\alpha$ with $\alpha = 0.51$. This gives an estimate of the variance, var $x_a \approx a^{-1/2}$. Right inset shows the probability distributions $p(x_1)$, $p(x_2)$, $p(x_3)$ and $p(x_6)$. Note, the distribution $p(x_1)$ is similar to the Wigner distribution, $p_1(x)$, shown by the shaded area.

Sect. 12.3. Contrary to the metallic regime, where $\langle x_a \rangle \propto a$ (Eq. 320), at the critical point we obtain (Fig. 41) that

$$\langle x_a \rangle^2 \propto a. \tag{154}$$

It is important to note that Eq. (154) is valid only for $a \leq L$. The upper part of the spectra, with $a > L$, is L dependent with $\langle x_a \rangle \propto a$. Since this upper part of the spectra does not contribute to the conductance, we will concentrate only on the lower part, given by Eq. (154).

Insets of Fig. 41 show that the distribution of x_1 is similar to the Wigner distribution p_1, and all higher parameters x_a, with $a > 2$ are distributed according to the Gaussian distribution with decreasing variance,

$$\text{var } x_a \sim a^{-\alpha}, \tag{155}$$

where the exponent α is close to 1/2 [91].

We use the statistical properties of x_a to estimate the behavior of the critical distribution for large g. From the expression for the conductance, given by Eq. (152) we see that we can obtain a large value of the conductance,

$$g \sim N \gg 1, \tag{156}$$
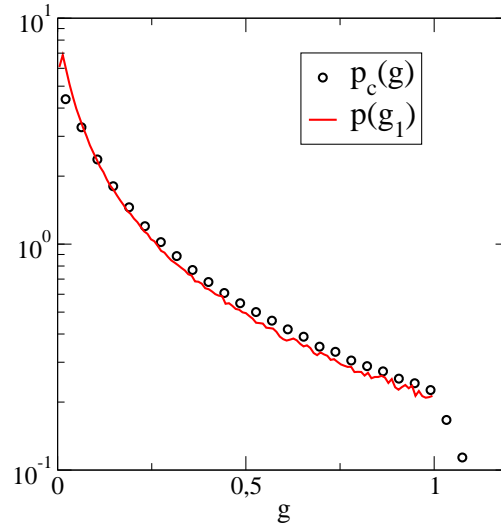
Fig. 42. Comparison of the critical conductance distribution with distribution $p(g_1)$ of the contribution of the first channel.

only when all x_a, $a = 1, 2, \ldots, N$ are small. However, since all parameters x_a are distributed with the Gaussian distribution, we obtain that the probability to have $x_N \ll 1$ is

$$\exp -\frac{\langle x_N \rangle^2}{\mathrm{var}\, x_N} \sim \exp -g^{1+\alpha}. \tag{157}$$

In Eq. (157) we used that $\langle x_N \rangle^2 \propto N = g$ and we estimated the variance $\mathrm{var}\, x_N \sim N^{-\alpha}$ with the use of Eq. (155). Eq. (157) confirms that $p_c(g)$ decreases *faster* than exponentially for large g. This is confirmed by our numerical data. The probability to have $g > 1$ is very small (less than 3%). The higher values of g appear with marginal probability. For instance, in an ensemble of $N_{\mathrm{stat}} = 10^7$ samples, we found only 470 samples with conductance $g > 2$ and only one with $g > 3$.

The most surprising property of the critical conductance distribution is that $p_c(g)$ seems to be non-analytical at $g = 1$. The right Fig. 40 shows that the first derivative, $\partial p_c(g)/\partial g$, is discontinuous at $g = 1$. The origin of the non-analyticity can be again explained from the spectra of the parameters x_a. The numerical data, for mean values, $\langle x_1 \rangle = 3.42$, $\langle x_2 \rangle = 5.52$, and $\langle x_3 \rangle = 7.07$, indicate that the conductance is given mostly by the first term, $g_1 = \cosh^{-2}(x_1/2)$. Indeed, the distribution $p(g_1)$ is a very good approximation to $p_c(g)$ for $g < 1$, as shown in Fig. 42. Since $g_1 \leq 1$, the function $p(g_1)$ has a cutoff when $g \to 1^-$. It is difficult to estimate the contribution of higher channels but it is reasonable to expect that the non-analyticity of the distribution survives also when the contribution of higher channels is included. This is supported by analytical calculations of Muttalib et al [109,110], who reported the non-analytical form of the conductance distribution in the weakly disordered quasi-1d systems with the mean conductance $\langle g \rangle \sim 1$.
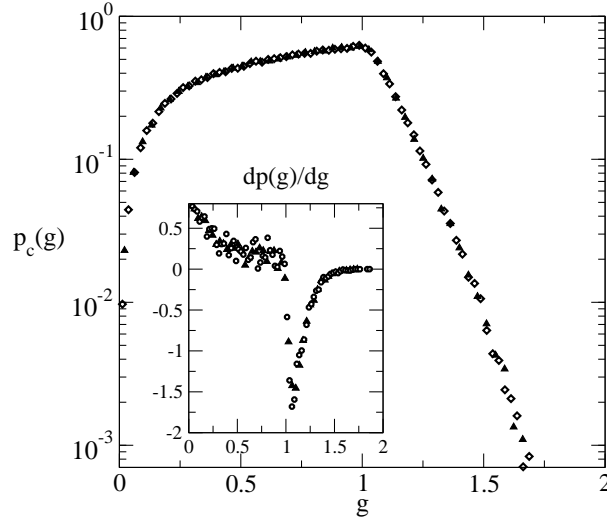
Fig. 43. The critical conductance distribution for the 2d Ando model. The different symbols correspond to the size of the system $L = 82$ and $L = 200$. The data prove that $p_c(g)$ is system size invariant. Note the logarithmic scale on the vertical axis. Inset describes the non-analyticity of the distribution at $g = 1$. The mean value of the conductance is $\langle g \rangle_c = 0.71 e^2 / h$. [54]

The above properties of the critical conductance distribution can be found also in other models, where the critical conductance is close to or less than to 1. For instance, Fig. 43 shows $p_c(g)$ for the 2d Ando model. The non-analyticity at $g = 1$ is clearly visible, too.

10.1   Properties of the critical conductance distribution

The properties of the critical conductance distribution are important for the formulation of the scaling theory. Besides the system size independence of $p_c(g)$, we need to understand its universality, i.e. how the form of $p_c(g)$ depends on microscopic details of the model, on the physical symmetry and on the dimension of the system. Especially the dimension dependence of $p_c(g)$ is important for the comparison of the theoretical predictions with numerical data.

As expected, the critical conductance distribution is independent of the size of the system. This is confirmed by numerical data shown in Figs. 39 and 43. For a given universality class, it does not depend on microscopic details of the model. This was confirmed in Refs. [111, 112] where the critical distribution, $p_c(g)$ was calculated for the 2d and 3d models with various distributions of random disorder. However, the form of $p_c(g)$ does depend on the symmetry class [107]. Also, the form of $p_c(g)$ depends on the topology of the lattice. For instance, $p_c(g)$ for the 3d Anderson model with triangular, hexagonal and rectangular lattice in the transversal direction possess different critical distributions $p_c(g)$ [113].

Surprising was the observation that $p_c(g)$ depends also on the boundary conditions in the directions perpendicular to the propagation [86, 114, 115]. This result is, however, consistent
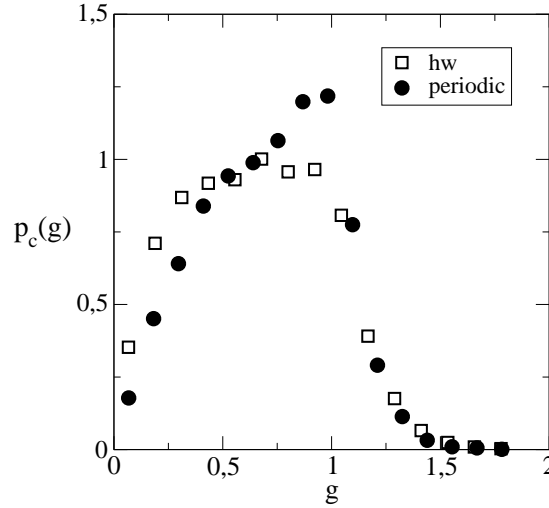
Fig. 44. The critical conductance distribution for the 2d Ando model with the hard wall and periodic boundary conditions in the direction perpendicular to the boundaries. The critical conductance is $\langle g \rangle = 0.655\ (0.71)\ e^2/h$, and the variance var $g = 0.43\ (0.36)\ (e^2/h)^2$ for the hard wall (periodic) boundary conditions, respectively.

with our understanding of the conductance as a measure of the sensitivity of eigenenergies to the boundary conditions [60]. We remind the reader that also the values of the universal conductance fluctuations depend on the boundary conditions. Nevertheless, the difference in the form of $p_c(g)$ is surprisingly large for the 3d Anderson model [115], Also, the mean values $\langle g \rangle_c$, are considerably different, being 0.445 (0.280) (e^2/h) for the periodic and hard wall boundary conditions, respectively [115]. In Fig. 44 we demonstrate the sensitivity to the boundary conditions for the 2d Ando model.

10.2 Dimension dependence of the critical conductance distribution

As discussed above, the analytical theories provide us only with the information about the critical conductance in systems with dimension close to the lower critical dimension, $d = 2 + \epsilon$. Since we do not expect that the analytical results could be applied also for $\epsilon = 1$, the numerical data for dimension $d = 3$ are not suitable for verification of the theory. Therefore, it might be interesting to calculate the critical conductance distribution on lattices with fractal dimension close to $d_c = 2$. This was done in Ref. [113].

By definition, the bifractal lattice [116] is linear in the direction of propagation and possesses the fractal transversal structure. Three fractals, discussed in Ref. [113] are shown in Fig. 45. For the analysis of critical phenomena on fractals, it is important to note that the "dimension" which is important for description of the critical phenomena is the *spectral* dimension of the lattice, not the fractal dimension, d_f. We remind the reader that spectral dimension, d_s, determines the
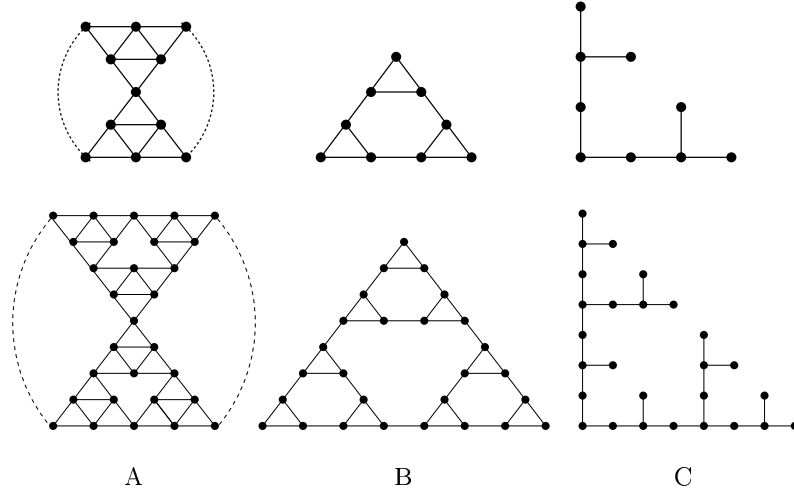
Fig. 45. Definition of three fractals used in the numerical analysis of the conductance distribution of fractals. Shown are the 2nd and the 3rd generations. All three fractals have the same fractal dimension, $d_f = \ln 3/\ln 2 \approx 1.58$. Fractals A and B have *spectral* dimension $d'_s = 1.365$, and fractal C has $d'_s = 1.226$. Note the different number of nearest-neighbor lattice sites. The bifractal lattice is created by combination of the fractal with the linear chain in the perpendicular direction. The spectral dimension of the bifractal is $d_s = d'_s + 1$. The number of lattice sites on fractal is 3^n in the nth generation, and the length along the linear chains is 2^n lattice sites.

low-frequency behavior of the phonon density,

$$\rho_{\text{phonon}}(\omega) \sim \omega^{d_s} \tag{158}$$

[116, 117], while the fractal dimension, d_f, determines an increase b^{d_f} of the "mass' (number of lattice points) when the scale of the system changes by a factor of b. Note that the spectral dimension of a regular system equals to its dimension, $d_s = d$.

All three fractals, shown in Fig. 45 have the same fractal dimension, $d_f = \ln 3/\ln 2 = 1.58$. Fractals A and B have the same spectral dimension, $d'_s = 1.365$, and fractal C has spectral dimension $d'_s = 1.226$, so that the spectral dimension is $d_s = d'_s = 2.365$ (2.226) for bifractals A and B (C), respectively. In Fig. 60 we will show that the critical exponent, ν is indeed a function of the spectral dimension only.

Critical conductance distributions are shown in Fig. 46. We see that the mean conductance increases when $d_s \to 2^+$ and the distribution $p_c(g)$ is similar to Gaussian, in agreement with theoretical prediction [104]. However, the width of the distribution, measured by the variance, var g, increases when $\epsilon \to 0$. This seems to be in contradiction with the analytical formula (147). The numerical data cannot confirm the power law decrease of the distribution, given by Eq. (148) for large values of g.

For completeness, we show in the right panel of Fig. 46 the critical distribution $p_c(\ln g)$ for the 4d Anderson model. The distribution is similar to that for the 3d system, including the non-
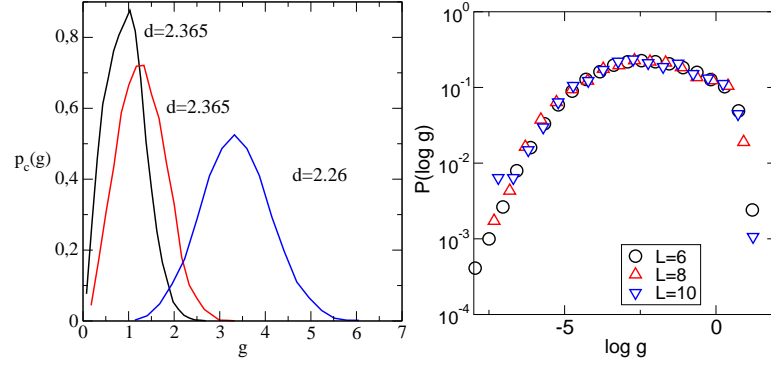
Fig. 46. Left: The critical conductance distribution for three bifractals, shown in Fig. 45. The legends give the spectral dimension, d_s, of the lattice. Critical distribution is close to Gaussian distribution when $d \to 2$. The power-law tail, predicted by the theory [104], is not observable in numerical simulations. Note, although two bifractals, A and B, have the same spectral dimension, the corresponding critical distributions differ from each other. This is because $p_c(g)$ depends on the topology of the lattice. Note also, the non-analyticity of the conductance distribution around $g = 1$ disappears, since more than one propagating channel contribute to the conductance in these models. Right: Distribution of $p_c(\ln g)$ for the 4d Anderson model.

linearity at $g = 1$. Similar to 3d models, the main contribution to the conductance is given by the first channel.

11   Localized regime

It is commonly believed that the distribution of the logarithm of the conductance is Gaussian, with the mean value

$$\langle \ln g \rangle = -2L/\lambda. \tag{159}$$

The variance,

$$\text{var } \ln g \propto -\langle \ln g \rangle \tag{160}$$

should be proportional to $-\langle \ln g \rangle$, with the coefficient of proportionality close to 2. This behavior is deduced from the analysis of the DMPK equation, discussed in Appendix B. It is argued that since all parameters $x_a \propto L_z$, the difference between x_2 and x_1 becomes large enough so that the contributions g_2, g_3 ... of higher channels become negligible in comparison with $g_1 = \cosh^{-2}(x_1/2) = \exp -x_1$. Since x_1 possesses the Gaussian distribution in the limit of large L_z, it is expected that the logarithm of the conductance, $\ln g \approx \ln g_1$ should posses a Gaussian distribution, too.

This argument is supported by the numerical data for the *normalized* difference, $\delta_{21} = x_2 - x_1$, shown in Fig. 47. As expected, $p(\delta_{21})$ differs considerably from the Wigner distribution, and is more similar (although not identical) to the Poisson distribution [20]. Although the
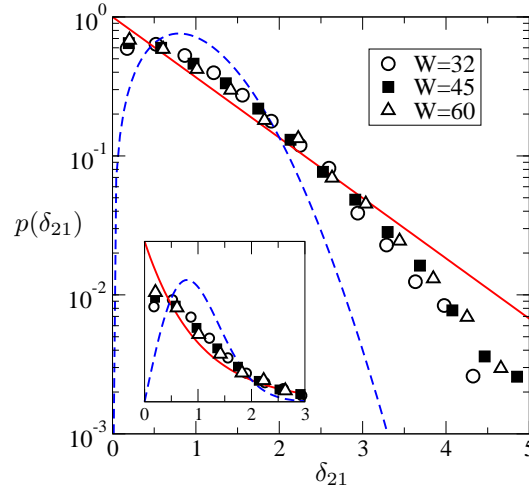
Fig. 47. The probability distribution of the *normalized* difference $\delta_{21} = x_2 - x_1$ for the 3d Anderson model ($L = 10$) compared with the Wigner distribution p_1 (dashed line) and Poisson distribution (solid line). Inset shows the same data in the linear scale [20].

deviations from the Poisson distribution indicate that x_2 and x_1 are not statistically independent, we expect that their correlation is small. Then, the contributions g_1 and g_2 can be assumed to be almost statistically independent and we can split the spectrum of the transfer matrix to the first eigenvalue, x_1, which determines the magnitude of the conductance, and the rest of the spectra, which have almost negligible contribution to g.

However, the above arguments are valid only in the quasi-1d weakly disordered systems (see Appendix B.3). As shown in Fig. 48, the probability distribution $p(\ln g)$ for the strongly disordered samples is not Gaussian. The origin of the difference between the strongly disordered 3d systems and weakly disordered quasi-1d systems lies in the spectra of parameters x_a. Contrary to the weakly disordered systems, parameters $\langle x_a \rangle$ do not increase linearly with a, but fulfill the relation

$$\langle x_a \rangle = \langle x_1 \rangle + \Delta_{a1}. \tag{161}$$

As is shown in Fig. 49, Δ_{a1} depends neither on the system size nor on the disorder.

Apart from the deviation from the Gaussian form, $P(\ln g)$ possesses also the non-analyticity at $\ln g = 0$, shown in Fig. 50. The origin of this non-analyticity is the same as in the case of the critical distribution, $p_c(g)$. The contribution to the conductance comes mostly from the first channel and the chance to have $g > 1$ is negligibly small.

More important is the question whether the variance is an unambiguous function of the mean value. This must be so if the one parameter scaling holds. The verification of the ambiguity is difficult in 2d and 3d. In 1d, analytical calculations [119] showed that there is no universal relation between the mean and the variance of x. This was confirmed by numerical simulations [20,120] of strongly disordered 1d systems, indicating the existence of the second relevant length scale in the strongly localized regime.
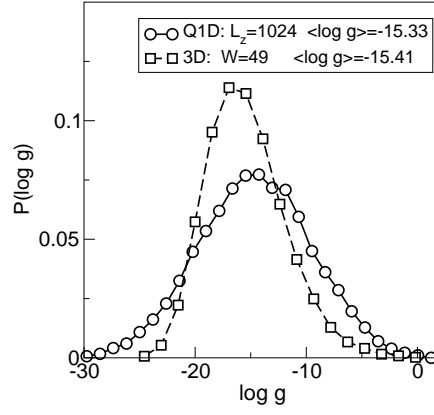
Fig. 48. Comparison of the conductance distribution for the quasi-1d weakly disordered system in the localized regime and strongly disordered 3d system. While the distribution of $p(\ln g)$ is Gaussian in the quasi-1d system, for the 3d system, the distribution is asymmetric and narrower. The size of the quasi-1d system is $8 \times 8 \times L_z$ and disorder $W = 4$. The size of the 3d system is 8^3 and the strength of the disorder, W, is chosen to have the same value of the mean logarithm of the conductance [118].
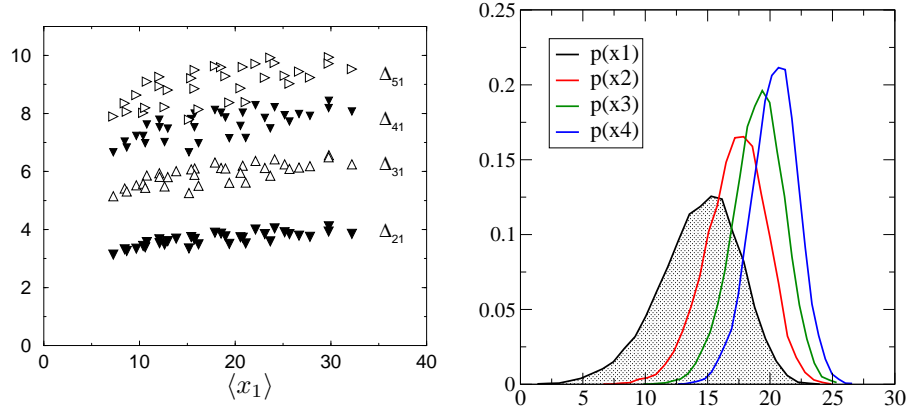
Fig. 49. Left: The differences $\Delta_{a1} = \langle x_a - x_1 \rangle$ for the 3d Anderson model [118]. Right: The probability distribution $p(x_a)$ for the strongly disordered cube ($W = 20$, $L = 18$). These data should be compared with those in Fig. 73 which shows the distribution $p(x_a)$ for long weakly disordered quasi-1d systems. Note, the mean values, $\langle x_a \rangle$ do not increase linearly. Also, the width of the distribution $p(x_a)$ decreases when a increases, similar to the distributions of parameters x at the critical point, shown in Fig. 41.

The second relevant length scale was indeed found in 1d systems [170] and estimated analytically by the formula

$$\ell_s = \frac{1}{\sin \pi \rho(E)}, \tag{162}$$
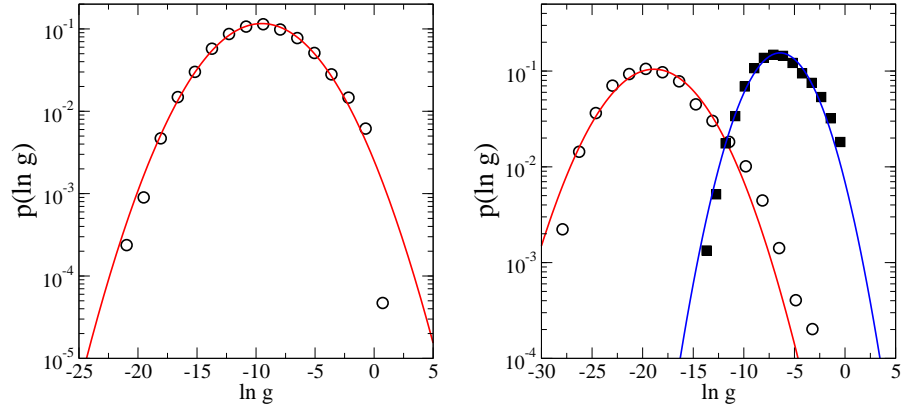
Fig. 50. The statistical distribution of the logarithm of the conductance in the strongly disordered squares (left) and cubes (right). The solid lines are Gaussian fits with the same mean and variance. Left: The 2d Anderson model, $W = 6$, $L = 200$, $\langle \ln g \rangle = -9.51$, $\mathrm{var}\ln g = 11.78$. Note the sharp decrease of the distribution at $\ln g = 0$. Right: The 3d Anderson model, $W = 32$, $L = 18$. $\langle \ln g \rangle = -18.88$, $\mathrm{var}\ln g = 14.57$ and $W = 14$ and $L = 10$ ($\langle \ln g \rangle = -6.42$, $\mathrm{var}\ln g = 6.63$).
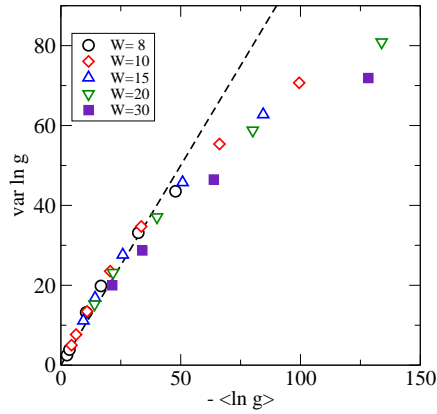
Fig. 51. The variance, $\mathrm{var}\ \ln g$ as a function of the mean value, $\langle \ln g \rangle$ for the 2d Anderson model. The expected linear relation, (160), is valid only for rather small values of $\langle \ln g \rangle$ [118].

where $\rho(E)$ is the density of states. Single parameter scaling is expected to be valid only when $\lambda > \ell_s$. This is not fulfilled in the band tail, where the density of states is small and, consequently, ℓ_s is large. The second relevant length scale was reported also in 2d systems in Ref. [121].

Figure 51 shows that the variance, $\mathrm{var}\ \ln g$ is *not* a linear function of the mean value, $\langle \ln g \rangle$. This was observed already in [120] for the 1d system. Very recently [121, 122], the non-linear

relation between the mean value and the variance of $\ln g$,

$$\text{var } \ln g \propto \begin{cases} (-\langle \ln g \rangle)^{2/3} & d = 2 \\ (-\langle \ln g \rangle)^{2/5} & d = 3 \end{cases} \tag{163}$$

was numerically observed.

Another test of the single parameter scaling was reported in Refs. [123, 124], where the electron wave function of large 2d disordered system was calculated numerically. The statistical distribution of the logarithm of the wave function at the distance r from the center of the lattice was discussed. The numerical data was fitted to the distribution function

$$H(-\ln |\Psi(\vec{r})|, r) = \frac{1}{\sqrt{2\pi\sigma}} \exp -\frac{(\ln |\Psi| + r/\lambda)^2}{2\sigma}. \tag{164}$$

The Gaussian form of the distribution H seems to be natural, since we expect that the wave function decreases exponentially at large distance. This decrease is controlled by the localization length, λ. Surprisingly, fitting the numerical data to the distribution (164) led to the r-dependent localization length, $\lambda(r)$. This result was interpreted as a failure of the scaling theory.

However, an assumption that the distribution function H, given by Eq. (164) is exactly Gaussian, is not correct. Indeed, the Gaussian distribution possesses a long tail for both negative and positive values of its argument, but the value of $-\ln |\Psi(\vec{r})|$ can not be negative if the wave function, Ψ, is normalized. Therefore, the distribution $H(x, r)$ must converge to zero when $x = -\ln |\Psi(\vec{r})| \to 0^+$, in the same way as the distribution $p(x)$, shown in Fig. 20. We believe that the fit of numerical data to the correct distribution function will recover the single parameter scaling.

11.1   3d versus quasi-1d systems

As discussed above, the statistical properties of the conductance in the 3d systems require numerical simulations. On the other hand, similar transition from the metallic to localized regime can be studied in weakly disordered quasi-1d systems. Indeed, such a system exhibits metallic behavior if the length of the system, L_z, fulfills the relations

$$\ell \ll L_z \ll N\ell \tag{165}$$

where ℓ is the mean free path and N is the number of channels. The conductance of such a system is $N\ell/L_z \gg 1$. By increasing L_z, the conductance decreases. There is an interval of L_z, where $g \sim 1$. Further increase of the system length draws the system into the localized regime, where $g \sim \exp -2L/\lambda$, where $\lambda = n\ell$ is the localization length.

This scenario is very similar to the metal-insulator transition. Of course, we do not have a critical behavior in quasi-1d system (there is no divergence of the correlation length), but it is reasonable to expect that the conductance distributions, obtained in all three regimes, $g \gg 1$, $g \sim 1$ and $g \ll 1$, might mimic the main properties of the conductance distributions in the metallic, critical and localized regime. The advantage of quasi-1d systems is that they might be, at least within some approximations, solved analytically.

The above idea was developed by Muttalib *et al.* [109, 110, 125]. By solving the DMPK equation in the regime of $g \sim 1$, they indeed found that the "critical" conductance distribution
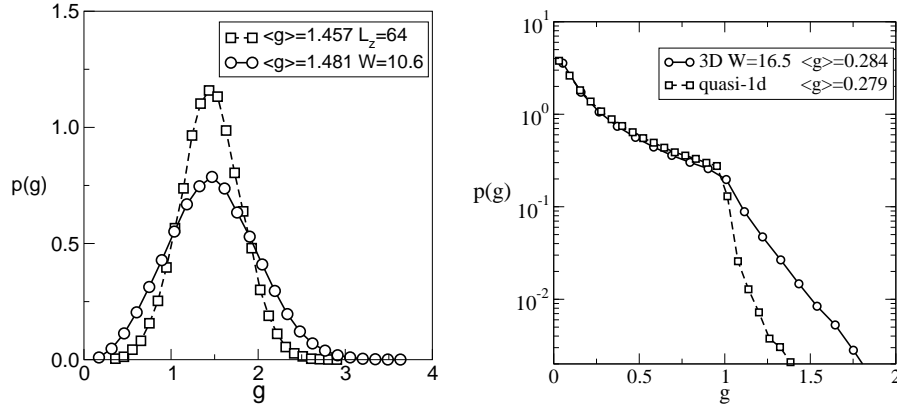
Fig. 52. Comparison of the conductance distribution for the quasi-1d systems (squares) and cubic systems (circles) [118]. Left: The metallic regime: $p(g)$ is Gaussian in both systems, but the widths of the distributions differ. This is consistent with our data for the universal conductance fluctuations, given in Table 1, since var g of quasi-1d systems differs from that of 3d. Right: The critical conductance distribution for the 3d Anderson model compared with the distribution of the conductance for quasi-1d weakly disordered ($W = 4$) system of the size $8 \times 8 \times 210$. Although the mean conductance is the same, the distributions differ in the region $g > 1$. The reason for this difference is that the difference, $\langle x_2 - x_1 \rangle = \langle x_1 \rangle$ in the quasi-1d system, while it is much smaller in the 3d system, as shown in Fig. 49. The non-analyticity of the distribution for the quasi-1d system was explained and qualitatively described in Ref. [110].

possesses non-analyticity close to $g = 1$ [110]. Also, in the localized regime, they observed that the distribution $p(\ln g)$ drops down at $\ln g = 1$. Similar results were observed numerically in Ref. [126] where the transport in the quasi-1d systems with a corrugated surface was investigated and the conductance distribution in the "critical" regime was studied.

However, these results provide us only with a qualitative description of the conductance distributions in the true critical regime and in the insulator. In the previous Section, we showed that the localized regime in the 3d system differs qualitatively from the localization in the weakly disordered quasi-1d systems. The origin of this difference lies in the different form of the spectra of parameters x_a.

To demonstrate the difference between the two insulating regimes, we showed in Fig. 48 the distribution $p(\ln g)$ for the 3d and the weakly disordered quasi-1d systems. Here, we compare in Fig. 52 the conductance distributions for both systems in the metallic and critical regime (Fig. 52). For a quantitative description of the critical and localized regimes, we need to study the systems with strong disorder.

12 Numerical scaling analysis

Since the analytical calculations are possible only in the limit of the dimension $d = 2 + \epsilon$ ($\epsilon \ll 1$), numerical simulations provides us at present with the most relevant information about the critical regime of the Anderson transition.

The main problem of the numerical scaling analysis is the calculation of critical exponent, ν in various physical models. Universality of the critical exponent for a given symmetry class and dimension is interpreted as evidence of the validity of the single parameter scaling.

Historically, the first numerical simulations were performed for quasi-1d system [17, 127]. The scaling of the smallest Lyapunov exponent was proved and the critical exponent, ν was found. Later, scaling of other variables was analyzed, mostly with the motivation to treat the true 3d systems and 2d systems with unitary and symplectic symmetry. We will discuss in this Section the scaling analysis of the conductance, conductance distribution and level statistics.

12.1   Scaling of the smallest Lyapunov exponent

Pichard and Sarma [127] were the first who proposed to use the finite size scaling analysis for the calculation of the critical parameters of the Anderson model. They considered the quasi-1d system of the size $L^{d-1} \times L_z$ ($d = 2$ and 3) and calculate numerically the *smallest* Lyapunov exponent, γ_1. As discussed in Appendix D.2, the Schrödinger equation for the Anderson model in the quasi-1d geometry can be written in the form

$$\begin{pmatrix} \Psi_{n+1} \\ \Psi_n \end{pmatrix} = M_n \begin{pmatrix} \Psi_n \\ \Psi_{n-1} \end{pmatrix}, \tag{166}$$

where M_n is the transfer matrix for the nth slice of the system,

$$M_n = \begin{pmatrix} E - \mathcal{H}_n & -1 \\ 1 & 0 \end{pmatrix}. \tag{167}$$

By multiplication of the transfer matrices, we obtain that the exponential decrease of the wave function along L_z is given by eigenvalues Λ_a of the matrix

$$M_{L_z} = \prod_{n=1}^{L_z} M_n. \tag{168}$$

Oseledec's theorem states that in the limit of $L_z \to \infty$, all Lyapunov exponents, γ_a of the matrix M_{L_z} posses the Gaussian distribution with the variance proportional to the mean value. The smallest (in absolute value) Lyapunov exponent, γ_1, determines the localization length in the z direction.

Since $\gamma_1 \propto L_z$, it is more convenient to use the parameter

$$\Lambda = \frac{L_z}{L\gamma_1}. \tag{169}$$

In this paper, we discuss the scaling behavior of parameter z_1,

$$z_1 = \frac{2}{\Lambda} = \frac{2L\gamma_1}{L_z}, \tag{170}$$

which is closely connected to parameter x_1, used in the previous Section for parametrization of the contribution to the conductance. From Oseledec's theorem it follows that z_1 converges in the limit of $L_z \to \infty$ to the mean value, and var $z_1 \propto L/L_z$. Consequently, the difference between the numerically calculated value of z_1 and the mean value is $\propto L_z^{-1/2}$ so that z_1 is free from any
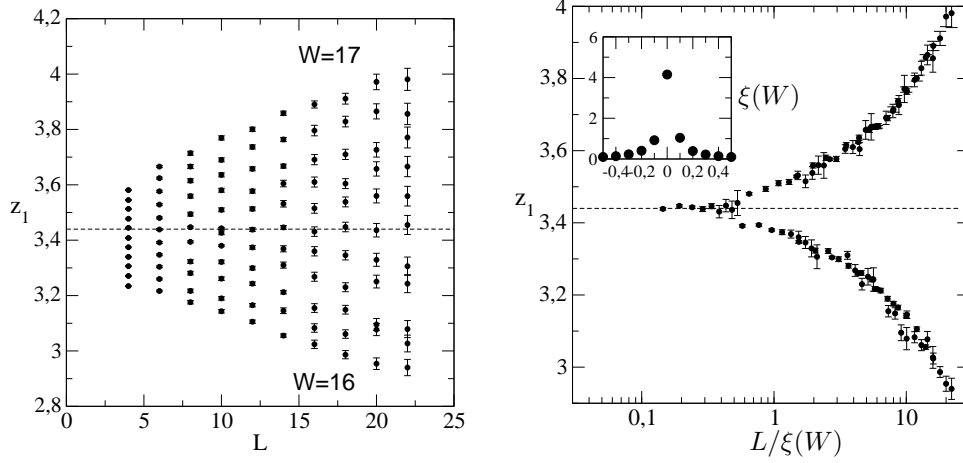
Fig. 53. Left: The L-dependence of the variable $z_1 = 2L\gamma_1/L_z$ for the 3d Anderson model. The data was calculated for the quasi-1d systems, $L^2 \times L_z$ and for disorder increasing from $W = 16$ (bottom) to $W = 17$ (top) with step $\Delta W = 0.1$. The length L_z is sufficiently long to guarantee the relative accuracy of 0.2% for small L, and of 1% for $L = 22$. The dashed line is the fit of the critical value $z_{1c} \approx 3.44$ [128]. Right: The same data plotted as a function of $L/\xi(W)$, Eq. (172). Note the logarithmic scale on the horizontal axis. The function F has two branches, the lower branch for the metallic regime, and upper one for the insulating regime. The data with $L = 4$ were excluded from the data sets, because they do not lie on the universal curve due to the finite size effects. Inset shows divergence of the correlation length, $\xi(W)$, at the critical point. Note, ξ is calculated up to a multiplicative factor.

statistical problems provided that the system is sufficiently long. Of course, z_1 is a function of the disorder, W, energy, E and the system width, L.

For a sufficiently large width L of the system, we can estimate the disorder and L dependence of z_1 from basic physical considerations. It is reasonable to expect that when the system is in the localized regime, $W \gg W_c$, then z_1 converges to the ratio $2L/\lambda$. On the other hand, in the metallic regime, $W \ll W_c$, we have that the spectrum of z_a is linear, as given by Eq. (320), of Appendix C.1. Therefore, $z_1 = \frac{2L}{N\ell}$, where N is the number of channels. Since $N \propto L^2$ in the case of the 3d Anderson model we obtain $z_1 \sim L^{-1}$ in the metallic regime. Finally, at the critical point, we expect that $z_1 = \text{const}$.

The above consideration can be summarized as follows:

$$z_1 = 2\gamma_1 \frac{L}{L_z} \sim \begin{cases} L^{-1} & W < W_c \\ \text{const} & W = W_c \\ L/\lambda & W > W_c. \end{cases} \tag{171}$$

Relation (171) enables us to identify the critical point from the numerical data. The left panel of Fig. 53 presents the numerical data for the quasi-1d Anderson model $L^2 \times L_z$. We indeed see that for disorder $W > W_c$, z_1 increases when L increases, while for $W < W_c$, z_1 decreases with L. From the L dependence of z_1, we estimate approximately the value of the critical disorder, $W_c \approx 16.5$ and the critical value, $z_{1c} = z_1(W = W_c) \approx 3.44$.
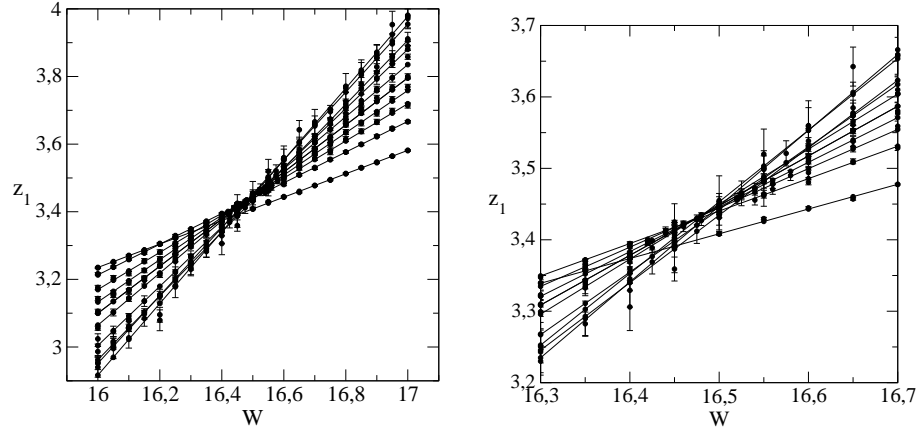
Fig. 54. Left: The same data as in left panel of Fig. 53 but plotted as a function of the disorder W. Solid lines are linear fits, given by Eq. (174) for $4 \ll L \ll 22$. In the ideal case, all lines have a common crossing point. This never happens for numerical data, as shown in the detailed plot in the right panel. The deviations from the universal scaling relation, given by Eq. (174) are either due to the finite size effects, discussed in Sect. 12.2, or due to the insufficient accuracy of numerical data.

The next step in the scaling analysis was done by MacKinnon and Kramer in Ref. [17]. They assumed that z_1 is a function of only one parameter,

$$z_1(L, W) = F(L/\xi(W)), \tag{172}$$

where $\xi(W)$ is the *correlation length*. Relation (172) follows from the assumption of the validity of single parameter scaling. The right panel of Fig. 53 shows that indeed all the data $z_1(L, W)$ lie on the universal curve.

Since $z_{1c} = z_1(W = W_c)$ does not depend on the system size, L, the correlation length must diverge at the critical point,

$$\xi(W) \propto |W - W_c|^{-\nu}. \tag{173}$$

Figure 54 confirms that $z_1 \propto (W - W_c)$ in the critical region. Therefore, if we expand the function $F(x)$ in the Taylor series, and keep only the first two terms, $F(x) = F(0) + Ax^\alpha$, we have that exponent $\alpha = 1/\nu$. Consequently, $z_1(L, W)$ is given in the critical region by the simple scaling equation,

$$z_1(L, W) = z_{1c} + A(W - W_c)L^{1/\nu}. \tag{174}$$

The fit of numerical data to Eq. (174) enables us to calculate both the critical exponent, ν, and critical disorder, W_c.

The easiest scaling analysis can be performed in the following two steps [129]. First, we can calculate the linear fit

$$z_1(L, W) = z_1^{(0)}(L) + W z_1^{(1)}(L). \tag{175}$$

Comparing the r.h.s. of Eq. (175) with Eq. (174), we have

$$z_1^{(0)} = z_{1c} - AW_c L^{1/\nu} \tag{176}$$

and

$$z_1^{(1)}(L) = AL^{1/\nu}. \tag{177}$$

Now, we can use Eq. (177) to calculate the critical exponent. Next, with the use of Eq. (177) we can write Eq. (176) in the form

$$z_1^{(0)} = z_{1c} - W_c z_1^{(1)}, \tag{178}$$

so that the slope of the linear fit $z_1^{(0)}$ *vs.* $z_1^{(1)}$ determines critical disorder, W_c.

The physical meaning of the correlation length, $\xi(W)$ can be estimated by comparing Eq. (172) with Eq. (171). Clearly, $\xi(W) = \lambda$ in the insulating side of the transition. Also, we find that $F(x) \sim x$ in the insulator and $F(x) \sim x^{-1}$ in the metal. Then, from the expression of $z_1 = 2L/(N\ell) = 2\langle g \rangle^{-1} = 1/(2L\sigma)$ (σ is the conductance) we find that in the metallic regime the correlation length $\xi(W) \propto \sigma^{-1}$ [17].

The correlation length $\xi(W)$ was first calculated numerically in Ref. [6]. The critical disorder, $W_c \approx 16.5$, and the critical exponent, $\nu \approx 1.50$, were calculated. These calculations were repeated by many other authors [130–132] with the use of various scaling analysis, and for increasing system size. Surprisingly, these new analysis did not bring any considerable corrections to the critical parameters, obtained in the pioneering work, [17]. At present, the most accurate estimation of the critical exponent is

$$\nu = 1.57 \pm 0.02, \tag{179}$$

obtained by very detailed scaling analysis of numerical data for z_1 in Ref. [133]. In Ref. [52], the phase diagram in the energy-disorder phase space (shown schematically in Fig. 6) was calculated for the first time for various distribution of random energies.

The scaling analysis [17] solved also the problem of the existence of the Anderson transition in the 2d orthogonal systems. It was shown, that there is no metallic phase, but the localization length, given by $\xi(W)$, is extremely large for small disorder (of orders of 10^6 lattice sites for $W = 1$. This result also explains why various previous works identify the Anderson transition also in 2d systems: these works analyzed only small systems [134]. The numerical data for the correlation length, $\xi(W)$ of the 2d Anderson model are given in Refs. [6,45] and for 3d Anderson model in Ref. [6].

12.2 Finite-size corrections

A more general formulation of Eq. (173) is

$$z_1 = F(\zeta_1, \eta_1, \eta_2, \ldots), \tag{180}$$

where η_i are further L-dependent parameters. They determine how z_1 depends on various microscopic parameters of the model, for instance distribution of the disorder, correlation length of the disorder, magnetic field. The one-parameter scaling is valid only if in the limit of $L \to \infty$ all

$\eta_i \to 0$. Only under this assumption, the equation (173) can be recovered, with $\zeta_1 = L/\xi(W)$. Thus, the assumption of the single parameter scaling requires that

$$\eta_i(L) \sim L^{-y_i}, \tag{181}$$

where y_i are irrelevant scaling exponents.

Although these parameters play no role for sufficiently large systems, they might influence the scaling analysis for smaller L. For instance, the one parameter scaling, given by Eq. (174) requires that all linear lines in Fig. 54 cross in one common point for $W = W_c$ and $z_1 = z_{1c}$. This is evidently not true for the smallest $L = 4$.

From Eq. (180) it follows that when L is not sufficiently large, one can generalize the scaling analysis by the inclusion of an additional term on the r.h.s. of Eq. (173). In the most simple case, when only one irrelevant parameter is considered, we obtain

$$z_1(L, W) = z_{1c} + A(W - W_c)L^{1/\nu} + BL^{-y}. \tag{182}$$

[135]. We can estimate the critical parameters by fitting the numerical data to the function (182). A more detailed scaling analysis might consider also higher order terms in powers of $\zeta_1 = (W - W_c)L^{1/\nu}$. The most detailed scaling analysis was performed in Ref. [133], where the numerical data were fitted to a function of 11 parameters.

Another possibility to eliminate the finite size scaling effects is to perform the scaling analysis with reduced data sets by omitting data for the smallest system size [54, 128]. Using only the numerical data for $L > L_{\min}$, one can study the $L_{\min}$ dependence of the critical parameters. We demonstrate this method in Fig. 55.

12.3 Scaling of higher Lyapunov exponents

As discussed in Sect. 10, the critical conductance distribution is not a self averaged quantity. Therefore, the scaling theory might, at least in principle, contain an infinite number of independent *relevant* parameters. To verify this possibility, it is worth to verify whether the higher Lyapunov exponents, z_a, scale in the same way as the z_1. This was done in Ref. [128] and reproduced in [112].

As shown in Fig. 56, already the most trivial scaling procedure, given by Eqs. (176-178), provides us with reliable evidence that the nine smallest Lyapunov exponents indeed scale with the same critical exponent, ν. This proves that all Lyapunov exponents can be expressed as a functions of only one variable, $L/\xi(W)$, with the same correlation length, $\xi(W)$.

Scaling of the higher Lyapunov exponent serves also as a nice example how the finite size effects influence the scaling analysis. As was shown in Fig. 55, the finite size corrections are almost negligible in the case of z_1, but they increase when a increases. The reason lies in the properties of the spectra of parameters z_a, or, equivalently, of x_a. In Section 10, we found that for a given size of the system, L, only parameters x_a with $a \leq L$ are size independent. The rest of the spectra depends on L. The same must hold for z_a. Therefore, only the data with $L > a$ are relevant for the scaling analysis of the higher Lyapunov exponent. In the case of z_9, only the data for $L \leq 12$ are relevant for the scaling analysis.
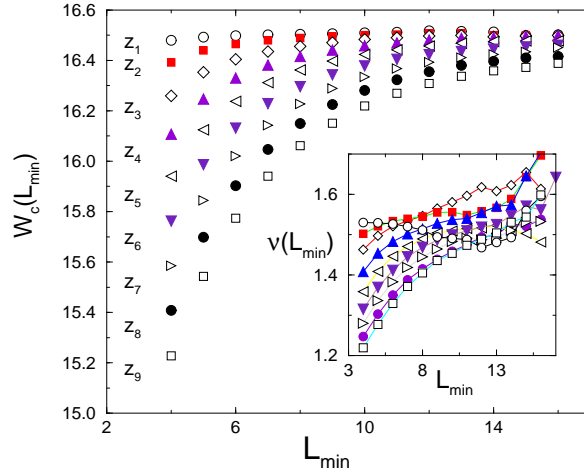
Fig. 55. The critical disorder, W_c, and the critical exponent, ν (inset) calculated from the finite size scaling analysis of the first 9 Lyapunov exponents [128]. The numerical data for $4 \leq L \leq 22$ were used. The critical disorder, W_c, converges to the 'correct' value, $W_c \approx 16.5$ when numerical data for smaller system size, $L < L_{\min}$ are not considered and $L_{\min}$ increases. The finite size effects are larger for the higher Lyapunov exponents, and may lead to wrong estimation of the critical parameters, when too small systems are considered. On the other hand, increase of $L_{\min}$ influences the accuracy of the numerical fits, especially in the case of the power fit (177) for the critical exponent. Note, the finite size effects are very small in the scaling analysis of the smallest Lyapunov exponent.
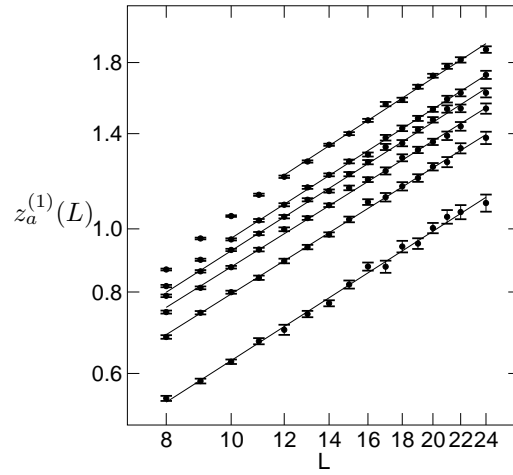
Fig. 56. Estimation of the critical exponent, ν, from the power fit, given by Eq. (177). Data for the smallest Lyapunov exponent, z_1, as well as for z_a, $a = 2 - 5$ and 9 are shown. We remind the reader that $z_a^{(1)}$ is the slope of the W dependence of z_a, defined by Eq. (176).

12.4 Scaling of the mean conductance

Numerical analysis of the quasi-1d systems provides us with the most accurate estimation of the critical parameters. Nevertheless, the use of quasi-1d geometry is rather artificial. It would be more suitable to prove the scaling of the conductance of the true d dimensional systems. This problem is rather complicated since, as we have seen in Sect. 10, the conductance is not self-averaged quantity in the critical region. We need therefore to calculate the mean value, $\langle g \rangle$ from the statistical ensemble of N_{stat} different cubes,

$$\langle\, g\, \rangle = \frac{1}{N_{\mathrm{stat}}} \sum_{i=1}^{N_{\mathrm{stat}}} g_i, \tag{183}$$

where g_i is the conductance calculated for the ith sample, and to estimate the accuracy of the mean value by using the relation

$$\mathrm{acc}\, g = \sqrt{\frac{\mathrm{var}\, g}{N_{\mathrm{stat}}}}. \tag{184}$$

Since both $\langle g \rangle$ and var g are of order of unity, we need $N_{\mathrm{stat}} \approx 10^6$ to reach the relative accuracy $\sim 0.1\%$.

The scaling formulas, presented in previous Sections, are valid for the scaling behavior of the mean conductance as well. Thus, we expect that the disorder and system size dependence of the mean conductance in the critical region is given by

$$\langle g \rangle = \langle g \rangle_c + A(W - W_c)L^{1/\nu}, \tag{185}$$

where $\langle g \rangle_c$ is the critical conductance. A similar equation can be constructed for $\langle \ln g \rangle$.

For the 3d Anderson model, the scaling of the mean conductance, $\langle g \rangle$, and of the typical conductance, $\exp\langle \ln g \rangle$ was numerically confirmed in Ref. [136]. The calculated critical exponent, $\nu = 1.57$, agrees with the result of the scaling analysis of the smallest Lyapunov exponent [133].

As an example of the scaling analysis of the conductance, we present the most recent numerical data for the mean conductance of the 2d Ando model [54]. The left panel of Fig. 57 shows the L-dependence of the mean conductance for fixed disorder. The metallic, localized and critical regime can be estimated in the same way as for z_1, with the only difference, that increasing $\langle g \rangle$ indicates the metallic phase in this case. The right panel of Fig. 57 shows the same data but as a function of L/ξ. The data confirms that indeed $\langle g \rangle = g(L/\xi)$ is a function of only one variable. Two branches of the function g correspond to two different transport regimes, metallic and localized.

The numerical proof of the scaling of the mean value is still not sufficient for the verification of whether or not one parameter scaling really works. Namely, we cannot exclude that the higher cummulants of the conductance do not scale. Of course, it is impossible to verify the scaling of all cummulants. Instead, we discuss in the next Section the scaling of conductance distribution, $p(g)$.

12.5 Scaling of the conductance distribution

In the previous Section we verified the scaling of the mean conductance, $\langle g \rangle$. However, we still cannot exclude the possibility that the length and disorder dependence probability distribution,
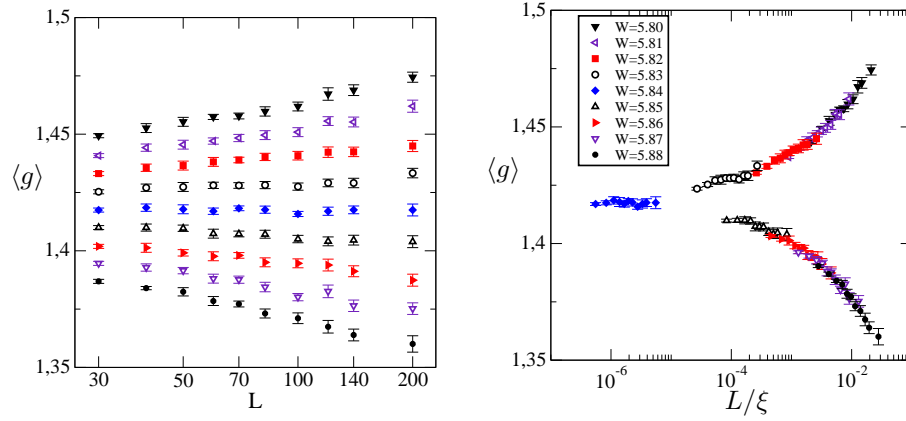
Fig. 57. Left: The L dependence of the mean conductance of the 2d Ando model. For disorder $W < W_c$, $\langle g \rangle$ increases with L, and for $W > W_c$, $\langle g \rangle$ decreases with L, in agreement with scaling hypothesis. Right panel shows the same data plotted as a function of only one parameter, $L/\xi(W)$ with $\xi \propto |W - W_c|^{-\nu}$. Appropriate choice of the correlation length, $\xi(W)$, for each value of the disorder, W enables us to scale all numerical data to one universal curve. Note the logarithmic scale on the horizontal axis.
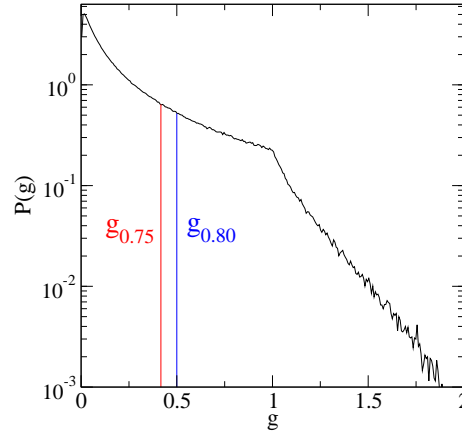
Fig. 58. Definition of percentiles. Note the logarithmic scale on the vertical axis.

$p(g)$, is determined by an infinite number of parameters, for instance all higher cummulants of the conductance. To prove that the entire conductance distribution scales as a function of only one parameter, the scaling of the percentiles, g_q was analyzed numerically in Ref. [137].

The percentile, g_q, is defined by the relation

$$q = \int_0^{g_q} p_L(g) \, \mathrm{d}g. \tag{186}$$

By definition (186), the probability that $g < g_q$, equals to q (Fig. 58).

In Ref. [137], the one parameter scaling of percentiles, g_q, was proved for four values of q, $q = 0.025, 0.17, 0.50$ (median) and 0.83. All four variables obey the one parameter scaling with the critical disorder W_c close to 16.5 and with the critical exponent $1.56 < \nu < 1.60$.

Suppose now that two percentiles, g_α and g_β, ($\alpha < \beta$) obey the single parameter scaling. Then, the percentile g_γ ($\alpha < \gamma < \beta$) must scale, too. Also, if g_α and g_β scale, then the difference $g_\beta - g_\alpha$ scales. Therefore, for the proof of the one parameter scaling, it is sufficient to prove the scaling of only a few percentiles, which was done in Ref. [137]. We conclude that the numerical verification of the single parameter scaling of a few percentiles provides us with the evidence that the entire probability distribution, $p(g)$, obeys the single parameter scaling in the critical region.

12.6   Scaling of the level statistics

As discussed in Sect. 5.2, the distribution $p(s)$ of the differences between the neighboring eigenenergies depends on whether the system is in the metallic, localized or critical regime. In Refs. [58, 138, 139], the scaling analysis of the level statistics was proposed and studied.

The critical parameters were calculated for the 2d Ando model [100], the 3d Anderson model [61, 140], and for the problem of quantum percolation in 3d system [141]. Recently, the scaling analysis of the level statistics was applied to the symplectic model on the fractal lattice with the aim to prove that the lower critical dimension for the symplectic systems is less than 2 [142].

12.7   Scaling of the inverse participation ratios

The scaling of inverse participation ratios, I_q, defined in Sect. 5, was performed recently in Ref. [56]. Contrary to the conductance, which is defined only for energies inside the unperturbed energy band, $|E| < 6V$, I_q can be calculated for the entire energy spectrum of the Hamiltonian, and can be used for the verification of the universality of the metal-insulator transition along the critical line. However, one has to keep in mind that I_q is not size-invariant at the critical point but behaves as

$$I_q \sim L^{-(q-1)d_q}, \tag{187}$$

as discussed in Sect. 5.

In the scaling analysis, the logarithm of I_q was used, since the values of $I_q(E_n)$ might fluctuate in orders of magnitude within a small energy interval, δE (Figs. 10, 11). The quantity of interest is then

$$\tilde{I}_q(L, W) = \langle \langle \ln I_q(E_n) \rangle_{\delta E} \rangle, \tag{188}$$

where the averaging is performed within the energy interval, δE, and over statistical ensemble of microscopically different samples. $\tilde{I}_q(L, W)$ is then fit to the scaling equation,

$$\tilde{I}_q(L, W) = A - (q-1)d_q \ln L + B(W - W_c)L^{1/\nu} \tag{189}$$

and critical parameters, W_c, d_q and ν are calculated for the 3d Anderson model with the Gaussian and box distribution of random energies.
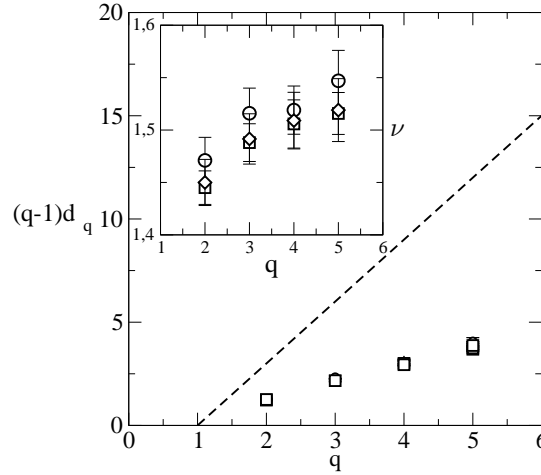
Fig. 59. The fractal dimension, d_q, obtained from the scaling analysis of the inverse participation ratios, I_q, for the 3d Anderson model with the Gaussian and box disorder. The dashed line is $(q-1)d$ for $d = 3$. Inset shows the estimated critical exponent for three critical points. At the band center with the Gaussian (circles) and box (boxes) distribution, and for the Gaussian disorder $W = 2$ with critical energy $E_c \approx 6.58$ (triangles). The electron eigenenergies and eigenfunctions were calculated numerically for cubes of the size $8 \le L \le 54$ [56].

Figure 59 shows that not only the critical exponent, ν, but also the fractal dimensions, d_q, are universal, independent of the microscopic details of the model and on the position of the critical point on the critical line. The fractal structure of the critical wave function was studied also in Refs. [143–146].

13   Scaling in the *d*-dimensional systems

The numerical scaling analysis provides us with rather accurate estimation of the critical exponent for the 3d Anderson model. However, the obtained results are in disagreement with expectations of the theory, which reports $\nu = 1$ for $d = 3$ [147]. It is therefore important, for the detailed comparison of the theory and numerical data, to calculate the dimension dependence of the critical exponent, and check, whether or not agreement with theory is better for, $d \to 2^+$ or for $d > 3$. We summarize here the very recent data for the critical exponent, calculated in Ref. [113] for $2 < d \le 4$, and we present also new data for $d = 5$.

13.1   Dimension $d = 2 + \epsilon$

Figure 60 shows the disorder dependence ($d = 2 + \epsilon$) of the critical exponent, ν, calculated from the finite size scaling of the smallest Lyapunov exponent of quasi-1d bifractal lattices with fractal structure of the cross-section, shown in Fig. 45. These data are compared with the theoretical prediction, based on the analytical calculation of the function $\beta(g)$.
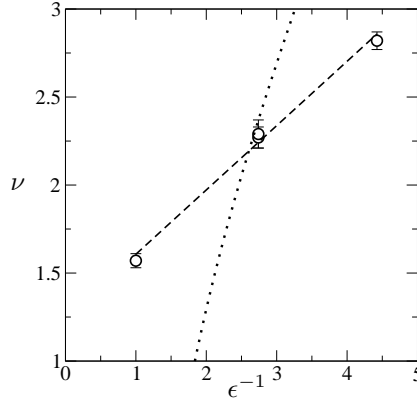
Fig. 60. The critical exponent, ν, as a function of ϵ^{-1} ($\epsilon = d - 2$). Shown are the data for three bifractals, discussed in Sect. 10.2 (Fig. 45), and for a cubic 3d system. The dashed line is the linear fit, $1.24 + 0.365/\epsilon$. The dotted line is the analytical ϵ - expansion of the critical exponent, given by Eq. (194). Note, there is no agreement between the theoretical prediction (dashed line) and the numerical data. Note also that two systems with the same spectral dimension have the same critical exponent, as expected.

In the limit of $\epsilon \ll 1$, the critical disorder $W_c \sim \epsilon \ll 1$ and the critical conductance $g_c \sim \epsilon^{-1} \gg 1$. The function $\beta(g)$ can be expanded in power series of g^{-1}. It is more convenient to use, instead of the conductance g, the parameter

$$t = \frac{1}{2\pi g}. \tag{190}$$

The size dependence of the parameter t is given by the equation

$$\frac{\partial t}{\partial \ln L} = \beta(t), \tag{191}$$

and the critical exponent, ν, is then given by the relation

$$\nu^{-1} = -\left.\frac{\partial \beta(t)}{\partial t}\right|_{t=t_c}. \tag{192}$$

For the orthogonal systems, the t-expansion of the function $\beta(t)$ reads [11]

$$\beta_{\mathrm{O}}(t) = \epsilon t - 2t^2 - 12\zeta(3)t^5 + \frac{27}{2}\zeta(4)t^6 + \dots. \tag{193}$$

In Eq. (193), $\zeta(3) = 1.202$ and $\zeta(4) = \pi^4/90$.

Since the expansion (193) is known only up to the 6th power in t, it is difficult to estimate the accuracy of the obtained results for the critical conductance and critical exponent, specially when ϵ is not small. For instance, for the 3d system, ($\epsilon = 1$) one finds, by solving the equation $\beta_{\mathrm{O}}(t_c) = 0$, that $t_c = 0.395$. This agrees qualitatively with the estimation of critical conductance, $g_c = 1/(2\pi t_c) \approx 0.40$ (we remind the reader that the numerically observed values of the

critical conductance are 0.445 and 0.280 for periodic and hard wall boundary conditions, respectively). However, from Eq. (192) we obtain $\nu = 0.67$, which is far from the numerical result, $\nu \approx 1.57$. The agreement with the numerical data is not better for small ϵ, as is shown in Fig. 60 which compares the critical exponent, calculated from the ϵ expansion,

$$\nu = \frac{1}{\epsilon} - \frac{9}{4}\zeta(3)\epsilon^2 \tag{194}$$

with our numerical data. Clearly, there is no agreement between the theory and results of numerical simulations.

For completeness, we add the ϵ expansion of the β function for symplectic systems. It can be obtained from expression (193) with the use of the symmetry relation [97]

$$\beta_{\mathrm{S}} = -2\beta_{\mathrm{O}}(-t/2), \tag{195}$$

which gives

$$\beta_{\mathrm{S}}(t) = \epsilon t + t^2 - \frac{3\zeta(3)}{4}t^5 - \frac{27\zeta(4)}{64}t^6 + \dots. \tag{196}$$

Note, $\beta_{\mathrm{S}}(t)$ is positive for $\epsilon \to 0$ which confirms the existence of the critical point in the 2d symplectic systems.

13.2   Dimension $d \geq 3$

The numerical data for the critical exponent in higher dimensions does not agree with the self-consistent theory [147] which predicts that

$$\nu(d) = \begin{cases} (d-2)^{-1} & 2 < d \leq 4 \\ 1/2 & d > 4. \end{cases} \tag{197}$$

For instance, for the 3d systems, Eq. (197) predicts $\nu = 1$, which clearly disagrees with the numerical result, $\nu = 1.57$.

In order to get insight into the dimension dependence of the critical exponents, the finite size scaling analysis for $d = 4$ was performed in Refs. [113, 116, 148], and for $d = 5$ in the present paper. Figure 61 presents numerical data for z_1 obtained for the quasi-1d systems $L^3 \times L_z$ and $L^4 \times L_z$. Although only the data for small L can be calculated, obtained results confirm the existence of the critical points in both systems. The simple scaling analysis, given by Eqs. (175-178) was used to estimate the position of the critical points and of the critical exponents. For the 4d Anderson model, we find

$$\nu_{4\mathrm{d}} = 1.12 \pm 0.05. \tag{198}$$

This result agrees with previously obtained data [113, 116]. To the best of our knowledge, there have been no published data for the critical exponent of the 5d Anderson model yet. Our estimation of the critical exponent is

$$\nu_{5\mathrm{d}} = 0.94 \pm 0.05. \tag{199}$$

Figure 62 summarizes all obtained numerical data for the critical exponent of the orthogonal Anderson model in d dimensions and compares them with predictions of analytical calculations. We conclude that there is no agreement of numerical data with the theory, neither for small dimension, nor for $d > 3$.
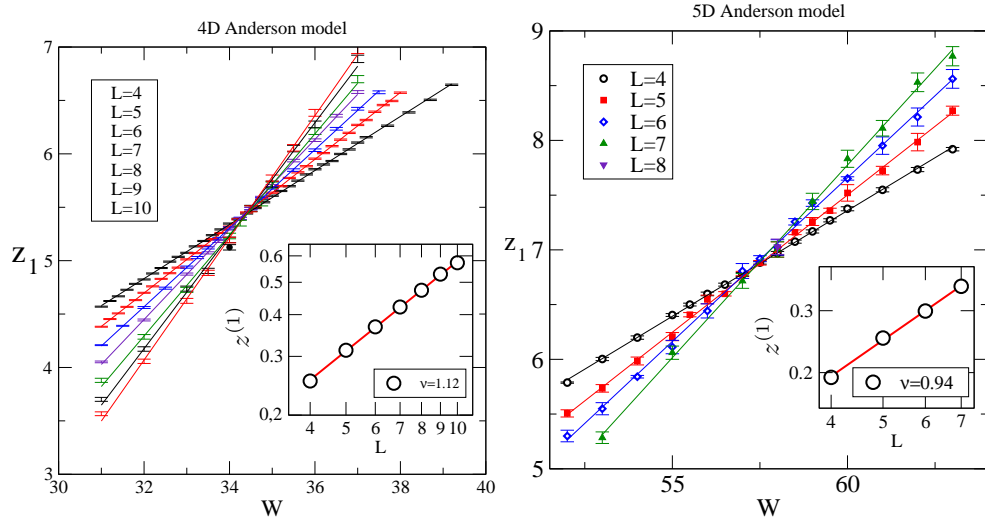
Fig. 61. The first Lyapunov exponent, z_1, as a function of disorder, W, for various L for the 4d (left) and 5d (right) Anderson model. The critical parameters are $W_c = 34.3 \pm 0.2$, $\nu = 1.12 \pm 0.05$ for 4d and $W_c = 57.26 \pm 0.2$, $\nu = 0.93 \pm 0.05$ for 5d. Inset shows the L-dependence of $z_1^{(1)}$, defined by Eq. (175). Power fit $z_1^{(1)}$ *vs.* L, given by Eq. (177) determines the critical exponent, ν.
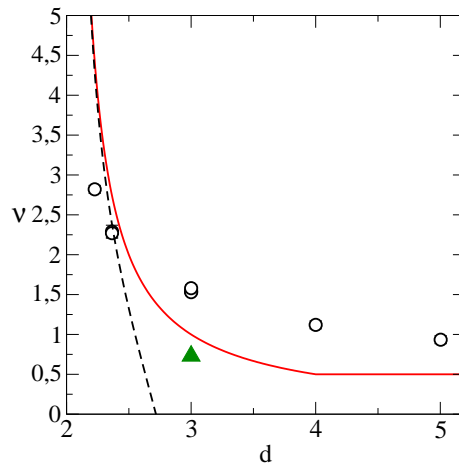
Fig. 62. Dimension dependence of the critical exponent. Numerical data differ considerably from the theoretical predictions, both for $d - 2 \ll 1$ and for $d \gg 2$. The dashed line is the ϵ-expansion, given by Eq. (194). Triangle is The estimation of Hikami, obtained by the Pade approximation of the ϵ expansion of the β function, $\nu_{\text{Hikami}} \approx 0.73$. The solid line is the analytical prediction (197)

13.3 Theory *vs* (numerical) experiment

Disagreement between the theoretical predictions and numerical data might lead to the conclusion that the numerical scaling analysis is insufficient or even wrong [149–151]. It is not our aim to discuss these objections here (see, for instance, the comment to Ref. [151], published in Ref. [152]). We only concentrate on the discussion of advantages and disadvantages of numerical analysis.

The main objection against the numerical methods is that they are always restricted to the systems of finite size. This limitation can be partially avoided by the scaling analysis, Eq. (173), and by including the irrelevant scaling variables, Eq. (182). Also, the accuracy of obtained critical parameters can be estimated by elimination of numerical data for small system size, as discussed in Sect. 12.2. Fortunately, the finite size effects seem to play a negligible role in higher dimension. The first estimation of the critical exponent for the 3d Anderson model, $\nu \approx 1.5$, obtained in pioneering work of MacKinnon and Kramer, [17], differs only in a few per cent from the best today's estimation, $\nu = 1.57$ [136]. Also, for the 4d Anderson model, the estimation $\nu = 1.1 \pm 0.1$ was obtained already in Ref. [116], where really small lattices, typically of the size $3^3 \times L_z$ were analyzed. Nevertheless, the analysis of larger samples, up to $7^3 \times L_z$, [113] brought no corrections to the critical exponent. As is shown in Fig. 61, the additional data for even large systems have no influence to the critical exponent, originally estimated for smaller systems. We conclude therefore that the numerical simulation provides us with reliable data in higher dimension.

Our belief that the numerical data for the critical exponent are correct, is supported also by results of the scaling analysis of various groups. In the 3d systems, various models were studied, isotropic and anisotropic [153], with diagonal or off-diagonal disorder [131, 132]. Scaling of various parameters was analyzed, inclusive the smallest Lyapunov exponent, higher Lyapunov exponents, conductance [136, 137], conductivity [154], level statistics [61, 141] and inverse participation ratio [56]. All these works report the critical exponent close to 1.5, with the accuracy which definitely excludes the possibility that $\nu = 1$.

As discussed in Sect. 14, finite size effects become stronger in lower dimension, The reason is that the mean free path, ℓ is larger (Fig. 28). A typical problem caused by the finite size of the system is shown in Fig. 37 which presents the latest numerical data for the mean conductance, $\langle g \rangle$ of the 2d Anderson model. Although we accept that there is no Anderson transition in $d = 2$, the numerical data seem to mimic the metallic behavior. For $W = 1$, the mean conductance $\langle g \rangle$ increases when L increases. One might argue that there is a critical disorder, $W_c \approx 2$. However, as discussed already in Sect. 8.6, the above conclusion is not correct. To determine the character of the transport regime, the size dependence of the conductance must be carefully analyzed. The increase of the mean conductance for $W = 1$ is the manifestation of the *ballistic* regime. Indeed, the mean free path $\ell \approx 17$ for $W = 1$ is comparable with the size of the system when $L \leq 100$. Also, the variance, var g, is much larger than expected universal value, typical for the metallic regime (Fig. 31).

Also, the decrease of the mean conductance with the system size for disorder $W = 3$ and $W = 4$ *cannot* be associated with localization. Indeed, the same data, plotted in Fig. 25 in the logarithmic scale, show that the decrease of the conductance is not exponential, but logarithmic, and is caused by the weak localization. To see the exponential localization, one needs much larger system size.

The big advantage of the numerical simulation is that it can relatively easy analyze statistical properties of any quantity of interest. No averaging is necessary in the course of calculations. All mean values can be calculated "from first principles". This cannot be done analytically. The analytical theory must solve the problem how to perform the average over the disorder. Wrong averaging might lead immediately to wrong results [151]. In our opinion, the discrepancy between the numerical data and results of analytical theories is due to the inability of analytical theories to analyze completely the statistical fluctuations in the critical regime.

14   Two dimensional critical regimes

The critical regime in the 2d models deserves a special attention. As discussed above, only systems with symplectic symmetry exhibits the metal insulator transition in dimension $d = 2$. The 2d systems with unitary symmetry posses, in the presence of strong magnetic field, the critical energies, E_c where the localization length diverges.

On first sight it seems that the 2d systems can be easier simulated numerically since the lower dimension of the system allows one to calculate the conductance for much larger samples. However, this advantage is "compensated" by much stronger finite size effects.

Besides the calculation of the critical exponents and critical conductance distribution, the 2d critical regime is suitable for the verification of the general relation between the conductance and conductivity,

$$\langle g \rangle = \sigma, \tag{200}$$

given by Eq. (109). Contrary to the orthogonal 2d systems, where Eq. (200) holds only in the diffusive regime, i.e. when the size of the system is smaller than the localization length, $L \ll \lambda$, Eq. (200) holds also in the limit of infinite system size at the critical point of the unitary and symplectic models.

Note, equation (200) compares two different quantities. The conductance, g, is given, by definition, by the transmission properties of the disordered sample at zero temperature. The value of the conductance depends on the actual distribution of disorder inside the sample. Owing to the quantum character of electron propagation, the conductance is not a self-averaged quantity.

On the other hand, the *conductivity*, σ, is a material parameter. It characterizes the transport properties of an *infinite* system. When calculated for the system of *finite size*, L, [5], σ fluctuates around the mean value, but the fluctuations decrease when L increases. Contrary to the conductance, the conductivity, σ *is* a self-averaged quantity.

For the critical 2d regimes, Falko and Efetov [158] derived the following relation between the fractal dimensions of the critical wave function, d_q, and the critical conductivity, σ, derived the relation

$$d_q = 2 - \frac{q}{\beta \pi \sigma (h/e^2)}. \tag{201}$$

Here, $\beta = 1$, 2 and 4 determines the symmetry of the system[6]. Eq. (201) holds for small q, when

---

[5]Numerical algorithm for the calculation of the conductance is described in Ref. [154, 156] and in Ref. [157] for the case of critical quantum Hall regime.

[6]Note, that $\beta = 1/2$, 1 and 2 is used in original papers, which adds an additional factor of 2 in the denominator on the r.h.s. of Eq. (201). Also, note that factor of 2 for two orientation of electron spin is not included in the definition of the conductivity, σ.

terms proportional to higher powers of q can be neglected. Since both the wave functions and the conductance can be calculated numerically in the critical point, we can verify the relation (201) by direct numerical simulations. It will be shown in next two Sections that indeed both Eqs. (200) and (201) are satisfied within the accuracy of numerical data.

14.1 Symplectic models

The difficulty of the analysis of the 2d symplectic models is manifested by a wide variety of values of the critical exponent, $2 \leq \nu \leq 2.88$, reported in the literature within the last 15 years [47, 49, 99, 100]. These discrepancies are due to the strong finite size effects. Recently, the finite size scaling of the smallest Lyapunov exponent on the SU(2) model, [49] provided the following estimate of the critical exponent,

$$\nu = 2.75 \pm 0.01. \tag{202}$$

This value can be considered as the most accurate estimation of the critical exponent. The analysis of the scaling of the mean conductance for the 2d Ando model, [54] led to the similar value,

$$\nu \approx 2.80 \pm 0.04. \tag{203}$$

The scaling behavior of the mean conductance, $\langle g \rangle$, is shown in Fig. 57. The critical conductance distribution for the 2d Ando model is shown in Fig. 27. Since the mean conductance,

$$\langle g \rangle_c \approx 0.71, \tag{204}$$

is close to 1, the distribution possesses all characteristic properties of the critical distribution for the 3d Anderson model (Fig. 43). Comparison of the critical distribution, calculated for the periodic and hard wall boundary conditions is shown in Fig. 44.

The numerical data for the conductance, together with Eq. (200) enables us to verify the relation (201) between the conductance and the fractal dimensions, d_q. To do so, the wave function of the 2d Ando model was calculated numerically for the disordered sample of size 260×260. Then, the sample was divided into the small squares Ω_a of size $L_0 \times L_0$, and the quantity

$$p_q(L_0) = \sum_a \left\{ \sum_{\vec{r} \in \Omega_a} |\Psi_n(\vec{r})|^2 \right\}^q \tag{205}$$

was calculated for the $N_{\text{stat}} = 10$ different realizations of the disorder. The wave function Ψ_n is the eigenfunction of the disordered Ando Hamiltonian, corresponding to the eigenvalue E_n, closest to the band center, $E = 0$. Since the wave function is expected to posses the multifractal spatial structure, the L_0-dependence of $p_q(L_0)$ is determined by the fractal dimensions, d_q,

$$p_q(L_0) \sim L_0^{-(q-1)d_q}. \tag{206}$$

Numerically calculated fractal dimensions, d_q are plotted in Fig. 63 as a function of q. The results confirm that d_q decreases linearly with q, for $q \leq 1$. The slope, given by Eq. (201), determines the critical conductivity, $\sigma_c = 0.71 e^2/h$, which is exactly equal to the critical conductance, $\langle g \rangle_c$.
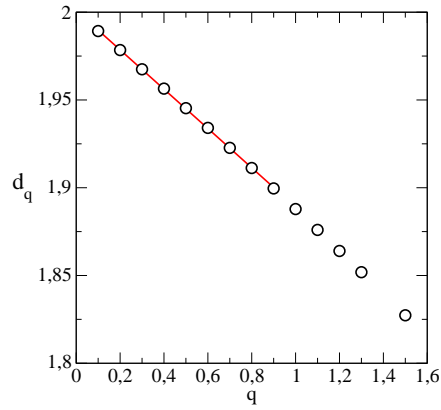
Fig. 63. The fractal dimension, d_q, as a function of q, calculated for the 2d Ando model. For $q \leq 1$, the fractal dimension, d_q, is a linear function of q, in agreement with Eq. (201). The solid line is the linear fit with the slope 0.11202 which determines the critical conductance, $\sigma_c = 0.71$, and which agrees with the estimation of the critical conductivity, $\langle g \rangle_c = 0.71$ [159].
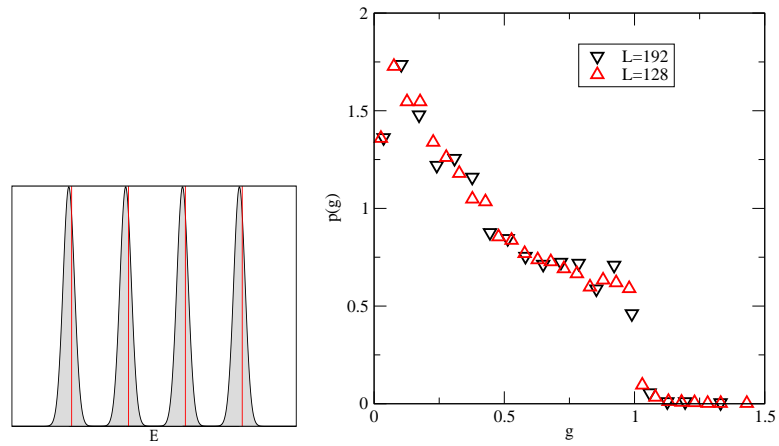
Fig. 64. Left: The density of states of the weakly disordered 2d system in a strong magnetic field. The energy spectrum consists of the Landau bands. Inside each Landau band there is a critical energy, E_c, where the localization length diverges. Note, the position of the critical energy depends on the strength of the disorder. Right: The critical conductance distribution for the first Landau band for $\phi = 2\pi/8a$. The disorder is $W = 1.4$ and the critical energy, $E_c = -3.29$.

14.2   Critical quantum Hall regime

The 2d disordered system in a strong magnetic field possesses, inside each Landau band, the critical energy, E_c shown schematically in the left panel of Fig. 64. When the Fermi energy

crosses the energy E_c, the transmission from one Hall plateau to another one appears [31, 160]. The existence of the critical energy, E_c, was numerically proved in Refs. [50]. The correlation length, ξ, diverges on both sides of the critical energy as

$$\xi(E) \propto |E - E_c|^{-\nu}, \tag{207}$$

with the critical index, $\nu \approx 2.33$ [32, 50].

The critical quantum Hall regime can be studied numerically within the Hamiltonian, (19) with the Peierls phase, $\phi = B(ea)^2/\hbar$. Since we are interested only in the critical parameters, the periodic boundary conditions are used in the direction perpendicular to the propagation. Then, the Peierls phase, ϕ, must fulfill the relation $\phi L = 2\pi n$, where L is the size of the lattice in the transversal direction, and n is an integer.

The numerical analysis of the critical regime is difficult, since the disorder W must be small in order to keep the Landau levels separated from each other. Then, however, the mean free path, ℓ is large. This problem can be avoided with he use of the spatially correlated disorder [29].

In Ref. [159], the sample averaged conductance, $\langle g \rangle$, and the conductivity, σ, were calculated for the first and the second Landau band. To eliminate the finite size effects, the random disorder was spatially correlated. Numerical data was fitted to the formulas

$$\langle g(L) \rangle = g_c - g_0 \left(\frac{L_0}{L} \right)^y \tag{208}$$

and

$$\sigma(L) = \sigma_c - \sigma_0 \left(\frac{L_0}{L} \right)^{y'}. \tag{209}$$

where $y \approx y'$ are irrelevant scaling exponents.

Numerical analysis, performed for various strength of the disorder proved that both the mean conductivity and conductance converge to the same values listed in Table 2. This data proves the relation (200) for the critical quantum Hall regime and they also shows that the critical conductance (or conductivity) is universal, independent of the microscopic model and on the Landau level.

Critical values listed in Table 2 are significantly larger than the commonly accepted value, $0.5e^2/h$, found in Ref. [161], and confirmed in previous numerical simulations [162]. However, they are in agreement with numerical data obtained on the Chalker Coddington model [163,

Tab. 2. The critical conductivity, σ_c, and the critical conductance, $\langle g \rangle$, (in units of e^2/h) for the two lowest Landau bands [159]. The data was obtained by fit of the numerical data to Eqs. (208) and (209) with $y \approx y' \approx -0.4$

critical conductivity	σ_c	0.58 ± 0.02
critical conductance		
1st. Landau band	g_{c1}	0.60 ± 0.02
2nd Landau band	g_{c2}	0.61 ± 0.03

164]. Critical conductance, $\sigma_c \approx 0.61 e^2/h$, is also consistent with the recently calculated fractal dimension, $d_1 = 1.739$, and with the relation (201),

$$\sigma = \frac{1}{2\pi(2 - d_1)} \frac{e^2}{h}.$$

(210)

The difference between the theoretical and numerical data is probably due to the spatial inhomogeneity of the electron distribution, which was neglected in the analytical calculations.

15 Possible theoretical description of the localized regime

In this Section, we present two possible descriptions of the localized regime. Both of them are based on the generalization of the theoretical methods developed for the analysis of the transport in diffusive regime. In Sect. 15.1, we discuss the possibility to generalize the DMPK equation, [165] and in Sect. 15.2, a simple generalization of random matrix theory is proposed [91].

15.1 Generalized DMPK equation

In Appendix B we present the DMPK equation, which describes successfully the transport properties of weakly disordered quasi-1d systems. The theory contains only one parameter - the mean free path ℓ, which measures the strength of the disorder.

The DMPK equation was derived under the assumption of the homogeneity of the matrices u and v which parametrize the transfer matrix (see Appendix A.3 for details). Physically, homogeneity of matrices u and v means homogeneous distribution of the electron on the opposite side of the sample. This is possible only if the electron has many paths to travel from one side of the sample to another side. Mathematically, this requirement is expressed by Eq. (276), which can be written in the form

$$K_{ab} = \left\langle \sum_c |u_{ac}|^2 |u_{bc}|^2 \right\rangle = \frac{1 + \delta_{ab}}{N + 1}.$$

(211)

Here, N is the number of channels. Clearly, this assumption is fulfilled only in the limit of weak disorder, when the electron can choose, on its travel through the sample, many equivalent paths. This is not true when the disorder is strong and the electron hardly finds a single trajectory propagating from one side of the sample to opposite one (Fig. 71).

Recently, Muttalib and Klauder [165] proposed the generalization of the DMPK equation. Without any restriction to the value of the matrix elements K_{ab}, they generalized the DMPK equation into the form

$$\frac{\partial p_{L_z}(\lambda)}{\partial(L_z/l)} = \frac{1}{J} \sum_a^N \frac{\partial}{\partial \lambda_a} \left[\lambda_a (1 + \lambda_a) K_{aa} J \frac{\partial p}{\partial \lambda_a} \right]$$

(212)

with the Jacobian

$$J \equiv \prod_{a < b}^N |\lambda_a - \lambda_b|^{\gamma_{ab}}, \qquad \gamma_{ab} \equiv \frac{2 K_{ab}}{K_{aa}}.$$

(213)

In Eq. (212), the symmetry parameter $\beta = 1$.

For the weak disorder, one can substitute for K_{ab} from Eq. (211) and obtain that Eq. (212) reduces to the "classical" DMPK equation. For strong disorder, the parameters K_{aa} and γ_{ab} represent the additional free parameters which must be estimated from numerical experiment.

To estimate values of γ_{ab} in the localized regime (regime with strong disorder), we remind the reader that the probability distribution of the difference, $\delta_a = x_{a+1} - x_a$ is similar to the Poisson distribution in the localized regime (Fig. 47). Therefore, it is natural to assume that the repulsion between the two levels in the Jacobian (213) is weaker than in the diffusive regime. Consequently, we assume that $\gamma_{ab} \to 0$ in the case of strong disorder. A similar conclusion was derived also in Ref. [91].

The second assumption made in Ref. [165] was that $K_{aa} \gg K_{ab}$ for $a \neq b$. In particular, in the localized regime, one can assume that

$$K_{aa} \propto L^0. \tag{214}$$

To understand the physical meaning of (214), note that

$$K_{aa} = \left\langle \sum_c |u_{ac}|^4 \right\rangle. \tag{215}$$

is nothing but the inverse participation ratio for the transversal wave function on the opposite side of the sample. In analogy with the properties of I_q, discussed in Sect. 5.1, we conclude that the condition (214) reflects the non-homogeneity of the distribution of the electron on the opposite side of the sample, which follows directly from the existence of only the single possible path through the sample (Fig. 71).

Conjecture (214) was numerically tested in Refs. [166, 167] by the direct numerical calculation of the matrix K_{ab}. The numerical method of calculation of the conductance, described in Appendix E.2, can be easily generalized for calculation of the eigenvectors u. To avoid the problem with evanescent modes, the calculations were performed for the anisotropic 3d Anderson model, defined by Eq. (9) with $t = 0.4$. This model exhibits the metal-insulator transition for critical disorder $W_c \approx 9.5$.

The numerical analysis confirmed that the parameters K indeed depend on the disorder. In Fig. 65 we see that the size dependence of parameters LK_{11} and γ_{12} differs depending on whether the system is in the metallic, localized or critical regime. Note, since $\lambda_1 < \lambda_2 < \ldots$, and the matrix $t^\dagger t$ has eigenvalues $(1 + \lambda_a)^{-1}$, the parameter K_{11} contains information about the spatial structure of the first eigenvector, u_1, which corresponds to the largest eigenvalue, and γ_{12} is a measure of the overlap of eigenvectors related to the two largest eigenvalues of $t^\dagger t$.

In the metallic regime, $LK_{11} \propto L^{-1}$, and γ_{12} converges to 1, as was assumed in the derivation of the "classical" DMPK equation. However, in the localized regime, LK_{11} increases with the system size, which indicates that indeed K_{11} is constant, in agreement with Eq. (214). Also, γ_{12} decreases when $W > W_c$ being $\propto L^{-1}$ in the limit of large system size.

At the critical point, both parameters, LK_{11} and γ_{12}, converge to the size independent constants, indicating that they could be used as the order parameters for the calculation of the critical parameters of the model by scaling theory. The size dependence of LK_{11} and γ_{12} is summarized in Table 3.
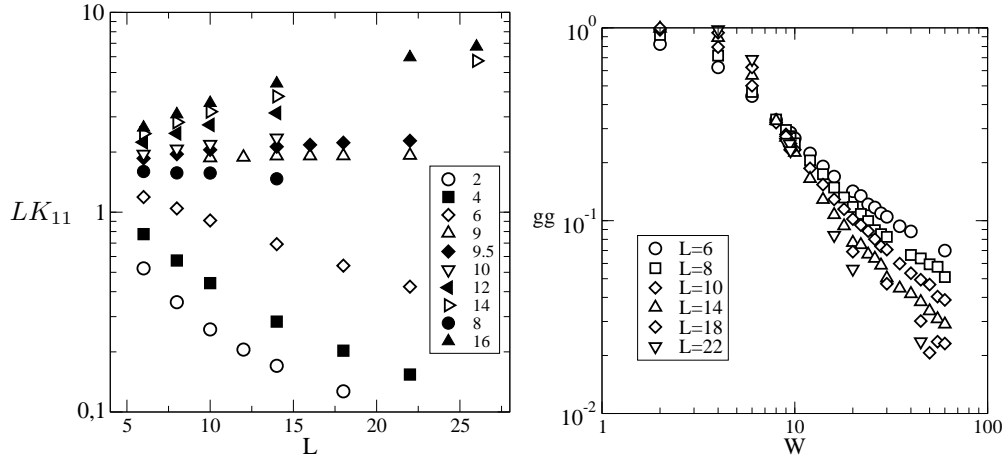
Fig. 65. Left: The disorder dependence of LK_{11} for the 3d anisotropic Anderson model, given by Eq. (215) with $t = 0.4$. The symbols correspond to the different disorder. The data confirm that LK_{11} decreases (increases) with L for $W < W_c$ ($W > W_c$), respectively. Here, the critical disorder $W_c \approx 9.5$. Note, LK_{11} does not depend on the system size when $W = W_c$. The right panel shows that $\gamma_{12} \to 1$ when $W < W_c$ and $L \to \infty$, but γ_{12} decreases with L when disorder $W > W_c$ (insulating regime). At the critical point, $\gamma_{12} \approx 0.25$ does not depend on the system size [167].

With known size dependence of K_{11} and γ_{12}, we need to estimate also other parameters, K_{ab}. Detailed numerical analysis, performed in Ref. [167] confirmed that these quantities can be expressed as a simple functions of indices a and b. It is also reasonable to assume that $K_{aa} = K_{11}$ and $\gamma_{ab} \approx \gamma_{12}$. This reduces the number of free parameters to two. The first one,

$$\Gamma = \frac{\ell}{L_z K_{11}} \tag{216}$$

measures the strength of the disorder, and the second one, γ_{12}, influences the mutual correlation of channels in the generalized DMPK equation. In the limit of

$$\gamma_{12} \sim \frac{\lambda}{L} \ll 1, \tag{217}$$

Tab. 3. The size dependence of parameters LK_{11} and γ_{12} in the metallic, localized and critical regime.

	$L \times K_{11}$	γ_{12}
$W \ll W_c$	L^{-1}	1
W_c	const	const
$W \gg W_c$	$\sim L/\xi$	L^{-1}
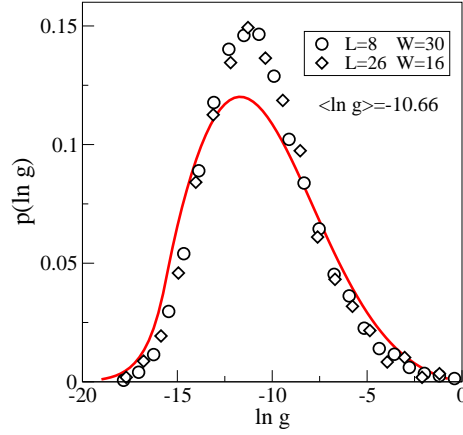
Fig. 66. Probability distribution of a strongly disordered three dimensional system. Symbols show data form numerical simulations, solid line is the solution of the generalized DMPK equation which gives the same value of $\langle \ln g \rangle$ and with $\gamma_{12} = \Gamma/2$. Dotted line is the distribution obtained for the same value of Γ but with $\gamma_{12} = 1$.

the probability distribution $p(g)$ can be obtained analytically by solving the generalized DMPK equation, given by Eq. (212), by methods developed in Refs. [109, 110] The obtained conductance distribution is shown in Fig. 66 and compared with the numerically calculated distribution $p(\ln g)$. Parameter Γ was chosen such that $\langle \ln g \rangle$, equals to the numerically obtained value. We see that the analytical model reproduces qualitatively correctly the numerical data. The quantitative difference is probably due to oversimplification of the model, which neglects the differences between K_{ab} for higher channels.

The generalized DMPK equation represents the most promising step toward the analytical description of the localized regime. However, the main assumption which allows the analytical solution is that γ_{12} is very small. This is not true at the critical point, as can be seen in Fig. 65. Therefore, it is not known at present, how accurately the generalized DMPK equation describes the critical regime.

15.2 Random matrix model of the Anderson transition

We have shown in Appendix C that in the diffusive regime, the probability distribution for the eigenvalues λ of the transmission matrix can be relatively easily obtained from the assumption that the matrix $(t^\dagger t)^{-1}$ belongs to the orthogonal class of random matrices. The form of the distribution was determined by the additional constrain that the density $\sigma(x)$ of parameters x,

$$\sigma(x) = \left\langle \sum_a \delta(x - x_a) \right\rangle, \tag{218}$$

is constant for $x < L_z/\ell$. This constraint follows directly from the linear dependence, $\langle x_1 \rangle \propto a$, shown in Fig. 76.
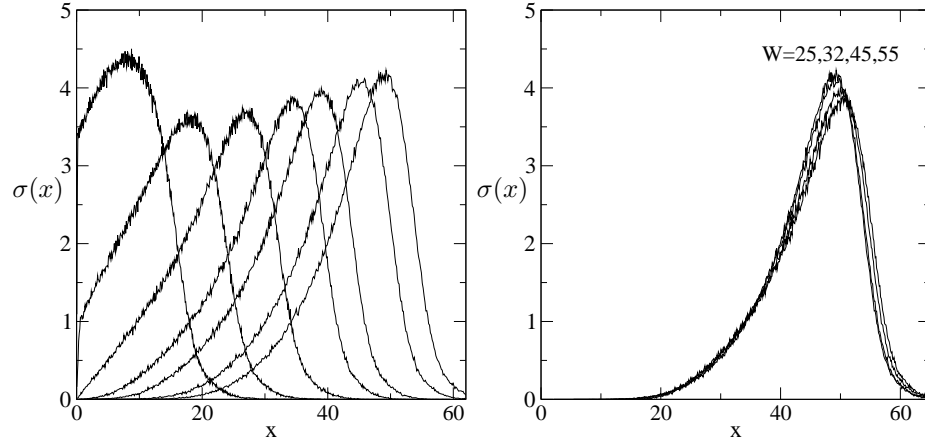
Fig. 67. Left: The density $\sigma(x)$ calculated numerically for the 3d Anderson model with disorder $W = 6$, 10, $W = W_c = 16.5$, and $W = 25$ and 32 (from left to the right). Note, at the critical point, the density is linear for $x \leq 10$. Right: $\sigma(x)$ for the strongly localized regime with disorder $W = 25$, 32, 45 and 55. To show the universality of the density, the data are shifted on the horizontal axis by the difference $\langle x_1(W) \rangle - \langle x_1(W = 55) \rangle$ [168].

Since the spectrum of x exhibits the universal properties also at the critical point and in the localized regime, it is tempting to try to generalize the random matrix analysis also for transport beyond the diffusive regime. This expectations are inspired by the numerical data for $\sigma(x)$, shown in Fig. 67.

In Sects. 10 we found that contrary to the diffusive regime, the density $\sigma(x)$ is not constant in the critical regime. Since $\langle x_a \rangle^2 \propto a$ at the critical point (Fig. 41), the density must be linear,

$$\sigma_{\mathrm{crit}}(x) \propto x, \tag{219}$$

at least in the lower part of the spectra. Note, only this part of the spectra is relevant for the description of the transport. The linearity of the density is confirmed numerically in the left panel of Fig. 67.

The right panel of Fig. 67 shows that in the localized regime, the density $\sigma(x)$ is a function of the difference, $x - 2L/\lambda$. This follows directly from Eq. (161).

It is therefore natural to postulate that the density $\sigma(x)$ behaves as

$$\sigma(x) = c(W) \times [x + a(W)], \tag{220}$$

where the function $a(W, L)$ changes the sign at the critical point [91].

The disorder and size dependence of functions a and c are not known. The analysis of the size dependence of of parameters x in the critical region [169] confirmed that

$$a(W, L) \sim \begin{cases} +2L/\xi(W) & W \ll W_c \\ 0 & W = W_c \\ -2L/\xi(W) & W \gg W_c \end{cases} \tag{221}$$
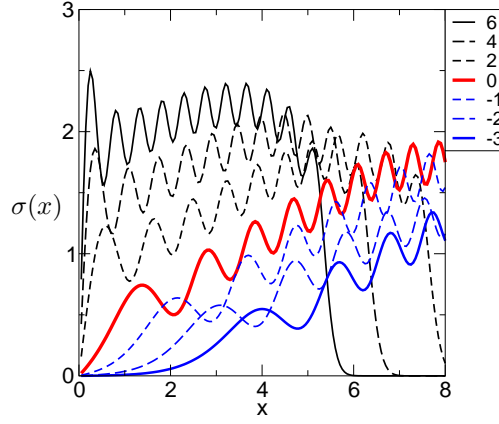
Fig. 68. The density, $\sigma(x)$, calculated from the random matrix model, given by Eq. (220). Various values of parameters a are given in the legend [168].

and that $c(W, L)$ is a size independent constant for $W = W_c$. In Eq. (221), $\xi(W)$ is the correlation length introduced in Sect. 12.1. In strongly localized regime, $\xi(W)$ equals to the localization length λ.

We can verify that the density $\sigma(x)$, given by Eqs. (220) and (221) reproduces numerical data for parameters x. Indeed, inserting in Eq. (220) we find that in the metallic regime, $\sigma(x) \sim$ const since $x \ll 2L/\xi(W)$ (we remind the reader that $\langle x_a \rangle = L/(N\ell)a$ in the metallic regime). Since $\sigma = cx$ at the critical point, we immediately recover that $\langle x_a \rangle^2 \propto a$. In the localized regime, $\sigma = c(x - 2L/\xi)$, so that the entire spectrum of parameters x shifts by $2L/\xi(W)$ for higher values of the disorder W.

Using the method explained in Appendix C.1, it was found in Ref. [91] that the distribution of parameters x at the critical point is given by the universal distribution Eq. (310) and (312), but with a cubic one particle potential,

$$V_{\text{crit}} = cx^3. \tag{222}$$

Then, applying the methods of orthogonal polynomials, [44], the density $\sigma(x)$ can be calculated within the random matrix model. Results, shown in Fig. 68, agree qualitatively with results of the numerical simulations, shown in the left panel of Fig. 67.

An interesting consequence of the expression (220) is the following scaling relation for higher Lyapunov exponents z_i:

$$[z_i - a(W, L)]^2 - [z_j - a(W, L)]^2 = \frac{1}{c}(i - j), \quad i, j \leq L \tag{223}$$

which enables us to find the critical parameters of the 3d Anderson model from numerical data for only one system size [169]. It also provides us with numerical evidence that the model (221), based on the change of the density at the critical point, is correct.

The simple form of the potential (222) indicates that the statistical description of the critical regime might be as simple as the analysis of the diffusive regime. However, we are not aware of any microscopic model which confirms the above phenomenological model.

16 Conclusion

We have discussed in this paper the main transport properties of the single electron disordered electronic systems. The quantum character of the electron propagation is responsible for the wide variety of interesting transport phenomena, which we demonstrated numerically.

In the limit of weak disorder, the weak localization and anti-localization corrections to the conductance and universal conductance fluctuations were observed and the conductance was found to exhibit the universal conductance fluctuations. In the localized regime, the exponential decrease of the wave functions and the conductance with the system length has been demonstrated and discussed.

One of the most important phenomena in the localization theory is the absence of the self averaging of the conductance. In the metallic regime, the electron wave function is spread over the entire sample, and is very sensitive to any change of the disorder configuration, as well as to the change of the boundary conditions. This remarkable property survives also in the limit of an infinite system size. The sensitivity of the energy spectra to the change of the boundary conditions can be used as a measure of the electron localization, and defines the main parameter of the localization theory, the conductance g.

The statistical properties of the conductance in the strongly localized regime are even more complicated. The transport is possible only by tunneling between localized centers, and the conductance decreases exponentially with the size of the sample. Still, a few samples exist in the statistical ensemble which possess rather high conductance. These samples determine the mean conductance, which might be in orders of magnitude larger than the typical (the most probable) conductance of the ensemble. For a given sample, the conductance is also very sensitive to the distribution of random impurities. Equivalently, a small change of the Fermi energy might cause a huge change in the conductance.

The critical regime of the metal-insulator transition has been discussed in detail. First, we have analyzed the statistical properties of the conductance, and we have presented numerical data for the critical conductance distribution. Then, the scaling theory of localization is introduced and verified by numerical scaling analysis of Lyapunov exponents and conductance distribution. In order to compare the numerical data for the critical parameters with predictions of the analytical theories, the critical electronic transport on lattices with dimension close to the lower critical dimension, $d_c = 2$ as well as with dimension $d = 4$ and $d = 5$ was simulated.

We have tried to convince the reader that the numerical data, collected within the last 25 years supports the validity of the one parameter scaling theory of localization. We believe that the numerical data provides us with the most reliable estimation of the critical exponents in various disordered models. We hope that the disagreement between the results of numerical simulations and theory will motivate further theoretical research [155].

Finally, we want to mention some other aspects of the single electron localization. We have not discussed the transport in systems with correlated disorder. The mobility edge in the 1d system with *correlated* disorder has been found in Ref. [171] (see Ref. [172] for review). Special

attention is deserved also for disordered systems with chiral symmetries [173]. Also, application of the concepts of the electron localization to the propagation of the electromagnetic [22, 24, 93, 174], and acoustic [175] waves in disordered media opens a new field for studies of the localization and promise further development of the localization theory.

17 Acknowledgments

A Properties of the transfer matrix

We summarize here the most important properties of the transfer matrix. For details, we refer the reader to Refs. [77, 177].

First, we derive the expression for the transfer matrix, given by Eq. (54). From Eq. (51) we obtain

$$
\begin{aligned}
C &= t^+ A + r^- D \,, \\
B &= r^+ A + t^- D \,.
\end{aligned}
\tag{224}
$$

If we have N incoming channels, then the amplitudes A, B, C and D are the (complex) vectors of length N, and the transmission and reflection amplitudes are the matrices of size $N \times N$.

We express D from the second equation (224) as

$$
D = (t^-)^{-1}B - (t^-)^{-1}r^+ A
\tag{225}
$$

and insert it in the first equation (A). We obtain that the transfer matrix is given by Eq. (54),

$$
\mathbf{T} = \begin{pmatrix} t^+ - r^-(t^-)^{-1}r^+ & r^-(t^-)^{-1} \\ -(t^-)^{-1}r^+ & (t^-)^{-1} \end{pmatrix}.
\tag{226}
$$

Note, t^- and r^- are the transmission and reflection amplitudes of the wave coming from the *right* side of the sample, and t^+ and r^+ are the transmission and reflection amplitudes of the wave coming from the *left* side of the sample.

A.1 The composition law

The transfer matrix given by Eq. (226) fulfills the composition law. If the sample consists of two subsystems, shown in Fig. 69, then the transfer matrix $\mathbf{T}_{12}$ of the whole sample can be calculated from the transfer matrices of the two subsystems as

$$
\mathbf{T}_{12} = \mathbf{T}_2 \mathbf{T}_1.
\tag{227}
$$

The resulting transfer matrix $\mathbf{T}_{12}$ has again the form (54). This composition law enables us to calculate the transmission of a complicated structure from the transfer matrices of its parts. In particular, the transmission through two scattering centers is given by the relation

$$
t_{12}^- = t_1^- \left[1 - r_2^+ r_1^-\right]^{-1} t_2^-.
\tag{228}
$$

Similarly for the reflection we obtain

$$
r_{12}^+ = r_1^+ + t_1^+ \left[1 - r_2^+ r_1^-\right]^{-1} r_2^+ t_1^-.
\tag{229}
$$

PSfrag replacements $\quad r_{12}^+$ ①   ② $\xrightarrow{t_{12}^+}$

t_{12}^-
r_{12}^-
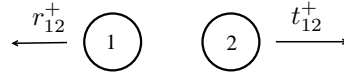
Fig. 69. The composition law for the transfer matrix.

A.2 Symmetries

The elements of the transfer matrix are not independent. Various physical symmetries provide important relations between the transmission and reflection amplitudes. Here, we investigate the consequences of the flux conservation and of the symmetry with respect to the inversion of time.

The *flux conservation* requires that the flux on the right-hand side of the sample equals to the flux on the left-hand side. This gives the following constrain to the transfer matrix [77],

$$\mathbf{T}^\dagger \begin{pmatrix} 1 & 0 \\ 0 & -1 \end{pmatrix} \mathbf{T} = \begin{pmatrix} 1 & 0 \\ 0 & -1 \end{pmatrix}. \tag{230}$$

Inserting

$$\mathbf{T} = \begin{pmatrix} T_{11} & T_{12} \\ T_{21} & T_{22} \end{pmatrix} \tag{231}$$

we obtain from Eq. (230) that

$$T_{22}^\dagger T_{22} - T_{12}^\dagger T_{12} = 1 \tag{232}$$

and

$$T_{11}^\dagger T_{11} - T_{21}^\dagger T_{21} = 1. \tag{233}$$

We also have

$$\begin{aligned} T_{11}^\dagger T_{12} - T_{21}^\dagger T_{22} &= 0 \\ T_{12}^\dagger T_{11} - T_{22}^\dagger T_{21} &= 0. \end{aligned} \tag{234}$$

With the use of the explicit form of the transfer matrix, given by Eq. (226), we obtain from Eq. (232) the relation

$$(t^-)^\dagger t^- + (r^-)^\dagger r^- = 1. \tag{235}$$

The second equation (234) gives

$$r^+ = -(t^-)^{-1\dagger}(r^-)^\dagger t^+, \tag{236}$$

which can be written in the form

$$r^-(t^-)^{-1} = -(t^+)^{-1\dagger}(r^+)^\dagger. \tag{237}$$

Inserting (236) into Eq. (233) gives, after some algebra, the relation

$$(t^+)^\dagger t^+ + (r^+)^\dagger r^+ = 1. \tag{238}$$

The equations (235) and (238) are a direct consequence of the flux conservation. They tell us that the electron either transmits through the sample or is reflected back.

The relation (237) enables us also to simplify the expression for T_{11},

$$\begin{aligned} T_{11} &= t^+ - r^-(t^-)^{-1}r^+ = t^+ + (t^+)^{-1\dagger}(r^+)^\dagger r^+ \\ &= (t^+)^{-1\dagger}\left[(t^+)^\dagger t^+ + (r^+)^\dagger r^+\right] \\ &= (t^+)^{-1\dagger}. \end{aligned} \tag{239}$$

The *time reversal symmetry* implies that the transfer matrix fulfills the relation

$$\begin{pmatrix} 0 & 1 \\ 1 & 0 \end{pmatrix} \mathbf{T} \begin{pmatrix} 0 & 1 \\ 1 & 0 \end{pmatrix} = \mathbf{T}^*. \tag{240}$$

From Eq. (240) we obtain that for systems with time reversal symmetry the transfer matrix can be written in the form

$$\mathbf{T} = \begin{pmatrix} T_{11} & T_{12} \\ T_{12}^* & T_{11}^* \end{pmatrix}, \tag{241}$$

where T_{11} and T_{12} are the $N \times N$ complex matrices. Also, from Eq. (230) we see that $|\det \mathbf{T}| = 1$ and from Eq. (240) we get $(\det \mathbf{T})^* = \det \mathbf{T}$. Consequently, $\det \mathbf{T} = 1$ when the time reversal symmetry is preserved.

From Eq. (241) we also find that in the case of time reversal symmetry the matrices t^+ and t^- are related by the relation

$$t^+ = (t^-)^T. \tag{242}$$

A.3 Parametrization of the transfer matrix

Consider now the system with time reversal symmetry. Then, the transfer matrix, T, is determined by two complex matrices, T_{11} and T_{12}, which are completely determined by $4N^2$ *real* parameters. However, these parameters are not independent of each other, since the matrices T_{11} and T_{12} must fulfill the relations of flux conservation.

We insert the expression (241) into Eq. (230) and from Eq. (233) we obtain the relation

$$T_{11}^\dagger T_{11} - T_{12}^T T_{12}^* = 1, \tag{243}$$

which implies N^2 additional relations between the elements of the matrices T_{11} and T_{12}. Other constraints are given by the first of Eq. (234),

$$T_{11}^\dagger T_{12} - T_{12}^T T_{11}^* = 0, \tag{244}$$

which can be written in the form

$$A^T = A, \quad \text{where} \quad A = T_{12}^T T_{11}^*. \tag{245}$$

Equation (245) requires that the complex matrix A is symmetric. This requirement implies $N_o(N_o - 1)$ relations between the elements of the matrices T_{11} and T_{12}. Finally, we have that the matrices T_{11} and T_{12} are fully determined by $N(2N + 1)$ real parameters.

Following Ref. [178] let us look for the solution of Eqs. (243) in the form

$$T_{11} = uLv \quad \text{and} \quad T_{12} = u'L'v', \tag{246}$$

where u, u', v, and v' are the unitary matrices and L, L' are the diagonal *real* matrices. Inserting into Eq. (243) we obtain that

$$
\begin{aligned}
v^\dagger L^2 v - (v')^T (L')^2 (v')^* &= 1, \\
v^\dagger L u^\dagger u' L' v' - (v')^T L' (u')^T u^* L v^* &= 0,
\end{aligned}
\tag{247}
$$

which can be solved with

$$u' = u, \qquad v' = v^*, \qquad (L')^2 = L^2 - 1. \tag{248}$$

Since the complex unitary matrices u and v are determined together by $2N^2$ real parameters and the real diagonal matrix L needs N real parameters, we see that the solution (248) is consistent with our estimation of the number of free parameters of the transfer matrix.

Taking $L = \sqrt{1 + \lambda}$ we obtain that the transfer matrix can be parametrized in the form

$$\mathbf{T} = \begin{pmatrix} u & 0 \\ 0 & u^* \end{pmatrix} \begin{pmatrix} \sqrt{1+\lambda} & \sqrt{\lambda} \\ \sqrt{\lambda} & \sqrt{1+\lambda} \end{pmatrix} \begin{pmatrix} v & 0 \\ 0 & v^* \end{pmatrix}, \tag{249}$$

where u, v are the $N_o \times N_o$ unitary matrices. We also use the following parametrization of the diagonal elements λ_a:

$$\lambda_a = \frac{1}{2} \left[\cosh x_a - 1 \right]. \tag{250}$$

It was shown in Ref. [178] that parametrization (249) is the most general one. Any transfer matrix of the orthogonal system can be expressed in the form given by Eq. (249). A similar parametrization can be derived for the transfer matrices with unitary and symplectic symmetry. For unitary symmetry, the transfer matrix has the form

$$\mathbf{T} = \begin{pmatrix} u_1 & 0 \\ 0 & u_2 \end{pmatrix} \begin{pmatrix} \sqrt{1+\lambda} & \sqrt{\lambda} \\ \sqrt{\lambda} & \sqrt{1+\lambda} \end{pmatrix} \begin{pmatrix} v_1 & 0 \\ 0 & v_2 \end{pmatrix}, \tag{251}$$

i. e., it is determined by four unitary matrices u_1, u_2, v_1 and v_2 and by the diagonal matrix λ. A detailed derivation of relations (249,251) can be found in Ref. [178].

A.4 Transfer matrix *vs* conductance

From the flux conservation (230) we obtain the following relations for the transfer matrix:

$$\left[\mathbf{T}^\dagger\right]^{-1} = \begin{pmatrix} 1 & 0 \\ 0 & -1 \end{pmatrix} \mathbf{T} \begin{pmatrix} 1 & 0 \\ 0 & -1 \end{pmatrix}, \tag{252}$$

and

$$\mathbf{T}^{-1} = \begin{pmatrix} 1 & 0 \\ 0 & -1 \end{pmatrix} \mathbf{T}^\dagger \begin{pmatrix} 1 & 0 \\ 0 & -1 \end{pmatrix}, \tag{253}$$

With the use of these equations we obtain

$$\left[\mathbf{T}^\dagger\mathbf{T}\right]^{-1} = \begin{pmatrix} 1 & 0 \\ 0 & -1 \end{pmatrix} \mathbf{T}^\dagger\mathbf{T} \begin{pmatrix} 1 & 0 \\ 0 & -1 \end{pmatrix}. \tag{254}$$

Using Eqs. (254) and (234) we obtain

$$\left[\mathbf{T}^\dagger\mathbf{T}\right]^{-1} + \mathbf{T}^\dagger\mathbf{T} = \begin{pmatrix} 4T_{11}^\dagger T_{11} - 2 & 0 \\ 0 & 4T_{22}^\dagger T_{22} - 2 \end{pmatrix}. \tag{255}$$

Inserting into Eq. (255) the matrix elements $T_{11} = (t^+)^{-1\dagger}$, given by Eq. (239), and $T_{22} = (t^-)^{-1}$ we obtain the formula of Pichard [179]

$$\begin{pmatrix} t^+(t^+)^\dagger & 0 \\ 0 & (t^-)^\dagger t^- \end{pmatrix} = \frac{1}{4}\left[\mathbf{T}^\dagger\mathbf{T} + (\mathbf{T}^\dagger\mathbf{T})^{-1} + 2\right]^{-1}. \tag{256}$$

Note that relation (256) follows directly from the requirement of flux conservation.

We can also use the parametric form of the transfer matrix, given by Eq. (251), and we express the inverse of the r.h.s. of Eq. (256) in the form

$$\frac{1}{4}\left[\mathbf{T}^\dagger\mathbf{T} + (\mathbf{T}^\dagger\mathbf{T})^{-1} + 2\right] = \begin{pmatrix} v_1^\dagger & 0 \\ 0 & v_2^\dagger \end{pmatrix} \begin{pmatrix} 1+\lambda & 0 \\ 0 & 1+\lambda \end{pmatrix} \begin{pmatrix} v_1 & 0 \\ 0 & v_2 \end{pmatrix}. \tag{257}$$

Comparing the l.h.s. of Eq. (256) with Eq. (257), we obtain that

$$t^+(t^+)^\dagger = v_1^\dagger(1+\lambda)^{-1}v_1 \tag{258}$$

and

$$(t^-)^\dagger t^- = v_2^\dagger(1+\lambda)^{-1}v_2. \tag{259}$$

Both equations are equivalent if time reversal symmetry is preserved. Indeed, $(t^+)^\dagger = ((t^+)^T)^* = (t^-)^*$ and $v_2 = v_1^*$.

The matrices v_1 and v_2, obey the relation of unitarity, $v^{-1} \equiv v^\dagger$. Using this relation we can express the Hermitian matrix $(t^-)^\dagger t^-$ in the form

$$(t^-)^\dagger t^- = v_2^{-1}\frac{1}{1+\lambda}v_2. \tag{260}$$

Thus, the eigenvalues of the matrix $(t^-)^\dagger t^-$ are $(1+\lambda_a)^{-1}$ and the unitary matrix v_2^{-1} contains in its columns the corresponding eigenvectors.

Using the eigenvalues of the matrices $(t^-)^\dagger t^-$ and $(t^+)^\dagger t^+$ we can express the transmission,

$$g = \frac{e^2}{h} \operatorname{Tr}(t^-)^\dagger t^- = \frac{e^2}{h} \sum_a \frac{1}{1+\lambda_a}. \tag{261}$$

A.5   Open channels and evanescent waves

In previous Sections, we assumed that there are only propagating states in the leads. This might not be true in real systems. For instance, for the 3d model, we see from the dispersion relation, given by Eq. (20), that the propagation along the leads, (which is the z direction in our notation), is determined by the z-component of the wave vector, k_z, given by the relation

$$2\cos k_z = E - 2\cos k_x - 2\cos k_y \; , \tag{262}$$

where the transversal wave vector k_x is given by

$$k_{n_x} = \frac{2\pi}{L_x} n_x, \quad n_x = 0, 1, \ldots, L_x - 1 \tag{263}$$

for the periodic boundary conditions and

$$k_{n_x} = \frac{\pi}{L_x + 1} n_x, \quad n_x = 1, \ldots, L_x \tag{264}$$

for the hard wall boundaries. Similar relations hold for k_y.

Using the eigenfunctions $\Phi_{n_x}(x)$ and $\Phi_{n_y}(y)$, related to the eigenvalues of k_x and k_y, we find that the wave function in the leads is

$$\Psi(\vec{r}) = \sum_{n_x n_y} \phi_{n_x}(x)\phi_{n_y}(y)\frac{e^{ik_z}}{\sqrt{2i\sin k_z}}. \tag{265}$$

The wave vector $k_z = k_z(n_x, n_y)$ possesses $N = L_x L_y$ values given by Eq. (262) (not necessarily different from each other). The propagating solutions exist only for such values of k_z, for which

$$|2\cos k_z(n_x, n_y)| < 2, \tag{266}$$

i. e. when k_z is real. Otherwise, k_z is purely imaginary. and determines the exponential decrease of the wave function with distance form the left (right) boundary of the sample. Therefore, we have to distinguish between N_o and N, where N_o is the number of propagating channels with k_z real, and N is the total number of channels.

Since we assume that both leads are semi-infinite, it is clear that the evanescent waves, emitted from the reservoirs, are not able to reach the sample. Therefore, the size of the transmission and reflection matrices is $N_o \times N_o$. The necessity to distinguish between N and N_o complicates the calculation of the conductance. Indeed, the size of the transmission matrix t^- is N_o but the size of the matrix T_{22} defined by Eq. (231) is $N \times N$. If we order the eigenvectors in the matrix R in such way that the eigenvectors with index $1 \leq a \leq N_o$ correspond to the propagating modes, and the remaining eigenvectors correspond to the evanescent modes, then the transmission is given only by the $N_o \times N_o$ sub-matrix $[T_{22}]_{ab}$, with $a, b \leq N_o$:

$$T = \sum_{ab=1}^{N_o} \left| \left[T_{22}^{-1}\right]_{ab} \right|^2. \tag{267}$$

Other matrix elements of T_{22} correspond to the scattering of the electron into the evanescent channels. Note, the composition laws for the transmission and reflection of the system given by
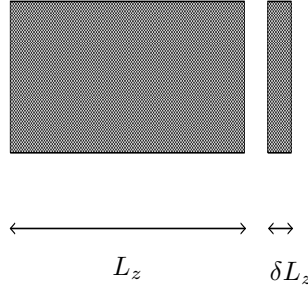
PSfrag replacements

$$L_z \qquad \delta L_z$$

Fig. 70. Small segment of length δL_z is added to the sample of length L_z.

Eqs. (228,229) are not valid in this case because evanescent waves between two subsystems can also contribute to the transport.

It is important to underline that the *analytical theories discussed in next two Appendices assume implicitly that there are no evanescent waves in the leads.*

In numerical simulations, we can avoid the evanescent waves for the band center ($E = 0$) by using anisotropic models, given, for instance, by Eq. (9). However, the evanescent waves cannot be completely excluded if we are interested in the transmission of the electron with energy close to the band edge. Indeed, from the E dependence of k_z, given by Eq. (262), we see that N_o is maximal for the band center and decreases to zero when the energy E approaches the band edge of the unperturbed system. Therefore, we have to consider evanescent waves in the numerical calculation of the conductance. The calculation of the conductance is described in Appendix E.

Note, there are no propagating channels for the energy E outside of the unperturbed band. Therefore, we are not able to calculate the conductance for such energies. This constrain complicates the scaling analysis of the conductance along the critical line shown in Fig. 6.

B   Dorokhov-Mello-Pereyra-Kumar (DMPK) Equation

The transfer matrix of the disordered system is a statistical variable. One can ask if there is a possibility to calculate the probability distribution $p(\mathbf{T})$, which is a joint probability distribution of all matrix elements of the transfer matrix, $\mathbf{T}$. This problem was solved by Mello *et al.* [7]. For the transfer matrix, given by expression (249), they derived the equation for the joint probability distribution of the parameters λ, which parametrize the transfer matrix in Eq. (249). Since the derivation of the DMPK equation is rather difficult, we present here only main ideas and refer the reader to the original work, [7].

Consider a weakly disordered system of length L_z, connected on both sides to the semi-infinite leads as shown in Fig. 18. There are N *open* channels in the leads, with N big enough to neglect all corrections of order N^{-1}. The channels are equivalent to each other. In the leads, each channel is characterized by the same wave vector k_z. The disorder is introduced inside the sample by random hopping terms between the channels.

Suppose we have a sample of length L_z and we know the probability distribution $p_{L_z}(\mathbf{T}')d\mathbf{T}'$. Now, we add to the sample of length L_z an additional random segment of length δL (Fig. 70).

The resulting sample will have length $L_z + \delta L_z$ and is characterized by the transfer matrix

$$\mathbf{T} = \mathbf{T}_\delta \mathbf{T}'. \tag{268}$$

We suppose that the length δL_z of the additional segment is sufficiently small so that the reflection coefficient of the segment is linear in δL_z,

$$R_\delta^+ = \mathrm{Tr}\,(r^+)^\dagger r^+ \propto a \frac{\delta L_z}{\ell}. \tag{269}$$

In Eq. (269), the length ℓ is the mean free path and we put $a = 1$. We also neglect all terms proportional to higher orders of δL_z. Equivalently, we can require that the trace,

$$\mathrm{Tr}\,\mathbf{T}_\delta^\dagger \mathbf{T}_\delta = 2N \left[1 + \frac{\delta L_z}{\ell}\right], \tag{270}$$

is linear in δL_z[7].

We also need to know the probability distribution $p_{\delta L}(\mathbf{T}_\delta)$ of matrix elements of the transfer matrix T_δ. This distribution represents the main building block of the theory. In Ref. [7], the Ansatz

$$p_{\delta L_z}(\mathbf{T}_\delta) \propto \exp -\frac{(N+1)\ell}{2\delta L_z}\mathrm{Tr}\,\lambda_\delta \tag{271}$$

was proposed. It represents the "most random" distribution of matrix elements of the transfer matrix T_δ. We remind the reader that parameters λ_δ for the transfer matrix T_δ are defined by Eq. (249). Clearly, $\mathrm{Tr}\,\langle\lambda_\delta\rangle = N\delta L_z/\ell$.

The probability distribution $p_{L_z + \delta L_z}(\mathbf{T})$ fulfills the Smoluchovsky equation,

$$p_{L_z + \delta L_z}(\mathbf{T}) = \int p_{L_z}(\mathbf{T}\mathbf{T}_\delta^{-1})p_{\delta L_z}(\mathbf{T}_\delta)d\mathbf{T}_\delta. \tag{272}$$

Inserting Eq. (271) into Eq. (272) leads, after rather complicated mathematical operations, to the equation for the joint probability distribution of eigenvalues λ:

$$\frac{\partial p_{L_z}(\{\lambda\})}{\partial(L_z/\ell)} = \frac{2}{\beta N + 2 - \beta}\,\frac{1}{J}\sum_a^N \frac{\partial}{\partial\lambda_a}\left[\lambda_a(1+\lambda_a)J\frac{\partial p_L(\{\lambda\})}{\partial\lambda_a}\right]. \tag{273}$$

Here, J is the Jacobian, given by

$$J \equiv \prod_{a<b}^N |\lambda_a - \lambda_b|^\beta \tag{274}$$

and β is the symmetry parameter, $\beta = 1, 2$ or 4 for orthogonal, unitary, or symplectic systems, respectively. Equation (273) is known in the literature as the DMPK equation. Note, the mean free path, ℓ, is the only parameter which enters the theory.

The DMPK equation, given by Eq, (273) does not contain any information about the matrices u and v. These variables were "integrated out" in the process of deriving Eq. (273). The main

---

[7]Note, in the case of zero reflection, the matrices $(t^-)^\dagger t^-$ and $t^+(t^+)^\dagger$ are diagonal and $\mathrm{Tr}\,T^\dagger T \equiv 2N$.
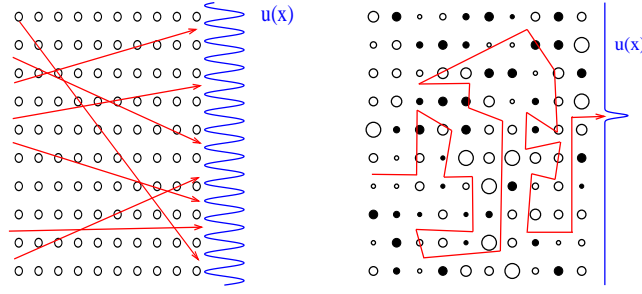
Fig. 71. The propagation of the electron through the disordered sample. Left: If the disorder is weak, then there are many paths through the structure. We expect that the wave function of the electron on the opposite side of the sample is spatially homogeneous. This corresponds to the assumption (275,276). Right: If the disorder is strong, there is in the best case only one path through the structure. Then, the wave function possesses sharp maxima at the opposite side of the sample; the positions of these maxima depend on the realization of the disorder in a given sample. It is clear that assumption (276) is not longer valid. Therefore, we do not expect that the DMPK equation, given by Eq. (273), describes the transport in strongly disordered systems.

assumption made in this process was that u, v and λ are statistically independent. Next, it was assumed that the elements of the matrix v fulfill the relations

$$\langle v_{ab}^* v_{cd} \rangle = \frac{1}{N} \delta_{ab} \delta_{cd} \tag{275}$$

and

$$\langle v_{ca}^* v_{cb}^* v_{da} v_{db} \rangle = \frac{1 + \delta_{ab}}{N(N+1)} \delta_{cd}, \tag{276}$$

and similar relations hold also for the matrix u. These assumptions limit the validity of the DMPK equation to the systems with weak disorder. It is implicitly assumed that there are many paths for the electron to propagate through the sample. Then, the density of the electron on the opposite side of the sample is homogeneous, as shown in the left panel of Fig. 71.

Another constraint of the DMPK equation is given by the assumption of the equivalence of all incoming and outgoing channels. In the real world, the channels are never equivalent, since they are determined by the incident angle (or by the transversal momentum) inside the leads, as shown in Fig. 18. The assumption that all channels are equivalent removes from the theory any information about the topology of the leads. Further, in the derivation of the DMPK it is assumed that channels are equivalent also *inside* the sample, since disorder was introduced by the random hopping between any two channels. Thus, the DMPK equation represents the simplest "mean field theory". In spite of the above constrains, the DMPK equation is surprisingly successful in the description of the electronic transport in weakly disordered quasi-1d systems. The DMPK equation can be easily generalized to description of more realistic systems. For instance, instead of the Ansatz (271) we can use more complicated probability distribution, which reflects the properties of the system, inclusive anisotropy and topology [180]. However, such generalization
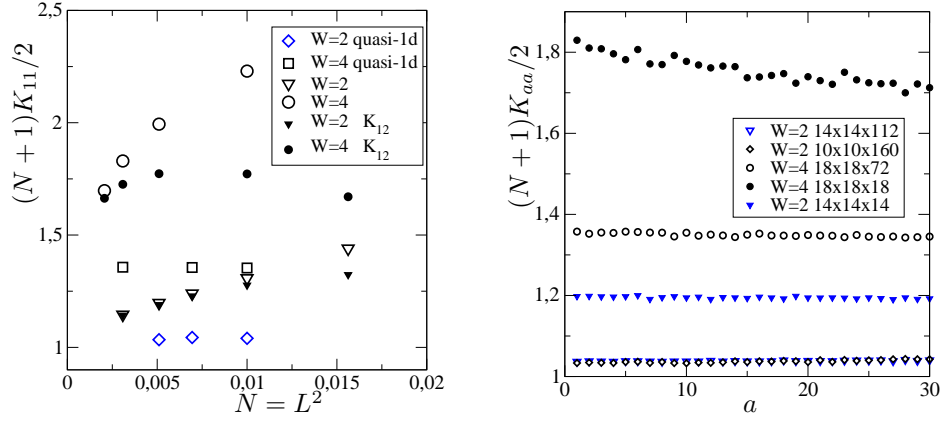
Fig. 72. Numerical verification of the validity of the DMPK equation. Left: The $N = L^2$ dependence of the $(N+1)K_{11}/2$ for the quasi-1d systems $L \times L \times 4L$ and for the cubes L^3. In the last case, also $(N+1)K_{12}$ is shown. The DMPK is applicable if these quantities converge to 1 in the limit of $L \to \infty$. Right: The a dependence of K_{aa} for the quasi-1d systems and for the cubes. Data were obtained for the anisotropic Anderson model with $t = 0.4$ with disorder $W = 2$ and $W = 4$, which corresponds to the mean free path $\ell = 9$ and $\ell = 1.8$, respectively [167].

does not bring any novel physical information. It only complicates the resulting formula for the transmission.

B.1   Numerical verification of validity of the DMPK equation

In Fig. 72 we verify numerically the validity of the relation (276). We consider the anisotropic Anderson model, given by Eq. (9) with $t = 0.4$ and calculate the matrix

$$K_{ab} = \left\langle \sum_c |u_{ac}|^2 |u_{bc}|^2 \right\rangle, \tag{277}$$

where, as usual, $\langle \ldots \rangle$ means averaging over the statistical ensemble. Requirement (276) is equivalent to

$$K_{ab} = \frac{1 + \delta_{ab}}{N + 1} \tag{278}$$

with $N = L^2$.

Our data show, that although the channels in the Anderson model are not equivalent to each other, the requirement (278) is perfectly fulfilled for the weakly disordered quasi-1d systems, as long as the mean free path, ℓ, is comparable to the width, L, of the system Agreement is worse for 3d systems. This is natural, since the 3d systems are expected to possess slightly different conductance statistics than the quasi-1d systems (see Table 1 which compares data for the universal conductance fluctuations, var g. in the quasi-1d, 2d and 3d systems). When disorder

increases, the mean free path decreases and the transversal structure of the sample becomes important. This could be included into the theory if a more detailed model for the distribution $p(\mathbf{T}_\delta)$ is considered.

B.2   Conductance

The DMPK equation can be directly used to calculate the first two moments of the conductance of the weakly disordered quasi-1d system. The method is described in Ref. [83]. When we are interested in the mean value of the function $F(\lambda)$, we multiply both sides of the DMPK equation, given by Eq. (273) by $F(\lambda)$ and integrate over λ. On the r.h.s., we obtain mean values of some other functions, $F_i(\lambda)$; repeating this procedure for F_i, we obtain a system of coupled equations for $\langle F \rangle$ and $\langle F_i \rangle$, which can be solved in the limit of $N \to \infty$. In this way, the mean conductance (in units of e^2/h) was calculated as

$$\langle g \rangle = \left\langle \sum_a \frac{1}{1 + \lambda_a} \right\rangle = \frac{N\ell}{L_z} - N\frac{\ell^2}{L_z^2} - \frac{1}{3}\left[1 - 3\frac{\ell}{L_z}\right] + \frac{L_z}{45N\ell} + \dots. \tag{279}$$

The first term, $N\ell/L_z$ can be identified with the conductivity, σ. Other terms represent the quantum corrections. Of particular interest is the diffusive regime, which is defined by the following relations between L_z and ℓ:

$$\ell \ll L_z \ll N\ell. \tag{280}$$

If the conditions (280) are fulfilled, then we can neglect the last term in Eq. (279). Assuming also that the system is sufficiently long, so that

$$N\frac{\ell^2}{L_z^2} \ll 1, \tag{281}$$

we can neglect also the 2nd term on the r.h.s. and we finally obtain the following estimation of the mean conductance:

$$\langle g \rangle = \frac{N\ell}{L_z} - \frac{1}{3}. \tag{282}$$

The correction, $\delta g = -1/3$, is the universal weak localization correction to the conductance of the quasi-1d system. This is a fully universal value, independent of any details of the system provided that the conditions (280,281) are fulfilled. The numerical verification of the relation (282) is shown in Fig. 28.

In a similar way, Mello and Stone calculated in Ref. [83] the variance,

$$\text{var } g = \langle g^2 \rangle - \langle g \rangle^2 = \frac{2}{15\beta}. \tag{283}$$

The variance of the conductance in the quasi-1d system is universal, given only by the physical symmetry (by the value of the parameter β). The same result was obtained in Ref. [9] by perturbation Green's function analysis.

The universal relations (282) and (283) hold only when the system is long enough (as required by Eq. (281)). In this case, the electron is scattered many times inside the sample so that its wave function and phase are sufficiently randomized. As required by Eq. (280), the length of the sample should not be too long, otherwise the effects of localization become important. This is analyzed in the next Section.

B.3 Limit $L_z \gg N\ell$

In the limit of $L_z \gg N\ell$, the localization appears. As shown in Appendix D, the wave function decreases exponentially in the limit of infinitely long system. This must be true also for the solution of the DMPK equation. Therefore, parameters $\lambda_a = (\cosh x_a - 1)/2$ increase exponentially with the system length. If we order the parameters λ,

$$\lambda_1 \ll \lambda_2, \ll \ldots, \ll \lambda_N, \tag{284}$$

then the Jacobian, given by Eq. (274), reduces to

$$J = \prod_{a=1} \lambda_a^{a-1} \tag{285}$$

and the DMPK equation splits into the N independent equations for the probability distributions $p(\lambda_a)$,

$$\frac{\partial p_L(\lambda_a)}{\partial(L/\ell)} = \frac{2}{\beta N + 2 - \beta} \; \lambda_a^{1-a} \frac{\partial}{\partial \lambda_a} \left[\lambda_a^{a+1} \frac{\partial p_L(\lambda_a)}{\partial \lambda_a} \right]. \tag{286}$$

In the derivation of Eq. (286 we used that $\lambda_a \gg 1$ so that $\lambda_a(\lambda_a + 1) \approx \lambda_a^2$. Substituting $\lambda_a = \exp x_a$, and using $\partial p(\lambda_a)/\partial \lambda_a = \lambda_a^{-1} \partial p(x_a)/\partial x_a$, we obtain

$$\frac{\partial p_{L_z}(x_a)}{\partial(L_z/\ell)} = \frac{2}{\beta N + 2 - \beta} \; \left[a \frac{\partial p_{L_z}(x_a)}{\partial x_a} + \frac{\partial^2 p_{L_z}(x_a)}{\partial x_a^2} \right], \tag{287}$$

which is the diffusion equation. The solution of Eq. (287) is

$$p_{L_z}(x_a) = \frac{1}{\sqrt{2\pi\sigma}} \exp - \frac{(x_a - \langle x_a \rangle)^2}{2\sigma} \tag{288}$$

with the mean value,

$$\langle x_a \rangle = 2 \frac{1 + \beta(a - 1)}{\beta N + 2 - \beta} \frac{L_z}{\ell}, \tag{289}$$

and variance,

$$\sigma = 2 \frac{2}{\beta N + 2 - \beta} \frac{L_z}{\ell}. \tag{290}$$

Thus, in the limit of $L_z/\ell \gg 1$, the parameters x_a become statistically independent. They possess Gaussian probability distributions with the same variance, σ, and with mean values which increase linearly as a function of index a:

$$\langle x_a \rangle = \langle x_1 \rangle + 2 \frac{\beta a}{\beta N + 2 - \beta} \frac{L_z}{\ell}. \tag{291}$$

The numerical data for the probability distributions $p_{L_z}(x_a)$ are shown in Fig. 73.

When calculating the conductance, we can neglect all contributions from the higher channels We obtain
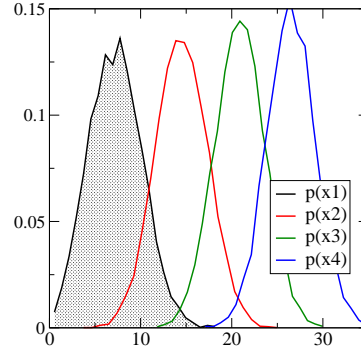
$$g \approx 4e^{-x_1} \tag{292}$$

Fig. 73. The statistical distributions of the parameters x_a for the weakly disordered quasi-1d system with the box disorder $W = 6$. The size of the system is $10 \times 10 \times 200$. Since disorder is weak, (the critical disorder $W_c = 16.5$ for the box distribution of random energies), we have $\langle x_a \rangle = a \langle x_1 \rangle$, in agreement with the DMPK equation. The length of the system, $L_z = 200$, is sufficient to localize all electronic states. All parameters x_a are large and posses the Gaussian distribution, as predicted by Eqs. (288-290).

which confirms that the conductance decreases exponentially when the system length increases. We also obtain that the *logarithm* of the conductance, $\ln g = -x_1 + \ln 4$, possesses the Gaussian probability distribution with the mean

$$\langle \ln g \rangle = -2 \frac{1}{\beta N + 2 - \beta} \frac{L_z}{\ell} + \ln 4 \tag{293}$$

and with the variance,

$$\operatorname{var} g = -2\langle \ln g \rangle - \ln 4. \tag{294}$$

The DMPK equation predicts the universal statistical properties of the conductance also in the localized regime.

However, it is important to mention that the localization described by the DMPK equation does not correspond to the true insulating regime. Note, the disorder is still weak in the system. The localization appears only due to the increase of the length of the system, L_z. We discuss in Sect. 11) that the localization in the weakly disordered quasi-1d systems differs qualitatively from the localization in the *strongly* disordered 3d systems.

C   Random matrix theory

Random matrix theory was developed 50 years ago for the description of the statistical properties of large matrices, which appear, for instance, in studies of the energy spectrum of big nuclei. The experimental data showed that the energy spectra possess common universal features - for instance, the repulsion of the neighboring eigenvalues, similar to that shown in the left panel of Fig. 12. It was suggested that the Hamiltonian of a big nucleus can be approximated by a random matrix. Then, the qualitative properties of the energy spectra can be obtained from the general

properties of the random matrices. Recently, the random matrix theory for the transfer matrix was developed to explain some universal properties of the electron transmission in the diffusive regime.

We present here the formula for the joint probability distribution $p(\Lambda)$ of the eigenvalues of the random matrix. More details about the theory can be found in Refs. [44, 179].

Consider a real symmetric $N \times N$ matrix $\mathbf{H}$ with random elements H_{ab}. Let us define the joint probability distribution of its elements, $P(\mathbf{H})d\mathbf{H}$. The measure $d\mathbf{H}$ is given as

$$d\mathbf{H} = \prod_{i=1}^{N} dH_{ii} \prod_{i<j} dH_{ij}. \tag{295}$$

Our aim is to find the expression for the joint probability distribution of the eigenvalues of the matrix H. Consider only the orthogonal symmetry class. Then the matrix $\mathbf{H}$ is real and symmetric. It can be diagonalized like

$$\mathbf{H} = \mathbf{Q}\Lambda\mathbf{Q}^{-1}, \tag{296}$$

with the helps of the orthogonal matrix $\mathbf{Q}$, which fulfills $\mathbf{Q}^{-1} = \mathbf{Q}^T$. It is evident that

$$\mathbf{Q}\mathbf{Q}^T = 1. \tag{297}$$

Then, each element H_{ij} can be expressed as

$$H_{ij} = \sum_{k=1}^{N} \Lambda_k Q_{ki} Q_{kj}. \tag{298}$$

Since $\mathbf{H}$ is a real symmetric matrix, it is fully determined by the $N(N+1)/2$ real independent parameters, H_{ij}, $i \leq j$. We want to express the measure dH in terms of the eigenvalues Λ_i and parameters x_a of the matrix Q (there are exactly $N(N-1)/2$ independent parameters x_a which determine matrix Q). We need to find the Jacobian, J, of the transformation

$$d\mathbf{H} = \prod_{i=1}^{N} dH_{ii} \prod_{i<j} dH_{ij} = J_N(\{\Lambda\}, \{Q_{ij}\}) \prod_{i=1}^{N} d\Lambda_i \prod_a x_a. \tag{299}$$

The Jacobian matrix can be schematically written in the form

$$\mathbf{J} = \begin{pmatrix} \dfrac{\partial H_{ii}}{\partial \lambda_\alpha} & \dfrac{\partial H_{ij}}{\partial \lambda_\alpha} \\ \dfrac{\partial H_{ii}}{\partial x_\mu} & \dfrac{\partial H_{ij}}{\partial x_\mu} \end{pmatrix}, \tag{300}$$

where the upper left quadrant is the $N \times N$ matrix, (i counts columns and α counts rows), and the lower right quadrant is a square matrix of size $N(N-1)/2$ ($i < j$ counts columns and μ counts rows of the matrix).

With the help of Eq. (298) we see that the first N rows of the matrix $\mathbf{J}$ do not contain Λ. Also, all elements in the lower $N(N-1)/2$ rows are linear in the eigenvalues. Therefore, $J = \det \mathbf{J}$ is a polynomial of order of $N(N-1)/2$ in the eigenvalues Λ. In order to find the form of this polynomial one has to realize that if the matrix $\mathbf{H}$ possesses two degenerate eigenvalues, $\lambda_a = \lambda_b$

for $a \neq b$, then diagonalization of $\mathbf{H}$ is not unique and the matrix $\mathbf{J}^{-1}$, which determines the transformation inverse to (296), must be singular. Therefore, $J = \det \mathbf{J} = 0$ for the degenerate matrix. Then, we easily find that

$$J = \prod_{a<b} |\Lambda_a - \Lambda_b| \, F(\{x\}), \tag{301}$$

where the function $F(x)$ does not contain any information about the eigenvalues Λ. We obtain

$$P(\mathbf{H})d\mathbf{H} = P(\{\Lambda\})J(\{\Lambda\}d\Lambda P(x)dx. \tag{302}$$

Now, we can integrate out all parameters x to obtain the probability distribution for eigenvalues, Λ.

In the case of unitary and symplectic systems, the Jacobian changes to

$$J_\beta = \propto \prod_{a<b} |\Lambda_a - \Lambda_b|^\beta, \tag{303}$$

where $\beta = 2$ ($\beta = 4$) for the unitary (symplectic) symmetry, respectively.

The expression (303) plays an important role in the theory of random matrices. It tells us that there is a zero probability to find degenerate eigenvalues. The level repulsion is a typical property of random matrices. We have shown already in Fig. 13, that the spectrum of weakly disordered Hamiltonian exhibits level repulsion.

To find an explicit form of the probability distribution $P(\Lambda)$, we look for the probability distribution $P(\Lambda)$ in the form

$$P(\Lambda) = J_\beta \exp \sum_a F(\Lambda_a). \tag{304}$$

Choosing the expression (304), we implicitly assume that $F(\Lambda)$ is a function of only one eigenvalue. We will see later that this assumption might not be fulfilled in some applications of random matrix theory.

In the limit of $N \to \infty$, we introduce the level density, $\sigma(\Lambda)$ and we write the distribution (304) in the continuum form,

$$P(\Lambda) = e^{-\beta H} \tag{305}$$

where

$$H = -\frac{1}{\beta} \int d\Lambda \sigma(\Lambda) F(\Lambda) - \frac{1}{2} \int \int d\Lambda d\Lambda' \sigma(\Lambda) \sigma(\Lambda') \ln |\Lambda - \Lambda'|. \tag{306}$$

To specify the function F, we must introduce some constrains. We can, for instance, require a specific form of the density, $\sigma(\Lambda)$ and look for the "most random" distribution $P(\Lambda)$ by minimizing the "Hamiltonian" H. The condition

$$\frac{\delta H}{\delta \sigma} = 0 \tag{307}$$

leads to the following expression for F:

$$F(\Lambda) = -\beta \int d\Lambda' \sigma(\Lambda') \ln |\Lambda - \Lambda'|. \tag{308}$$

In the next Section, we apply the above formulas to the transfer matrix.

C.1   Application to transfer matrix

Assuming that the transmission matrix

$$\left[t^\dagger t\right]^{-1} = v^\dagger(1+\lambda)v \tag{309}$$

of the diffusive system belongs to the class of random matrices, we immediately obtain that the distribution of parameters λ has a form

$$P(\{\lambda\}) = e^{-\beta H} \tag{310}$$

with

$$H = -\sum_{a<b} \ln|\lambda_a - \lambda_b| + \sum_a \int_0^\infty d\lambda \sigma(\lambda) \ln|\lambda - \lambda_a|. \tag{311}$$

The first term is the Jacobian, and the second term is the one particle potential, given by Eq. (308).

It is more useful to express the distribution (310,311) in terms of variables x_a instead of λ. Inserting $\lambda_a = (\cosh x_a - 1)/2$ into Eq. (311) we obtain

$$H(\{x\}) = -\sum_{a<b}^N \ln|\cosh x_a - \cosh x_b| - \frac{1}{\beta}\sum_a^N \ln|\sinh x_a| + \sum_a V(x_a). \tag{312}$$

The second term on the r.h.s. of Eq. (312) is the Jacobian of the transformation $\lambda \to x$, and we have used $\sigma(\lambda)d\lambda = \sigma(x)dx$. The last term is the one particle potential,

$$V(x) = \int_0^\infty dx' \, \sigma(x') \ln|\cosh x - \cosh x'|. \tag{313}$$

The density $\sigma(x)$ can be estimated from the numerical data. Fig. 41 shows that $\langle x_a \rangle \sim a$. This leads to the constant density

$$\sigma(x) = \begin{cases} \frac{N\ell}{L_z} & x < L_z/\ell \\ 0 & \text{otherwise.} \end{cases} \tag{314}$$

We insert expression (314) into Eq. (313), and we calculate the potential $V(x)$ following the method given in Ref. [181]. The first derivative of Eq. (313) reads

$$\frac{\partial V(x)}{\partial x} = \frac{N\ell}{L_z} \int_0^\infty \frac{\sinh x}{\cosh x - \cosh x'} dx'. \tag{315}$$

With the new variable, $y = e^{x'}$, we obtain

$$\frac{\partial V(x)}{\partial x} = \frac{N\ell}{L_z} \int_1^A \left[\frac{1}{y - e^{-x}} - \frac{1}{y - e^{+x}}\right] dy, \tag{316}$$

with $A = \exp L_z/\ell \gg 1$. Since $x > 0$, the first integral gives $\ln|A - e^{-x}| - \ln|1 - e^{-x}|$. The function $1/(y - e^x)$ possesses a singularity at e^x. Since the (negative) contribution to the integral from 1 to e^x cancels with the (positive) contribution from e^x to $2e^x - 1$, we obtain that
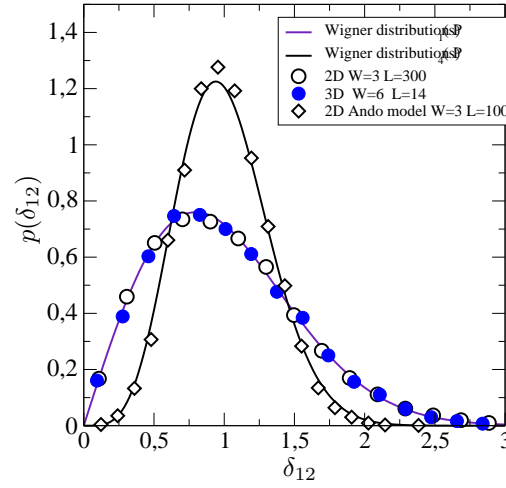
Fig. 74. The probability distribution $p(\delta_{12})$ of the *normalized* difference $x_2 - x_1$ for three models in the diffusive regime. Two systems with orthogonal symmetry have the same distribution p_1, given by Eq. (32). This confirms that the important property in the diffusive regime is not determined by the dimension of the sample, but by the randomization of the electronic wave function due to the multiple scattering. The third statistical ensemble, given by the 2d Ando model, possesses the symplectic symmetry ($\beta = 4$) The solid lines are the Wigner distributions.

the second integral gives $\ln|A - e^x| - \ln|e^x - 1|$. For $A >> e^x$ the difference of the two integrals is $\ln|e^x - 1| - \ln|1 - e^{-x}| \equiv x$. We finally obtain

$$\frac{\partial V(x)}{\partial x} = \frac{N\ell}{L_z}\,x. \tag{317}$$

Thus, we have the *quadratic* one particle potential,

$$V(x) = \frac{N\ell}{2L}x^2. \tag{318}$$

The probability distribution $P(x)$ is similar to the statistical sum of the one dimensional Coulomb gas. In the Coulomb gas analogy, the parameters x_a represent the position of the ath particle confined in the quadratic potential $V(x)$ and interacting with the other particles by the two particle logarithmic interaction. The parameter β is the "temperature". A detailed analysis of the probability distribution $p(x)$ and of the consequences for the diffusive transport are given in a series of papers of Pichard *et al.* [179, 181–184].

The most simple consequence of the probability distribution $p(x)$ is the "level repulsion". From random matrix theory it follows that the *normalized* difference

$$\delta_{a,a+1} = \frac{x_{a+1} - x_a}{\langle x_{a+1} - x_a \rangle} \tag{319}$$

is distributed with the Wigner distribution p_β. This was confirmed by numerical simulations [102, 181, 182]. In Fig. 74 we plot $p(\delta_{12})$ for three statistical ensembles for the 2d and 3d
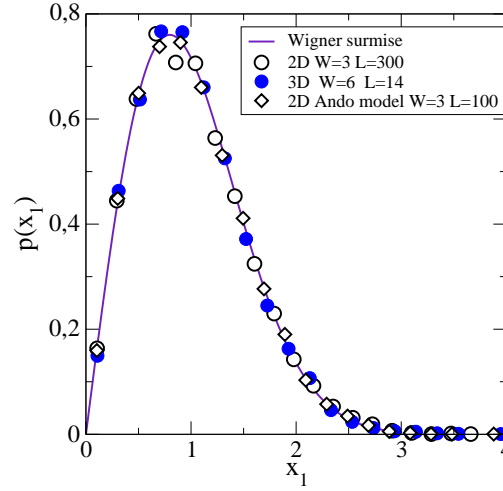
Fig. 75. The distribution $p(x_1)$ of the *normalized* parameter x_1 for three different models in the diffusive regime. The solid line is the Wigner distribution, given by Eq. (32). Note, the distribution $p(x_1)$ does not depend on the physical symmetry of the model.

orthogonal systems, and for the 2d Ando model. The data confirm that the distributions $p(\delta_{12})$ are indeed very similar to the Wigner distributions.

Note, the term $\ln \sinh x$ in the "Hamiltonian" (312) can be interpreted as the interaction of the particle located at x with its "mirror image", i. e. the particle located at $-x$. Therefore, the distribution of $p(x_1)$ is given by the Wigner distribution, too. However, since the "interaction", $\ln \sinh x$, does not depend on β, the distribution $p(x_1)$ should not depend on the physical symmetry [181]. This is confirmed in Fig. 75.

Figure 76 confirms that the spectrum of parameters x_a is linear in the diffusive regime, both in the 2d and 3d systems,

$$\langle x_a \rangle = [1 + (a-1)\beta] \langle x_1 \rangle. \tag{320}$$

For $\beta = 1$, a more accurate estimation, which agrees also with results of numerical simulations, can be derived from random matrix theory,

$$x_a \propto \sqrt{X_a}, \tag{321}$$

where X_a are zeros of Laguerre polynomials L_N [90, 91], $X_a \approx [4(N+1/2)]^{-1} j_0^2(a)$, where $j_0(a)$ is the ath zero of the Bessel function $J_0(x)$. In the limit of $a \gg 1$, $j_0(a) \approx \pi(a - 1/4)$, so that Eq. (321) gives $x_a \propto a$.

The right Fig. 76 shows the a dependence of parameters g_a,

$$g_a = \cosh^{-2} x_a/2. \tag{322}$$

Clearly, g_a is the contribution of the ath channel and
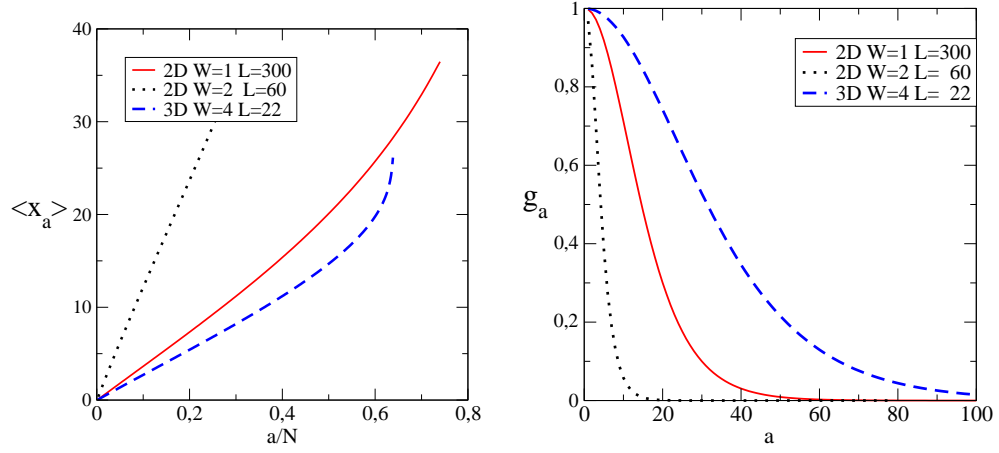
$$g = \sum_a g_a. \tag{323}$$

Fig. 76. The index dependence of the mean $\langle x_a \rangle$ (left) and g_a (right) for the 2d and 3d weakly disordered systems. The data confirm the linearity given by Eq. (320). To calculate $\langle x_a \rangle$, we have to diagonalize the matrix $t^\dagger t$ for each sample, extract x_a from the eigenvalue $(1 + \lambda_a)^{-1}$. The mean value, $\langle x_a \rangle$ is obtained by averaging over the statistical ensemble. Note, the data for large a are not present since $\cosh^2(x_a/2)$ exceeds the numerical accuracy of the computers for such large values of x_a. The conductance $\langle g \rangle = 16.1$, 4.3 for the 2d systems with $W = 1$ and $W = 2$, respectively, and $\langle g \rangle = 42.1$ for the 3d system. In the last model, the anisotropy, $t = 0.4$ was used to avoid the evanescent channels in leads.

Because of the rigidity of the spectrum, the fluctuations of x_a are of the order of the mean spacing, which is $\sim L_z/N\ell$. We see that g_a are very close to 1 for small a and exponentially small when $a \to N$. There is N_{eff} channels for which $x_a \leq 1$. Higher channels, with $a > N_{\text{eff}}$ give only negligible small contribution to transport Then, the conductance $g \approx N_{\text{eff}}$. The slope of the linear dependence, $\langle x_1 \rangle$, determines the conductance: if $\langle x_{N_{\text{eff}}} \rangle = 1$, then we have, from Eq. (320) that

$$\langle g \rangle = N_{\text{eff}} = 1 + \frac{1}{\beta}\left(\frac{1}{\langle x_1 \rangle} - 1\right). \tag{324}$$

This expression simplifies for $\beta = 1$:

$$\langle g \rangle = N_{\text{eff}} = \frac{1}{\langle x_1 \rangle}. \tag{325}$$

Since $g = N\ell/L_z$, we immediately see that

$$\langle x_1 \rangle = \frac{L_z}{N\ell}. \tag{326}$$

Thus, all parameters x_a increase linearly with the length of the system. The mean value, $\langle x_a \rangle$, as well as the spacing between two neighboring parameters, $\langle x_a \rangle$, decreases as N^{-1}.

The rigidity of the spectrum of parameters x_a was used for the explanation of the universality of conductance fluctuations in Ref. [92].

Random matrix theory represents a powerful tool for the analysis of transport in disordered systems. More details are given in Refs. [35, 179, 185].

C.2 DMPK equation versus random matrix theory

Both the DMPK equation and the random matrix theory were successfully applied to the transport in disordered systems. Originally it was believed that the theories are equivalent. This would mean that the probability distribution $p(\lambda)$, given by random matrix theory, solves the DMPK equation.

However, these two approaches are not equivalent. The discrepancy between the two approaches was observed when Beenakker [85] calculated the variance of the conductance from random matrix theory. The obtained result, var $g = 1/8\beta$ differs from the exact value, var $g = 2/15\beta$, obtained by the diagrammatic expansion [9] and from the DMPK equation [83]. This proves that random matrix theory is not exact. Beenakker and Rejaei [186] solved the DMPK equation for $\beta = 2$. Both in the metallic and localized regimes, the solution reads

$$p(x) = \exp -\beta \left[\sum_a V(x_a) + \sum_{a<b} u(x_a, x_b) \right], \tag{327}$$

with the interacting term

$$u(x_a, x_b) = -\frac{1}{2} \ln |\cosh x_a - \cosh x_b| - \frac{1}{2} \ln |x_a^2 - x_b^2| \tag{328}$$

and with the one-particle potential,

$$V(x_a) = \frac{N\ell}{2L_z} x_a^2 - \frac{1}{4} \ln(x_a \sinh x_a). \tag{329}$$

This solution is very similar to the probability distribution derived from random matrix theory. However, note, that it cannot be obtained from the Ansatz (304), since the two particle interaction, given by Eq. (328), is not determined by the Jacobian only. Therefore, the one parameter function $F(\lambda)$, introduced in Eq. (304), is not sufficient for obtaining the distribution (327).

D Lyapunov exponent

D.1 One-dimensional case

The Lyapunov exponent, $\gamma(E)$, of the one dimensional disordered system is defined by the relation

$$\gamma(E) = \lim_{L_z \to \infty} \frac{1}{2L_z} \ln \left(\Psi_{L_z}^2 + \Psi_{L_z+1}^2 \right), \tag{330}$$

Note also, that the wave function

$$|\Psi_{L_z}| \propto e^{-\gamma L_z} \tag{331}$$

decreases exponentially when L_z increases. From Eq. (330) we see that the real part of the Lyapunov exponent determines the localization length,

$$\text{Re } \gamma(E) = \lambda^{-1}. \tag{332}$$

Thouless [187] showed that the *imaginary part* is related to the density of states by the relation

$$\rho(E) = \frac{2}{\pi} \frac{\partial}{\partial E} \text{Im } \gamma(E). \tag{333}$$

In the 1d systems, the Lyapunov exponent can be found analytically in the limit of weak disorder. For the Anderson model, defined by Eq. (75), we find

$$\gamma(E) = ik + \frac{\langle \varepsilon^2 \rangle}{2(4 - E^2)}, \tag{334}$$

with $E = 2 \cos k$. Note that the expression (334) fails when close to the band edge, $|E| \to 2$. A more detailed analysis [188, 189] showed that in this case $\gamma \propto W^{2/3}$. In general, the weak disorder expansion exhibits a peculiar behavior in the neighborhood of energies $E = 2 \cos \pi p/q$, with p and q being integers. At the band center, $E = 2 \cos \pi/2 = 0$, the fourth order term of the expansion diverges and gives rise to the correction of the 2nd order term [188, 189]. For instance, $\text{Re}\gamma = W^2/96$ for $E = 0$ and the box disorder, defined by Eq. (10), since $\langle \varepsilon^2 \rangle = 1/12$. Correct expression, which takes into account the higher order terms of the expansion, gives $\text{Re}\gamma = W^2/105.4$, which agrees with numerical data.

The Lyapunov exponent plays an important role in the theory of localization. In the next Section, we generalize the 1d case to the quasi-1d systems. Note that the Schrödinger equation,

$$\Psi_{n+1} + (\varepsilon_n - E)\Psi_n + \Psi_{n-1} = 0, \tag{335}$$

can be written in the matrix form

$$\begin{pmatrix} \Psi_{n+1} \\ \Psi_n \end{pmatrix} = \begin{pmatrix} E - \varepsilon_n & -1 \\ 1 & 0 \end{pmatrix} \begin{pmatrix} \Psi_n \\ \Psi_{n-1} \end{pmatrix}. \tag{336}$$

Then we can write

$$\Psi_{L_z+1}^2 + \Psi_{L_z}^2 = (\Psi_{L_z+1}, \Psi_{L_z}) \begin{pmatrix} \Psi_{L_z+1} \\ \Psi_{L_z} \end{pmatrix} = (\Psi_1, \Psi_0)(\mathbf{M}^{(L_z)})^T \mathbf{M}^{(L_z)} \begin{pmatrix} \Psi_1 \\ \Psi_0 \end{pmatrix}, \tag{337}$$

where we have introduced the transfer matrix,

$$\mathbf{M}^{(L_z)} = \prod_{n=1}^{L_z} \mathbf{M}_n = \prod_{n=1}^{L_z} \begin{pmatrix} E - \varepsilon_n & -1 \\ 1 & 0 \end{pmatrix}. \tag{338}$$

Thus, in the limit of $L_z \to \infty$, γ is given by the eigenvalues of the matrix $\mathbf{M}^{(L_z)}$. Since $\mathbf{M}^{(L_z)}$ contains the random energies ε_i, γ is a statistical variable, too.

Oseledec [190] proved that the probability distribution, $p(\gamma)$ is Gaussian with the mean value $\langle \gamma \rangle \propto L_z$ and variance, $\text{var } \gamma \propto \langle \gamma \rangle$. Therefore, the variable

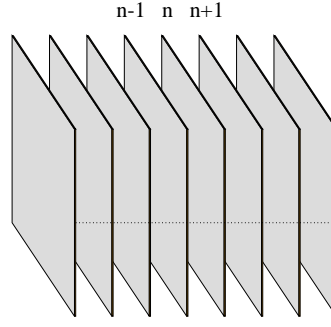$$z = \frac{2L}{L_z} \times \gamma \tag{339}$$

Fig. 77. We cut the quasi-1d system into the $L \times L$ vertical slices. The propagation of the electron in slice n is given by the Hamiltonian $\mathcal{H}_n$.

is a self-averaged quantity in the limit of long samples.

Self-averaging of the Lyapunov exponent can be intuitively understood from the expression (337). The Lyapunov exponent represents the logarithm of the eigenvalue of the matrix $(\mathbf{M}^{(L_z)})^T \mathbf{M}^{(L_z)}$, which is the product of the random matrices. Naively speaking, γ can be considered as a sum of logarithm of eigenvalues of the random matrices $\mathbf{M}_n$, $n = 1, 2, \ldots L_z$. Then, applying the central limit theorem we expect, that both the mean value and variance of γ are proportional to L_z.

D.2   Quasi-1d case

Consider the quasi-1d system of the size $L^{d-1} \times L_z$, and suppose that $L_z \gg L$. For the purpose of numerical analysis, we divide the system into a set of vertical slices, shown in Fig. 77 and we write the Schrödinger equation in the form

$$\Psi_{n+1} = (E - \mathcal{H}_n)\Psi_n - \Psi_{n-1}, \tag{340}$$

where $\mathcal{H}_n$ is the Hamiltonian related to the nth slice in Fig. 77, and Ψ_n is the vector which contains in its elements the wave function in sites of the nth slice. The length of the vector Ψ_n is $N = L^{d-1}$.

Equation (340) can be rewritten in the matrix form,

$$\begin{pmatrix} \Psi_{n+1} \\ \Psi_n \end{pmatrix} = \mathbf{M}_n \begin{pmatrix} \Psi_n \\ \Psi_{n-1} \end{pmatrix}, \tag{341}$$

where the transfer matrix, $\mathbf{M}_n$, is given by the relation

$$\mathbf{M}_n = \begin{pmatrix} E - \mathcal{H}_n & -1 \\ 1 & 0 \end{pmatrix}. \tag{342}$$

This relation is formally equivalent to Eq. (336) but now the matrix $\mathbf{M}_n$ has the size $2N \times 2N$. Note, det $M_n \equiv 1$. Also, the eigenvalues of $\mathbf{M}_n$ appear in pairs, λ and λ^{-1}.

Now we calculate the $2N \times 2N$ matrix

$$\mathbf{M}^{(L_z)} = \prod_{n=1}^{L_z} \mathbf{M}_n = \prod_{n=1}^{L_z} \begin{pmatrix} E - \mathcal{H}_n & -1 \\ 1 & 0 \end{pmatrix}. \tag{343}$$

The matrix $\mathbf{M}^{(L_z)}$ determines the behavior of the wave function at long distances. Since the system is effectively one dimensional, the wave function must decrease exponentially when the length of the system, L_z, increases. This exponential decrease is given by the eigenvalues, $\exp{-\gamma_a}$, with $\gamma_a > 0$. Clearly, the smallest γ_a determines the localization length.

Since the matrices $\mathbf{M}_n$ contains the random variables, ε_n, α_a are also statistical variables, and we need to know their probability distributions. Following Oseledec [190], we have that in the limit of $L_z \to \infty$ all the eigenvalues of the matrix

$$[\mathbf{M}^{(L_z)}\mathbf{M}^{(L_z)}]^{L/L_z} \tag{344}$$

converge to $\lambda_a = e^{\zeta_a}$ and $\lambda_{N+a} = e^{-\zeta_a}$ where

$$\zeta_a = \frac{2L}{L_z} \times \gamma_a. \tag{345}$$

The mean value, $\langle \zeta_a \rangle$, does not depend on L_z, and the variance,

$$\text{var } \zeta_a = \langle \zeta_a^2 \rangle - \langle \zeta_a \rangle^2 \propto \frac{L}{L_z}. \tag{346}$$

Thus, Oseledec theorem states that the parameters ζ_a are the self-averaged quantities in the limit of $L_z \to \infty$. For a given realization for the disorder, the eigenvalues of the matrix (344) converge to their mean values. In numerical simulations, the length L_z is finite, so that the obtained numerical data, ζ_a, differs from the limited mean values, $\langle \zeta_a \rangle$. Oseledec theorem enables us to estimate the typical difference,

$$\zeta_a - \langle \zeta_a \rangle \sim \sqrt{\text{var } \zeta_a} \propto \left(\frac{L}{L_z} \right)^{1/2}. \tag{347}$$

Thus, we can avoid the problem of statistical fluctuations in numerical calculations. It is sufficient to calculate the product of the transfer matrices, $\mathbf{M}^{(L_z)}$, for a sufficiently large system length, L_z, and then to calculate the eigenvalues, ζ_a. If L_z is large enough, then the obtained values ζ_a lie close to the mean values, $\langle \zeta_a \rangle$. This procedure is applied in the finite size scaling analysis of Lyapunov exponents, discussed in Section 12.1.

In what follows we order $\zeta_1 > \zeta_2 > \ldots > \zeta_N$. That means that

$$\zeta_a = z_{N+1-a}, \tag{348}$$

where z_a are discussed in Sect. 12. Clearly, the smallest Lyapunov exponent, z_1, equals to the smallest eigenvalue ζ_N.

In the numerical simulations, we need to calculate the smallest (in absolute value) parameter $\zeta_N = z_1$. This can be done by the following numerical algorithm.

1. Choose the required accuracy ε of ζ_N. Then, start with the following variables: first, we need the $N \times 2N$ matrix $\mathbf{V}$ which contains in N columns the mutually orthogonal vectors v_a of the length $2N$. We will also need the vectors d_a and e_a of the length N and put their stating values, $d_a = (0, 0, \ldots 0)$ and $e_a = (0, 0, \ldots 0)$. Also, put $L_z = 0$.

2. Calculate the n_i iterations

$$\mathbf{U} = \prod_{n=1}^{n_i} \mathbf{M}_n \mathbf{V}. \tag{349}$$

3. Perform the Schmidt orthogonalization of vectors u_a, given by columns of the matrix $\mathbf{U}$. Obtain new vectors w_a, which are already orthogonal to each other.

4. Calculate the norm of vectors w_a, and add these norms into vectors d and e as follows:

$$d_a = d_a + \ln |w_a| \tag{350}$$

and

$$e_a = e_a + (\ln |w_a|)^2. \tag{351}$$

5. Put

$$u_a = w_a / |w_a| \tag{352}$$

and the length,

$$L_z = L_z + n_i. \tag{353}$$

Calculate $\zeta_a = d_a / L_z$, $\eta_a = e_a / L_z$ and the accuracy

$$\varepsilon_a = \frac{\sqrt{\eta_a - \zeta_a^2}}{\zeta_a}. \tag{354}$$

6. If $\varepsilon_N > \varepsilon$ then go to the step 2, otherwise stop.

The obtained value of ζ_N is the required smallest Lyapunov exponent z_1.

The length L_z, necessary for the calculation of the smallest Lyapunov exponent, depends on the required accuracy, ε. For the 3d Anderson model, the length of the system, L_z was estimated in Ref. [91] as

$$L_z = \frac{1}{2\varepsilon^2} L. \tag{355}$$

In numerical simulations, the accuracy $\varepsilon = 0.001$ is usually required. Then, $L_z = 500.000 \times L$. The number of iterations between two successive Schmidt orthogonalization is $n_i \approx 6 - 8$ for the critical disorder, and smaller (larger) when $W \gg W_c (W \ll W_c)$, respectively.

E   Calculation of the conductance

E.1   1d case

It is convenient to write the Schrödinger Equation (75) in the form

$$\left(\begin{array}{c} \Psi_{n+1} \\ \Psi_n \end{array} \right) = \mathbf{M}_n \left(\begin{array}{c} \Psi_n \\ \Psi_{n-1} \end{array} \right) = \left(\begin{array}{cc} E - \varepsilon_n & -1 \\ 1 & 0 \end{array} \right) \left(\begin{array}{c} \Psi_n \\ \Psi_{n-1} \end{array} \right). \tag{356}$$

To calculate the conductance, consider the sample of the length L_z sites[8], connected to two semi-infinite ideal leads. This means that $\varepsilon_n = 0$ for both $n \leq 0$ and for $n > N - 1$.

Note that the transfer matrix $\mathbf{M}$, defined in Eq. (356) does not have the structure of the transfer matrix $\mathbf{T}$. Indeed, $\mathbf{T}$ connects the propagating waves on the left and right hand side of the sample, while $\mathbf{M}$ relates the wave functions in the the site representation. Both matrices are connected by the transformation,

$$\mathbf{T}_n = \mathbf{Q}^{-1}\mathbf{M}_n\mathbf{Q} = \mathbf{Q}^{-1} \left(\begin{array}{cc} E - \varepsilon_n & -1 \\ 1 & 0 \end{array} \right) \mathbf{Q}, \tag{357}$$

where

$$\mathbf{Q} = \left(\begin{array}{cc} 1 & 1 \\ e^{-ik} & e^{+ik} \end{array} \right). \tag{358}$$

Consider the electron coming from the right hand side of the system. Then, on the left hand side of the system, there is only a transmitted wave going to the left. Its wave function at the sites $n = 0$ and $n = -1$ can be written as

$$\begin{array}{rcl} \Psi_{-1} & = & e^{+ik} \\ \Psi_0 & = & 1. \end{array} \tag{359}$$

The wave function on the right-hand side of the system is given by superposition of the incoming and reflected waves. We can use the transfer matrix, $\mathbf{M}$, to express the wave function at sites L_z and $L_z - 1$:

$$\left(\begin{array}{c} \Psi_{L_z} \\ \Psi_{L_z-1} \end{array} \right) = \mathbf{M}_{L_z-1}\mathbf{M}_{L_z-2}\dots\mathbf{M}_1\mathbf{M}_0 \left(\begin{array}{c} \Psi_0 \\ \Psi_{-1} \end{array} \right) = \mathbf{M}^{(L_z)} \left(\begin{array}{c} \Psi_0 \\ \Psi_{-1} \end{array} \right). \tag{360}$$

Now we multiply both sides of the of Eq. (360) by the matrix $\mathbf{Q}^{-1}$. We get

$$\mathbf{Q}^{-1} \left(\begin{array}{c} \Psi_{L_z} \\ \Psi_{L_z-1} \end{array} \right) = \mathbf{Q}^{-1}\mathbf{M}^{L_z}\mathbf{Q}\mathbf{Q}^{-1} \left(\begin{array}{c} \Psi_0 \\ \Psi_{-1} \end{array} \right). \tag{361}$$

We obtain that

$$\frac{1}{2i \sin k} \left(\begin{array}{c} e^{ik}\Psi_{L_z} - \Psi_{L_z-1} \\ -e^{-ik}\Psi_{L_z} + \Psi_{L_z-1} \end{array} \right) = \mathbf{T}^{(L_z)} \frac{1}{2i \sin k} \left(\begin{array}{c} e^{ik}\Psi_0 - \Psi_{-1} \\ -e^{-ik}\Psi_0 + \Psi_{-1} \end{array} \right), \tag{362}$$

---

[8]For simplicity, we use the lattice constant, a as the unit length

where we used the relation (357). between the transfer matrices $\mathbf{M}$ and $\mathbf{T}$. Using the explicit form of Ψ_0 and Ψ_{-1}, given by Eqs. (359) we find that the r.h.s. of Eq. (362) equals to

$$\mathbf{T}^{(L_z)} \begin{pmatrix} 0 \\ 1 \end{pmatrix}. \tag{363}$$

From Eq. (362) we obtain

$$\frac{1}{2i \sin k} \begin{pmatrix} e^{ik}\Psi_{L_z} - \Psi_{L_z-1} \\ -e^{-ik}\Psi_{L_z} + \Psi_{L_z-1} \end{pmatrix} = \begin{pmatrix} r^+(t^-)^{-1} \\ (t^-)^{-1} \end{pmatrix}. \tag{364}$$

So we obtain the transmission coefficient in the form

$$T = |t^-|^{-2} = \frac{4\sin^2 k}{|e^{-ik}\Psi_{L_z} - \Psi_{L_z-1}|^2}. \tag{365}$$

Equation (365) is very useful for numerical calculations of the transmission T.

E.2   Quasi-1d case

To calculate the conductance in the quasi-1d case, we have to generalize the method of the previous Section. We again assume that our system is connected to two semi-infinite leads with zero disorder, $W = 0$. The electron is coming from the right and is scattered by the sample. The resulting waves either continue to the left in the left lead, or travel back to the right in the right side lead.

In numerical simulations, we use the transfer matrix $\mathbf{M}$, given by Eq. (343)

$$\mathbf{M}^{(L_z)} = \prod_{n=1}^{L_z} \mathbf{M}_n = \prod_{n=1}^{L_z} \begin{pmatrix} E - \mathcal{H}_n & -1 \\ 1 & 0 \end{pmatrix}. \tag{366}$$

Similarly as in the case of the 1d problem, discussed in the previous section, we have to transform this transfer matrix into the "wave" representation. In this representation, the transfer matrix in the leads is diagonal. Therefore, in the first step we have to diagonalize the transfer matrix

$$\mathbf{M}_0 = \begin{pmatrix} E - \mathcal{H}_0 & -1 \\ 1 & 0 \end{pmatrix}, \tag{367}$$

where $\mathcal{H}_0$ is Hamiltonian of the transversal slice *without* disorder.

In general, the transfer matrix has some eigenvalues with modulus equal to 1, i.e. $\lambda = \exp ik_z$. The corresponding eigenvectors represent the propagating waves. Other eigenvalues are of the form $\lambda = \exp \pm \kappa$. They correspond to the evanescent modes. Note, if λ is an eigenvalue, then λ^{-1} is also an eigenvalue corresponding to the wave traveling in the opposite direction.

As the transfer matrix $\mathbf{M}_0$ is not Hermitian, we have to calculate both the left and right eigenvectors. Then, we construct four matrices: The $N \times 2N$ matrix R_{left} (R_{right}) which contains in its columns N right eigenvectors, for waves traveling to the *left*, (*right*), respectively. Similarly, matrices L_{left} and L_{right} are $2N \times N$ matrices which contains in N rows the left eigenvectors of the transfer matrix $\mathbf{M}_0$ which represent the waves traveling to the left and to the right, respectively. Then, by definition of the transfer matrix,

$$\mathbf{T} = \begin{pmatrix} T_{11} & T_{12} \\ T_{21} & T_{22} \end{pmatrix} = \begin{pmatrix} L_{\text{right}}\mathbf{M}R_{\text{right}} & L_{\text{right}}\mathbf{M}R_{\text{left}} \\ L_{\text{left}}\mathbf{M}R_{\text{right}} & L_{\text{left}}\mathbf{M}R_{\text{left}} \end{pmatrix} \tag{368}$$

so that

$$T_{22} = L_{\text{left}} \mathbf{T} R_{\text{left}}. \tag{369}$$

At this point we have to distinguish between the propagating and evanescent modes. If there are evanescent modes, then $T_{22} \neq [t^-]^{-1}$ because the two matrices have different size. If we order the eigenvectors in the matrix R in such a way that the eigenvectors with index $1 \leq a \leq N_{\text{o}}$ correspond to the propagating modes, and the remaining eigenvectors correspond to the evanescent modes, then the transmission is given by the $N_{\text{o}} \times N_{\text{o}}$ sub-matrix $[T_{22}]_{ab}$, with $a, b \leq N_{\text{o}}$:

$$T = \sum_{ab=1}^{N_{\text{o}}} \left| \left[T_{22}^{-1} \right]_{ab} \right|^2. \tag{370}$$

Other matrix elements of T_{22} correspond to the scattering of the electron into the evanescent channels. They do not contribute to the transmission since evanescent waves decay to zero in the semi-infinite leads.

It seems that the relation (369) solves our problem completely. However, the above algorithm must be modified. The reason is that the elements of the matrix $(t^-)^{-1}$ are given by their largest eigenvalues. We are, however, interested in the largest eigenvalues of the matrix t^-. As the elements of the transfer matrix increase exponentially in the iteration procedure given by Eq. (366), any information about the smallest eigenvalues of $(t^-)^{-1}$ will be quickly lost. We have therefore to introduce some re-normalization procedure. We use the procedure described in Ref. [72].

Relation (369) can be written as

$$T_{22} = L_{\text{left}} r^{(L_z)}, \tag{371}$$

where we have defined the $N \times 2N$ matrices $r^{(n)}$, $n = 0, 1, \ldots L_z$ as

$$r^{(n)} = \mathbf{M}_n r^{(n-1)}, \quad \text{and} \quad r^{(0)} = R_{\text{left}}. \tag{372}$$

Each matrix $r^{(n)}$ can be written as

$$r = \begin{pmatrix} r_1 \\ r_2 \end{pmatrix} \tag{373}$$

with r_1, r_2 being the $N \times N$ matrices. We transform r as

$$r = r' r_1, \qquad r' = \begin{pmatrix} 1 \\ r_2 r_1^{-1} \end{pmatrix} \tag{374}$$

and define $r^{(n)} = \mathbf{M}_n (r')^{(n-1)}$. In contrast to the matrices r_1 and r_2, all eigenvalues of the matrix $r_2 r_1^{-1}$ are of the order of unity. The relation (371) can now be re-written into the form

$$T_{22} = L_{\text{left}} \begin{pmatrix} 1 \\ r_2^{(n)} \left[r_1^n \right]^{-1} \end{pmatrix} r_1^{(n)} r_1^{(n-1)} \ldots r_1^{(1)} r_1^{(0)} \tag{375}$$

from which we get

$$[T_{22}]^{-1} = \left[r_1^{(0)} \right]^{-1} \left[r_1^{(1)} \right]^{-1} \ldots \left[r_1^{(n)} \right]^{-1} \left[L_{\text{left}} \begin{pmatrix} 1 \\ r_2^{(n)} \left[r_1^{(n)} \right]^{-1} \end{pmatrix} \right]^{-1}. \tag{376}$$

All elements of the matrices on the r.h.s. of Eq. (376) are of the order of unity.

References

[1] P. W. Anderson: Phys. Rev. **109**, 1492 (1958)

[2] I. M. Lifshitz: Sov. Phys. Uspekhi **7**, 549 (1965)

[3] E. Abrahams *et al.*: Phys. Rev. Lett. **42**, 673 (1979)

[4] R. Landauer: IBM J. Res. Dev. **1**, 223 (1957); R. Landauer: Phil. Mag. **21**, 683 (1970)

[5] N. F. Mott, W. D. Twose: Adv. Phys. **10**, 107 (1961)

[6] A. MacKinnon, B. Kramer: Z. Phys. B **53**, 1 (1983)

[7] P. A. Mello, P. Pereyra, N. Kumar: Ann. Phys. (NY) **181**, 290 (1988)

[8] J. S. Langer, T. Neal: Phys. Rev. Lett. **16**, 984 (1966)

[9] P. A. Lee, A. D. Stone: Phys. Rev. Lett. **55**, 1622 (1985); P. A. Lee, A. D. Stone, H. Fukuyama: Phys. Rev. B **35**, 1039 (1987)

[10] F. Wegner: Z. Phys. B **25**, 327 (1976); *ibid* **35**, 207 (1979)

[11] S. Hikami: in [37] p. 429

[12] B. L. Altshuler, V. E. Kravtsov, I. V. Lerner: Sov. Phys. JETP **64**, 1352 (1986); JETP Lett. **43**, 441 (1986)

[13] B. L. Altshuler: JETP Lett. **41**, 648 (1985); B. L. Altshuler, D. E. Khmelnitskii: JETP Lett. **42**, 359 (1985); O. Tsyplyatyev *et al.*: cond-mat/0306613

[14] S. Washburn, R. A. Webb: Adv. Phys. **35**, 375 (1986)

[15] A. B. Fowler, J. J. Wainer, R. A. Webb: IBM J. Res. Dev. **32**, 372 (1988)

[16] P. W. Anderson, D. J. Thouless, E. Abrahams, D. S. Fisher: Phys. Rev. B **22**, 3519 (1980)

[17] A. MacKinnon, B. Kramer: Phys. Rev. Lett. **47**, 1546 (1981)

[18] D. J. Thouless: Phys. Rev. Lett. **39**, 1167 (1977)

[19] R. A. Serota, R. K. Kalia, P. A. Lee: Phys. Rev. B **33**, 8441 (1986)

[20] P. Markoš, B. Kramer: Annalen der Physik **2**, 339 (1993)

[21] E. Abrahams, S. V. Kravchenko, M. P. Sarachik: Rev. Mod. Phys. **73**, 251 (2001)

[22] C. M. Soukoulis *et al.*: Phys. Rev. Lett. **62**, 575 (1989)

[23] M. C. W. van Rossum, Th. M. Nieuwenhuizen: Rev. Mod. Phys. **71**, 313 (1999)

[24] M.Stoychev, A. Z. Genack: Phys. Rev. Lett. **79**, 309 (1997)

[25] G. Bergmann: Phys. Rep. **107**, 1 (1984)

[26] D. J. Thouless: Phys. Rep. **13**, 93 (1974)

[27] P. A. Lee, T. V. Ramakrishnan: Rev. Mod. Phys. **57**, 287 (1985)

[28] M. Janßen: Phys. Rep. **295**, 1 (1998)

[29] M. Janßen: Int. J. Mod. Phys. B **8**, 943 (1994)

[30] B. Kramer, A. MacKinnon: Rep. Prog. Phys **56**, 1469 (1993)

[31] K. von Klitzing: Rev. Mod. Phys. **58**, 519 (1986); B. Huckestein: Rev. Mod. Phys. **67**, 357 (1995)

[32] B. Kramer, T. Ohtsuki, S. Ketteman: Phys. Rep. **417**, 211 (2005)

[33] K. B. Efetov: Adv. Phys. **32**, 53 (1983)

[34] A. Mirlin: Phys. Rep. **326**, 259 (2000)

[35] C. W. J. Beenakker: Rev. Mod. Phys. **69**, 731 (1997)

[36] B. Kramer, G. Schön (Eds.) *Anderson Transition and Mesoscopic Fluctuations* Proc. of Workshop, Braunschweig 9-12 January 1990. Physica A **167** (1990) n. 1

[37] B. Kramer (Ed.) *Quantum Coherence in Mesoscopic Systems* NATO ASI **254**, Plenum Press NY and London (1991)

[38] T. Brandes and S. Ketteman (Eds.) *The Anderson Transition and its Ramifi cations - Localisation, Quantum Interference, and Interactions* Springer Verlag "Lecture Notes in Physics" vol. **630**, (2003) (ISBN 3-540-40785-5). Proceedings of the B. Kramer 60th Birthday Conference, Hamburg, September 4-6, 2002

[39] E. N. Economu: *Green's Functions in Quantum Physics* 2nd ed. Springer (1990)

[40] N. F. Mott, E. A. Davis: *Electron processes in non-crystalline materials*, Clarendon Press, Oxford 1979

[41] Y. Imry: *Introduction to Mesoscopic Physics*, Oxford Univ. Press (2000)

[42] S. Datta: *Electronic Transport in Mesoscopic Systems*, Cambridge University Press, Cambridge, UK (1995)

[43] Ping Sheng: *Introduction to Wave Scattering, Localization, and Mesoscopic Phenomena*, Academic Press (2000)

[44] M. L. Mehta: *Random Matrices* (Academic, NY 1991)

[45] K. Slevin, Y. Asada, L. I. Deych: Phys. Rev. B **70**, 054201 (2004)

[46] J. M. Ziman: J. Phys. C **1**, 1532 (1968); *ibid* **2**, 1232, (1969); **2**, 1704 (1969)

[47] S. N. Evangelou, T. Ziman: J. Phys. C **20**, L235 (1987)

[48] T. Ando: Phys. Rev. B **40**, 5325 (1989)

[49] Y. Asada, K Slevin, T. Ohtsuki: Phys. Rev. Lett. **89**, 256601 (2002); Phys. Rev. B **70**, 035115 (2004)

[50] B. Huckestein, B. Kramer: Solid State Comm. **71**, 445 (1989); Phys. Rev. Lett. **64**, 1437 (1990); B. Huckestein: in [37] p. 441.

[51] J. T. Chalker, P. D. Coddington: J. Phys. C **21**, 2665 (1998)

[52] B. Bulka, B. Kramer, A. MacKinnon: Z. Phys. B: Condens. Matt. **60**, 13 (1985)

[53] N. F. Mott: Philos. Mag. **26**, 1015 (1972)

[54] P. Markoš, L. Schweitzer: J. Phys. A **39**, 3221 (2006)

[55] S. N. Evangelou: J. Phys. A **23**, L317 (1990)

[56] J. Brndiar, P. Markoš: cond-mat/0606056

[57] P. Markoš, L. Schweitzer, *unpublished*

[58] B. I. Shklovskii *et al.*: Phys. Rev. B **47**, 11487 (1993)

[59] A. G. Aronov, V. E. Kravtsov, I. V. Lerner: JETP Lett. **59**, 40 (1994); Phys. Rev. Let. **74** 1174 (1995)

[60] D. Braun, G. Montambaux, M. Pascaud: Phys. Rev. Lett. **81**, 1062 (1998)

[61] I. Kh. Zarekeshev, B. Kramer: Phys. Rev. Lett. **79**, 717 (1997)

[62] J. T. Edwards, D. J. Thouless: J. Phys. C **5**, 807 (1972)

[63] D. C. Licciardello, D. J. Thouless: J. Phys. C **8**, 4157 (1975)

[64] E. N. Economou, C. M. Soukoulis: Phys. Rev. Lett. **46**, 618 (1981); *ibid* **47** 973 (1981)

[65] M. Azbel: Phys. Lett. A **78**, 410 (1980)

[66] D. S Fischer, P. A. Lee: Phys. Rev. B **23**, 6851 (1981)

[67] D. C. Langreth, E. Abrahams: Phys. Rev. B **24**, 2978 (1981)

[68] R. Landauer: Z. Phys. B **68**, 217 (1987)

[69] D. Braun *et al.*: Phys. Rev. B **55**, 7557 (1997)

[70]   A. Abrikosov, I. A. Rhyzkin: Adv. Phys. **27**, 147 (1978); V. I. Melnikov: Fiz. Tverd. Tela **23**, 444 (1981); A. Abrikosov: Solid State Commun. **37**, 997 (1981)

[71]   P. D. Kirkman, J. B. Pendry: J. Phys. C: Solid St. Phys. **17**, 4327 (1984); *ibid* 5705 (1984)

[72]   J. B. Pendry, A. MacKinnon, P. J. Roberts: Proc. R. Soc. London A **437**, 67 (1992)

[73]   O. N. Dorokhov: JETP Lett. **36**, 318 (1982)

[74]   P. A. Mello: Phys. Rev. B **35**, 1082 (1987)

[75]   B. Shapiro: Philos. Mag. B **56**, 1032 (1987)

[76]   P. Vagner *et al.*: Phys. Rev. B **67**, 165316 (2003)

[77]   P. Markoš, C. M. Soukoulis: *Wave propagation*, Princeton Univ. Press (submitted)

[78]   M. Moško *et al.*: Phys. Rev. Lett. **91**, 136803 (2003)

[79]   D. Maily, M. Sanquer: in [37] p. 401

[80]   P. Markoš, B. Kramer: Solid State Comm. **90**, 615-617 (1994)

[81]   M. Kaveh, N. F. Mott: J. Phys. C **14**, L177 (1981)

[82]   Y. Asada, K. Slevin, T. Ohtsuki: cond-mat/0509718

[83]   P. A. Mello, A. D. Stone: Phys. Rev. B **44**, 3559 (1991)

[84]   E. N. Economou. C. M. Soukoulis, A. D. Zdetsis: Phys. Rev. B **30**, 1686 (1984) *ibid.* **31**, 6483 (1985)

[85]   C. W. J. Beenakker: Phys. Rev. B **47**, 15763 (1993)

[86]   D. Braun *et al.*: Phys. Rev. B **64**, 155107 (2001)

[87]   M. Rühländer, P. Markoš, C. M. Soukoulis: Phys. Rev. B **64**, 172202 (2001)

[88]   I. Travěnec: Phys. Rev. B **69**, 2004 (033194)

[89]   M. C. W. van Rossum *et al.*: Phys. Rev. B **55**, 4710 (1997)

[90]   K. A. Muttalib: Phys. Rev. Lett **65**, 745 (1990)

[91]   P. Markoš: J. Phys.: Condens. Matter **7**, 8361 (1995)

[92]   Y. Imry: Europhys. Lett. **1**, 249 (1986)

[93]   P. Markoš, C. M. Soukoulis: Phys. Rev. B **71**, 054201 (2005)

[94]   Th. M. Nieuwenhuizen, M. C. W. van Rossum: Phys. Rev. Lett. **74**, 2674 (1995)

[95]   E. Kogan, M. Kaveh: Phys. Rev. B **52**, R3813 (1995)

[96]   K. Tankei, M. Ikegami, Y. Nagaoka: J. Phys. Soc. Jpn. **63**, 1090 (1994)

[97]   F. Wegner: Nucl. Phys. B **316**, 623 (1989)

[98]   S. Hikami: Phys. Rev. B **24**, 2671 (1981)

[99]   U. Fastenrath *et al.*: Physica A **172**, 302 (1991)

[100] L. Schweitzer, I. Kh. Zarekeshev: J. Phys.: Condens. Matt. **9**, L441 (1997)

[101] B. Shapiro: Phys. Rev. Lett. **65**, 1510 (1990)

[102] P. Markoš, B. Kramer: Philos. Mag. B **68**, 1993 (357-379)

[103] A. Cohen, Y. Roth, B. Shapiro: Phys. Rev. B **38**, 12125 (1988)

[104] A. Cohen, B. Shapiro: Int. J. Mod. Phys. B **6**, 1243 (1992)

[105] P. Markoš: Phys. Rev. Lett. **83**, 1999 (588)

[106] M. Rühländer, P. Markoš, C. M. Soukoulis: Phys. Rev. B **64**, 212202 (2001)

[107] K. Slevin, T. Ohtsuki: Phys. Rev. Lett. **78**, 4083 (1997)

[108] P. Markoš: in [38]

[109] V. A. Gopar, K. A. Muttalib, P. Wölfle: Phys. Rev. B **66**, 174204 (2002)

[110] K. A. Muttalib *et al.*: Europhys. Lett. **61**, 95 (2003)

[111] P. Markoš: Europhys. Lett. **26**, 431 (1994)

[112] K. Slevin, T. Ohtsuki: Phys. Rev. B **63**, 45108 (2001)

[113] I. Travěnec, P. Markoš: Phys. Rev. B **65**, 114109 (2002)

[114] C. M. Soukoulis *et al.*: Phys. Rev. Lett. **80**, 668 (1999); K. Slevin, T. Ohtsuki: Phys. Rev. Lett. **80**, 669 (1999)

[115] K. Slevin, T. Ohtsuki, T. Kawarabayashi: Phys. Rev. Lett. **84**, 3915 (2000)

[116] M. Schreiber, H. Grußbach: Phys. Rev. Lett. **76**, 1687 (1996)

[117] R. Rammal, G. Thoulouse: J. Phys. Lett. (France) **44**, 1983 (L13); R. Burioni, D. Cassi, S. Regina: cond-mat/9710273

[118] P. Markoš: Phys. Rev. B **65**, 104207 (2002)

[119] P. J. Roberts: J. Phys.: Condens. Matt. **4**, 7795 (1992)

[120] K. M. Slevin, J. B. Pendry: J. Phys.: Condens. Matt. **2**, 2821 (1990)

[121] J. Prior, A. M. Somoza, M. Ortuno: Phys. Rev. B **72**, 024206 (2005)

[122] A. M. Somoza, J. Prior, M. Ortuno: Phys. Rev. B **73**, 184201 (2006)

[123] J. W. Kantelhardt, A. Bunde: Phys. Rev. B **66**, 035118 (2002)

[124] S. L. A. de Queiroz: Phys. Rev. B **66**, 195113 (2002)

[125] K. A. Muttalib, P. Wölfle: Phys. Rev. Lett. **83**, 3013 (1999); P. Wölfle, K. A. Muttalib: Ann. Phys. (Leipzig) **8**, 753 (1999)

[126] L. S. Froufe-Prez *et al.*: Phys. Rev. Lett. **89**, 246403 (2002) A. Garcia-Martin, J. J. Saenz: Waves in Random and Complex Media **15**, 229 (2005) and references therein

[127] J.-L. Pichard, G. Sarma: J. Phys. C **14**, L127 (1981); *ibid*, L167

[128] P. Markoš: J. Phys. A: Math. Gen. **33**, L393 (2000)

[129] S. N. Evangelou: *private communication*

[130] B. Kramer, M. Schreiber, A. MacKinnon: Z. Phys. B **56**, 297 (1984); M. Schreiber, B. Kramer, A. MacKinnon: J. Pys. C: Solid State Phys. **17**, 4111 (1984); B. Kramer, K. Broderix, A. MacKinnon, M. Schreiber: Physica A **167**, 163 (1990)

[131] P. Cain, R. A. Römer, M. Schreiber: Ann. Phys. (Leipzig) **8**, SI-33 (1999)

[132] R. A. Römer, M. Schreiber: in [38] p. 3.

[133] K. M. Slevin, T. Ohtsuki: Phys. Rev. Lett. **82**, 382 (1999)

[134] A. MacKinon, B. Kramer: Phys. Rev. Lett. **49**, 695 (1982)

[135] A. MacKinnon: J. Phys.: Condens. Matt. **6**, 2511 (1994)

[136] K. Slevin, P. Markoš, T. Ohtsuki: Phys. Rev. Lett. **86**, 3594 (2001)

[137] K. Slevin, P. Markoš, T. Ohtsuki: Phys. Rev. B **67**, 155106 (2003)

[138] B. L. Altshuler *et al.*: Sov. Phys. JETP **67**, 625 (1988)

[139] E. N. Evangelou: Phys. Rev. B **39**, 12895 (1989); *ibid.* **49**, 16805 (1994)

[140] M. Batsch *et al.*: Phys. Rev. Lett. **77**, 1552 (1996)

[141] A. Kaneko, T. Ohtsuki: Ann. Phys. (Leipzig) **9**, 121 (1999)

[142] K. Slevin, Y. Asada, T. Ohtsuki: Phys. Rev. B **73**, (2006)

[143] F. Evers, A. D. Mirlin: Phys. Rev.Lett. **84**, 3690 (2000); A. D. Mirlin, F. Evers: Phys. Rev. B **62**, 7920 (2000); A. Mildenberger, F. Evers, A. D. Mirlin: Phys. Rev. B **66**, 033109 (2002)

[144] F. Evers, A. Mildenberger, A. D. Mirlin: Phys. Rev. B **64**, 241303(R) (2001)

[145] E. Cuevas: Phys. Rev. B **66**, 233103 (2002)

[146] E. Cuevas *et al.*: Phys. Rev. Lett. **88**, 016401 (2002)

[147] D. Vollhardt, P. Wölfle: *Self-Consistent Theory of Anderson Localization*, in *Electronic Phase Transitions*, Ed. by W. Haake and Yu. V. Kopaev, Elsevier Sci. Publ. 1992 1992

[148] P. Markoš, M. Henneke: J. Phys.: Condens. Matter **6**, L765 (1994)

[149] I. M. Suslov: cond-mat/0105325 2001; cond-mat/0106357 (2001)

[150] I. Suslov: J. Exp. Theor. Phys. **101**, 661 (2005)

[151] V.N. Kuzovkov, V. Kashcheyevs, W. von Niessen: J. Phys.: Cond. Matt. **69**, 1683 (2004)

[152] P. Markoš, L. Schweitzer, M. Weyrauch: J. Phys.: Condens. Matt. **16**, 2004 (1679-1681)

[153] I. Zambetaki *et al.*: Phys. Rev. Lett. **76**, 3614 (1996); Phys. Rev. B **56**, 12221 (1997)

[154] A. Croy, R. A. Roemer, M. Schreiber: in *Lecture Notes in Computational Science and Engineering* (Springer, Berlin), (cond-mat/0602300)

[155] V. Dobrosavljevic, A. A. Pastor, B. K. Nikolic: Europhys. Lett. **62**, 76 (2003)

[156] A. MacKinnon: Z. Phys. B **59**, 385 (1985)

[157] L. Schweitzer: in [38]

[158] V. I. Fal'ko, K. B. Efetov: Europhys. Lett. **32**, 627 (1995); Phys. Rev. B bf 52, 17413 (1995)

[159] L. Schweitzer, P. Markoš: Phys. Rev. Lett. **95**, 256805 (2005)

[160] A. Hansen *et al.*, Annual Rev. of Comp. Phys. **5**, Ed. by D. Stauffer (World Scientific, Singapore, 1997 (cond-mad/9703026)

[161] S. Kivelson, D. H. Lee, S. C. Zhang: Phys. Rev. B **46**, 2223 (1992)

[162] X. Wang, Q. Li, C. M. Soukoulis: Phys. Rev. B **58**, 3576 (1998)

[163] Z. Wang, B. Jovanovic, D. H. Lee: Phys. Rev. Lett. **77**, 4426 (1996)

[164] T. Ohtsuki, K Slevin, B. Kramer: Physica E **22**, 248 (2004)

[165] K. A. Muttalib, J. R. Klauder: Phys. Rev. Lett. **82**, 4272 (1999); K. A. Muttalib, V. A. Gopar: Phys. Rev. B **66**, 115318 (2002)

[166] P. Markoš *et al.*: Europhys. Lett. **68**, 867 (2004)

[167] K. A. Muttalib, P. Markoš, P. Wölfle: Phys. Rev. B **72**, 125317 (2005)

[168] P. Markoš: Ann. Physik (Leipzig) **8**, SI 165 (1999)

[169] P. Markoš: J. Phys. A: Math. Gen. **30**, 3441 (1997)

[170] L. I. Deych, A. A. Lisyansky, B. I. Altshuler: Phys. Rev. Lett **84**, 2678 (2000); Phys. Rev. B **64**, 224202 (2001); L. I. Deych, M. V. Erementchouk, A. A. Lisyansky: Phys. Rev. Lett. **90**, 126601 (2003); Physica B **338**, 79 (2003)

[171] F. M. Izrailev, A. A. Krokhin: Phys. Rev. Lett. **82**, 4062 (1999); F. M. Izrailev, A. A. Krokhin, S. E. Ulloa: Phys. Rev. B **63**, 041102 (2001)

[172] F. M. Izrailev, N. M. Makarov: J. Phys. A **49**, 10613 (2005)

[173] Ch. Mudry, P. W. Brouwer, A. Furusaki: Phys. Rev. B **62**, 8249 (2000); P. M. Brouwer: *et al.*: cond-mat/0511622 (2005) and references therein

[174] A. A. Asatryan *et al.*: Phys. Rev. E **71**, 036623 (2005)

[175] E. Larose *et al.*: Phys. Rev. Lett. **93**, 048501 (2004)

[176] P. Cain *et al.*: cond-mat/0106005 (2001); K. Slevin, T. Ohtsuki: cond-mat/0106006 (2001)

[177] K. Slevin, T. Nagao: Int. J. Mod. Phys. **21**, 2665 (1988)

[178] P. A. Mello, J.-L. Pichard: J. Phys. I **1**, 493 (1991)

[179] J.-L. Pichard: in: [37] p. 369.

[180] P. A. Mello, S. Tomsovìc: Phys. Rev. B **46**, 15963 (1992)

[181] J.-L. Pichard *et al.*: J. Phys. France **51**, 587 (1990)

[182] N. Zannon, J.-L. Pichard: J. Phys. France **49**, 907 (1988)

[183] K. M. Slevin, J.-L. Pichard, K. A. Muttalib: J. Phys. France I **3**, 1387 (1993)

[184] Y. Avishai, J.-L. Pichard, K. A. Muttalib: J. Phys. France **3**, 1387 (1991)

[185] T. A. Brody *et al.*: Rev. Mod. Phys. **53**, 385 (1981)

[186] C. W. J. Beenakker, R. Rajaei: Phys. Rev. Lett. **71**, 3689 (1993); Phys. Rev. B **49**, 7499 (1994)

[187] D. J. Thouless: J. Phys. C **5**, 77 (1972)

[188] M. Kappus, F. Wegner: Z. Phys. B **45**, 15 (1981)

[189] B. Derrida, E. Gardner: J. Physique **45**, 1283 (1984)

[190] V. I. Oseledec: Trans. Moscow Math. Soc. **19**, 197 (1968)